WATER IN EVOLVED LUNAR ROCKS

A DISSERTATION SUBMITTED TO THE GRADUATE DIVISION OF THE UNIVERSITY OF HAWAIʻI AT MĀNOA IN PARTIAL FULFILLMENT OF THE REQUIREMENTS FOR THE DEGREE OF

DOCTOR OF PHILOSOPHY

IN

GEOLOGY AND GEOPHYSICS

MAY 2015

By

Katharine Lynn Robinson

Dissertation Committee:

G. Jeffrey Taylor, Chairperson
Gary R. Huss
Kazuhide Nagashima
Eric Hellebrand
Michael J. Mottl

Keywords: Moon; Lunar water; Evolved rocks; Hydrogen isotopes; Felsites; Lunar evolution

ACKNOWLEDGEMENTS

This research was supported by the National Aeronautics and Space Administration through the NASA Astrobiology Institute under Cooperative Agreement No. NNA09DA77A issued through the Office of Space Science, and by NASA Lunar Advanced Science and Exploration Research Grants NNX11AE85G and NNX08AY88G to G. Jeffrey Taylor. I also received funding from the Fred M. Bullard Graduate Fellowship and Subagreement No. 02235-03 on Award number NNA14AB07A (NASA SSERVI).

On a more personal note, I would like to thank my advisor, Jeff Taylor, for being an amazing boss, teacher, and co-author for the past four-odd years. None of this work would have been possible without Jeff, and only Jeff could have made it so much fun. I also thank my past advisors, Albert Colman and Allan Treiman, for teaching me the fundamentals of research and helping me get my foot in the planetary geology door. The Grad Family at large is too numerous to thank individually, but thanks, everyone, for being my surrogate island family. Special thanks to Sarah Crites, Sarah Maher, and Lydia Baker for all the fun, beach days, hugs, and hand-holding through all the usual grad student milestones: quals, comps, conference presentations, and finally, the dissertation defense. To my real family (Mom, Dad, Alex, and Ben): *grazie mille*. I couldn't have done any of this without you.

ABSTRACT

The Moon was thought to be completely anhydrous until indigenous water was found in lunar samples in 2008. This discovery raised two fundamental questions about the Moon: how much water is present in the bulk Moon and is water uniformly distributed in the lunar interior? To address these questions, I studied a suite of lunar samples rich in a chemical component called KREEP (K, Rare Earth Elements, P), all of which are incompatible elements. Water behaves as an incompatible element in magmas, so KREEP-rich lunar samples are potentially water rich. In this dissertation, I present the results of a petrologic study of KREEP-rich lunar rocks, measurements of their water contents and deuterium (D) to hydrogen (H) ratios (D/H), and examined where these rocks fit into our understanding of water in the Moon as a whole.

We performed a study of highly evolved, KREEP-rich lunar rocks called felsites and determined that they contain quartz. Using cooling rates derived from quartz-Ti thermometry, we show the felsites originated at a minimum pressure of ~1 kbar, corresponding to a minimum depth of 20-25 km in the lunar crust. We calculate that at that pressure water would have been soluble in the melt, indicating that degassing of H_2O from the felsite parental melts was likely minimal and hydrogen isotopes in intrusive rocks are likely unfractionated.

We then measured D/H in apatite in KREEP-rich intrusive rocks to clarify the solar system source of the Moon's water. When viewed in the context of other lunar D/H studies, our results indicate there are at least three distinctive reservoirs in the lunar interior, including an ultra-low D reservoir that could represent a primitive component in the Moon's interior. Furthermore, our measurements of residual glass in a KREEP basalt show that the KREEP basaltic magmas contained 10 times less water than the source of the Apollo 17 pyroclastic glass beads, indicating

that, though wetter than previously thought, the concentration of water in the bulk Moon is still much lower than bulk Earth. The origin of these diverse reservoirs likely reflects a combination of complex processes during lunar formation and differentiation.

TABLE OF CONTENTS

Abstract....iii

List of Tables....vii

List of Figures....viii

List of Abbreviations and Variables....x

Chapter 1. Introduction....1

Chapter 2: Evolved lunar magmatism and the origin of the felsite suite....3

2.1 Introduction....3

2.2 Methods....7

2.2.1. Raman spectroscopy....7

2.2.2. Ti Thermometry....7

2.3 Results: Mineralogy and Petrology....9

2.3.1. Petrography and mineralogy of felsites and related rocks....9

2.3.2. Ti concentrations in quartz....16

2.4 Discussion: Thermometry, cooling rates, and physical setting for felsite formation....18

2.5 Implications for silicic domes....25

2.6 Implication for retention of H species in magmas....26

2.7 Conclusions....28

Chapter 3: Water in evolved lunar rocks: evidence for multiple reservoirs....29

3.1 Introduction....29

3.2 Samples....32

3.3 Methods....35

3.3.1. Secondary Ion Mass Spectrometry (SIMS) protocols....35

3.3.2. Cosmic ray exposure....40

3.4 Results....44

3.5 Discussion....45

3.5.1. Heterogeneous water concentrations....48

3.5.2. Hydrogen isotopic composition: Multiple reservoirs.....54
3.5.3. Implications for the lunar interior.....57
3.6 Conclusions.....59

Chapter 4: Heterogeneous distribution of water in the Moon.....60
4.1 Introduction.....60
4.2 Water in glassy volcanic deposits.....63
4.3 Water in lava flows from the lunar maria.....66
4.4 Drier nonmare rocks.....67
4.5 Heterogeneous distribution of water in the Moon.....71
4.6 Conclusions.....75

Chapter 5: Conclusions.....76

Appendix 1: Why lunar scientists thought the Moon was dry.....80

Appendix 2: Water jargon, isotopes, and cosmic ray corrections.....82

Appendix 3: Extrapolating from samples to source.....84

Work Referenced.....86

LIST OF TABLES

Table 2.1 Felsite samples studied in this paper……..9

Table 2.2 Average Ti concentration in quartz for a representative group of felsites……...16

Table 3.1 δD and H_2O abundances of lunar apatites and glasses...……...41-42

LIST OF FIGURES

Figure 2.1 Representative Raman spectra of quartz in felsites compared to Raman spectra of other SiO_2 polymorphs……...6

Figure 2.2 Representative BSE images of felsites…….12

Figure 2.3 Optical images of a small felsite clast in breccia...…….....13

Figure 2.4 Feldspar compositions for selected felsites.....14

Figure 2.5 Felsite enclave in QMD 14161,7069.....15

Figure 2.6 BSE image of felsite 1, 72215,180.....17

Figure 2.7 SiO_2 phase diagram.....19

Figure 2.8 Felsite cooling rates based on Ti closure temperatures in quartz.....22

Figure 2.9 Calculation of felsite magmatic body size by calculated cooling rates.....24

Figure 2.10 Curves showing the relationship of solubility of water in basaltic and rhyolitic magmas with pressure.....27

Figure 3.1 Representative backscattered electron (BSE) images of samples described in this chapter.....33

Figure 3.2 Sample calibration curves for ims-1280 analysis.....37

Figure 3.3 Apatite data for KREEP-rich intrusive samples.....43

Figure 3.4 Plots showing δD value (normalized to V-SMOW) versus ppm H_2O of lunar apatites.....47

Figure 3.5 KREEP basalt 15358.....50

Figure 3.6 Weighted averages of all apatite analyses.....53

Figure 4.1 Microscopic views of lunar volcanic glass.....62

Figure 4.2 Volatiles in orange glass beads.....65

Figure 4.3 Hydrogen isotopic composition and water contents of lunar materials.....69

Figure 4.4 Broad view of hydrogen isotopic composition.....73

Figure 5.1 Histogram of the lowest analyzed δD from lunar samples.....77

Figure 5.2 Tl vs. La plot for lunar and terrestrial samples.....79

Figure A2 Spallation corrections in low H and higher H samples.....83

LIST OF ABBREVIATIONS AND VARIABLES

Abbreviation/Variable	Definition
$\delta^{37}Cl$	$^{37}Cl/^{35}Cl$ ratio normalized to the mean Cl isotopic composition in terrestrial ocean
A	Pre exponential factor in the diffusion coefficient
a	Grain radius
Ab	Albite
An	Anorthite
a_{TiO2}	Activity of titanium
b	Half width of an intrusion
BSE	Backscattered electron image
CI	Crystallization interval
CI	CI chondrites
CM	CM chondrites
CR	Cooling rate
CRE	Cosmic ray exposure
D	^{2}H or deuterium
D/H	Deuterium to hydrogen ratio
E	Activation energy
EMPA	Electron microprobe analysis
FeNi	Iron-nickel metal
FeS	Iron sulfide

FTIR	Fourier transform infrared spectroscopy
G	Shape factor
HIGP	Hawaii Institute of Geophysics and Planetology
JFC	Jupiter Family Comets
kb	Kilobars
kbar	Kilobars
K-feldspar	Potassium feldspar
KREEP	K, Rare Earth Elements, P
L	Latent heat of crystallization
Ma	Million years ago
MORB	Mid ocean ridge basalt
Myr	Million years
OCC	Oort Cloud Comets
Or	Orthoclase
OU	Open University
PEC	Correction for crystallization
ppm	Parts per million
q	Cooling rate
Q	Quality factor
QMD	Quartz monzodiorites
R	Gas constant
REE	Rare earth elements

RRUFF	An online database of spectral data for minerals
RTI	Real time isotope imaging
SIMS	Secondary ion mass spectrometry
SLI	Silicate-liquid immiscibility
T	Temperature
T_c	Closure temperature
T_m	Initial temperature of the melt
T_o	Temperature of the country rock
t_s	Solidification time
UH	University of Hawaii
urKREEP	Chemical component related to the last 2% of the lunar magma ocean
UVVIS	Ultraviolet and visible wavelengths
V-SMOW	Vienna Standard Mean Ocean Water
wt.%	Weight percent
X_{qtzTi}	Ti content of quartz in ppm
Yr	Year
Z	Atomic mass
δD	The deuterium delta is the D/H ratio relative to terrestrial Vienna Standard Mean Ocean Water
κ	Thermal diffusivity
λ_2	Constant describing the position of the crystallizing front in an intrusion

CHAPTER 1: INTRODUCTION

With the arrival of the first lunar samples during the Apollo program, the Moon was regarded as "bone dry". The absence of common water-bearing minerals in lunar rocks, such as micas and amphiboles, led scientists to the conclusion the Moon was an anhydrous body. The idea of the dry Moon persisted until 2008, when Saal et al. reported the discovery of water in pyroclastic glass beads returned by the Apollo 15 and 17 missions. These glass beads were known to have volatile-rich coatings (Baedeker et al. 1974; Morgan et al., 1974; Wasson et al. 1976) but water had not been previously been reported in them. Soon after, McCubbin et al. (2010a) reported the identification of water in lunar apatite, a phosphate mineral which can incorporate hydroxyl into its chemical structure, and the analysis of lunar materials for water with modern analytical techniques began in earnest.

Initial analytical efforts focused on the water content of pyroclastic glass beads and apatites from lunar basalts (e.g. Saal et al., 2008, McCubbin et al., 2010b, Boyce et al., 2010). Greenwood et al., (2011) reported the first hydrogen isotope measurements in lunar apatites in mare basalts. The deuterium to hydrogen (D/H) ratio of water can provide information about igneous processes and/or the solar system source (e.g. Alexander et al. 2012) of that water. These early water measurements focused on the mare basalts, rather than more evolved lunar lithologies, which are relatively rare in the Apollo sample collection. As non-mare lithologies comprise the most ancient lunar samples, understanding the role water may have had in their formation is critical for understanding the source and behavior of water in the early Moon. Additionally, non-mare rocks rich in a chemical component called KREEP (**K**, **R**are **E**arth **E**lements, **P**) have the potential to be the most water-rich lunar samples on the basis of their extreme enrichment in incompatible elements, which could include water.

For this dissertation, I have studied the petrology of KREEP-rich lunar rocks, measured their water contents and D/H ratios, and examined where these rocks might fit into our understanding of water in the Moon as a whole. The three chapters are briefly described below.

Chapter 2: Evolved Lunar Magmatism and the Origin of the Felsite Suite.

Evolved (silica-rich) rocks are relatively rare on the Moon. The felsites, sometimes called granites in the literature, are the best known lunar silicic rocks. They are related to the incompatible element-enriched KREEP basalts, and likely formed in small intrusive bodies by extensive fractional crystallization. This chapter examines the petrology of felsites, establishes their origins in small intrusive bodies, and examines their thermal history and formation depth in the lunar crust with the ultimate goal of determining whether or not they could have preserved volatiles such as water.

Chapter 3: Water in Evolved Lunar Rocks: Evidence for Multiple Reservoirs

This chapter builds upon the conclusions of Chapter 1: that the felsites and related differentiated rocks formed in small intrusive bodies at pressure high enough to potentially avoid the degassing of hydrogen species and therefore the fractionation of deuterium from hydrogen, in order to preserve a more representative D/H ratio, for the lunar interior. Apatite in felsites and other evolved, intrusive lithologies was measured for D/H and water content. The extreme range of hydrogen isotope variation (δD -750 to +934) in apatite from these samples indicates that there are two or more different water reservoirs inside the lunar interior.

Chapter 4: Heterogeneous Distribution of Water in the Moon

This chapter recounts the history of the study of water in the Moon and contains a comprehensive analysis of all available water data for lunar samples, originally published as an invited review paper in *Nature Geoscience*. Compiling all available data for lunar water, including data from pyroclastic glass beads, melt inclusions in olivine grains, as well as apatite, allowed us to avoid some of the biases caused by only looking at one type of data at a time, which has led to claims that the bulk Moon contains terrestrial levels of water. The complied data provide further evidence for the heterogeneous distribution of water in the lunar interior and show that the Moon is indeed depleted in water with respect to Earth.

CHAPTER 2: EVOLVED LUNAR MAGMATISM AND THE ORIGIN OF THE FELSITE SUITE

To be submitted for publication as Robinson, K.L., Hellebrand, E., and Taylor G.J. Evolved lunar magmatism and the origin of the felsite suite.

Abstract

Sample-based evidence for past evolved magmatism on the Moon consists of a rare lunar rock type called felsite. The felsites are highly evolved, silica-rich rocks that consist of intergrowths of K-feldspar and a silica polymorph. Identifying that silica polymorph provides information on the formation and thermal history of the felsite suite, which in turn has important implications for the history of evolved magmatism on the Moon. Using Raman spectroscopy on 19 thin sections of felsites, we have determined that the silica polymorph is quartz. Based on the presence of quartz and cooling rates derived from quartz-Ti thermometry, we estimate that the felsites formed in small, 15-300 m intrusions at a minimum pressure of ~1 kbar, corresponding to a minimum depth of 20-25 km in the lunar crust. At that pressure, at least 3 wt. % H_2O would have been soluble in the melt, indicating that hydrogen-isotope fractionation due to degassing of H_2O from the felsite parental melts likely did not occur.

2.1. Introduction

The presence of rare felsite clasts in lunar soils returned by the Apollo missions suggests that silicic magmatism might have taken place on the Moon (Warren et al. 1983; Jolliff et al. 1991). This silicic magmatism was a separate phenomenon from mare basalt volcanism, but could have been related to the formation of KREEP basalts (Malin 1974; Wood and Head, 1975). Silicic rocks are rare in the lunar sample suite. The felsites are highly evolved rocks, sometimes called granites in the literature because of their high (~70 wt. %) SiO_2 content (Ryder et al. 1975). Most have igneous textures that feature graphic intergrowths of K-feldspar and a silica polymorph, and generally contain between ~10-15 wt.% Al_2O_3 and elevated K_2O, ~5-10 wt.% (Ryder et al. 1975; Taylor et al. 1980; Warner et al. 1978; Warren et al. 1983, 1987; Jolliff 1991). Felsites are generally low in Fe, but with a high Fe/Mg ratio that is indicative of evolved rocks (Taylor et al. 1980). When pyroxene is present, it is often finely exsolved. Sampled

felsites occur exclusively as small clasts in breccias, sometimes coexisting with Fe-rich, low-Si clasts (e.g., 77538, Warner et al. 1978).

The relationship between felsites and KREEP basalts has been recognized for many years due to the felsites' elevated K and rare-earth-element (REE) contents (Ryder et al. 1975; Warner et al. 1978; Taylor et al. 1980). The felsites are also related to another evolved lunar lithology, the quartz monzodiorites (QMDs) (Jolliff 1991). Like the QMDs, felsites are enriched in the incompatible element Th (Warner et al. 1978; Taylor et al. 1980, Warren et al. 1983; Jolliff 1991). This Th enrichment is characteristic of evolved rocks, because Th (along with other incompatible lithophile elements) becomes enriched in the residual liquid of a melt as other phases crystallize out. Minor phases present in felsites include ilmenite, apatite, merrillite, zircon, iron-rich pyroxene and olivine, and glass (Jolliff et al. 1999; James and Hammarstrom 1977, Warren et al. 1983, 1987; Warner et al. 1978, Taylor et al. 1980). Some felsites also occur in tandem with Fe-rich minerals (James and Hammarstrom 1977; Warner et al. 1978; Taylor et al. 1980). The pairing of high-Fe with high-Si compositions is strikingly similar to immiscible melt pairs observed experimentally (Rutherford et al. 1976, Hess et al. 1975, Hess et al., 1978), in the mesostasis of mare basalts (Roedder and Weiblen 1970, 1971), and in some quartz monzodiorite (Jolliff 1991, Jolliff et al. 1999). This has led many investigators to propose that felsites formed by silicate liquid immiscibility (Hess et al. 1975, Ryder et al. 1975, Taylor et al. 1980). However, it is unclear that silicate liquid immiscibility could produce large enough volumes of lava to form large lunar silicic structures, such as the Gruithuisen Domes or Hansteen Alpha (Hagerty et al., 2006).

The lunar red spots, high-albedo spectral anomalies which exhibit strong ultraviolet absorptions, have long been thought to be related to ancient silicic volcanism on the Moon (Whitaker 1972, Head and McCord 1978; Bruno et al. 1991, Hagerty et al. 2006, Glotch et al. 2010). Red spots occur on the lunar nearside in several locations, all within the Th-rich Procellarum KREEP Terrane (Jolliff et al., 2000). They formed before mare volcanism took place, as many of them are embayed by younger mare basalts, and probably covered a much larger area than they appear to today (Bruno et al., 1991; Hawke et al., 2003). They are spectrally and compositionally different from surrounding maria and highlands (Whitaker 1972). FeO and TiO_2 maps derived from Clementine UVVIS data show that the red spots are low in

both Fe and Ti (Lucey et al., 2000; Hawke et al., 2003). Based on the morphologies of certain red spots, several workers have proposed that they are of highlands volcanic origin (Head and McCord, 1978; Hagerty et al., 2006 and references therein). Hawke et al. (2003) suggest that some features resemble terrestrial rhyolite domes. The Gruithuisen domes, Hansteen Alpha, the Lassell massif, and the Compton-Belkovich feature all appear dome-like, dominated by silicic minerals and abundant in Th (Hagerty et al., 2006; Glotch et al., 2010; Jolliff et al. 2011).

Ancient lunar highlands volcanism has important implications for lunar thermal history and crustal evolution, but until recently the direct detection of silica-rich minerals from lunar orbit has not been possible (Hawke et al. 2003; Glotch et al. 2010). The mid-infrared Diviner experiment onboard NASA's Lunar Reconnaissance Orbiter can detect the Christiansen feature, a spectral feature between 7.5 and 8.5μm that is indicative of the bulk SiO_2 content of a mineral. Diviner recently detected minerals indicative of silicic volcanism at several lunar red spots but it cannot determine which minerals (or glasses) are present (Glotch et al. 2010; Jolliff et al. 2011). To get a sense for the possible mineralogy and petrology of these silicic domes, we must look to the collection of returned samples.

To evaluate whether the felsites could be related to silicic domes and to understand felsite petrogenesis, we studied a suite of felsites and related evolved rocks to assess their thermal histories and pressures of formation. We identified the SiO_2 polymorph present in the samples and estimated their cooling rates using Ti thermometry (Wark and Watson, 2006). Besides helping to test the link between the felsites and the silicic domes, the formation depth and thermal histories have great bearing on whether H_2O or other volatiles could be retained in KREEP basaltic magma bodies. Initial studies show that felsites and other KREEP-related rocks have lower H contents than do mare basalts and pyroclastic glasses (Robinson and Taylor, 2014; Barnes et al., 2014).

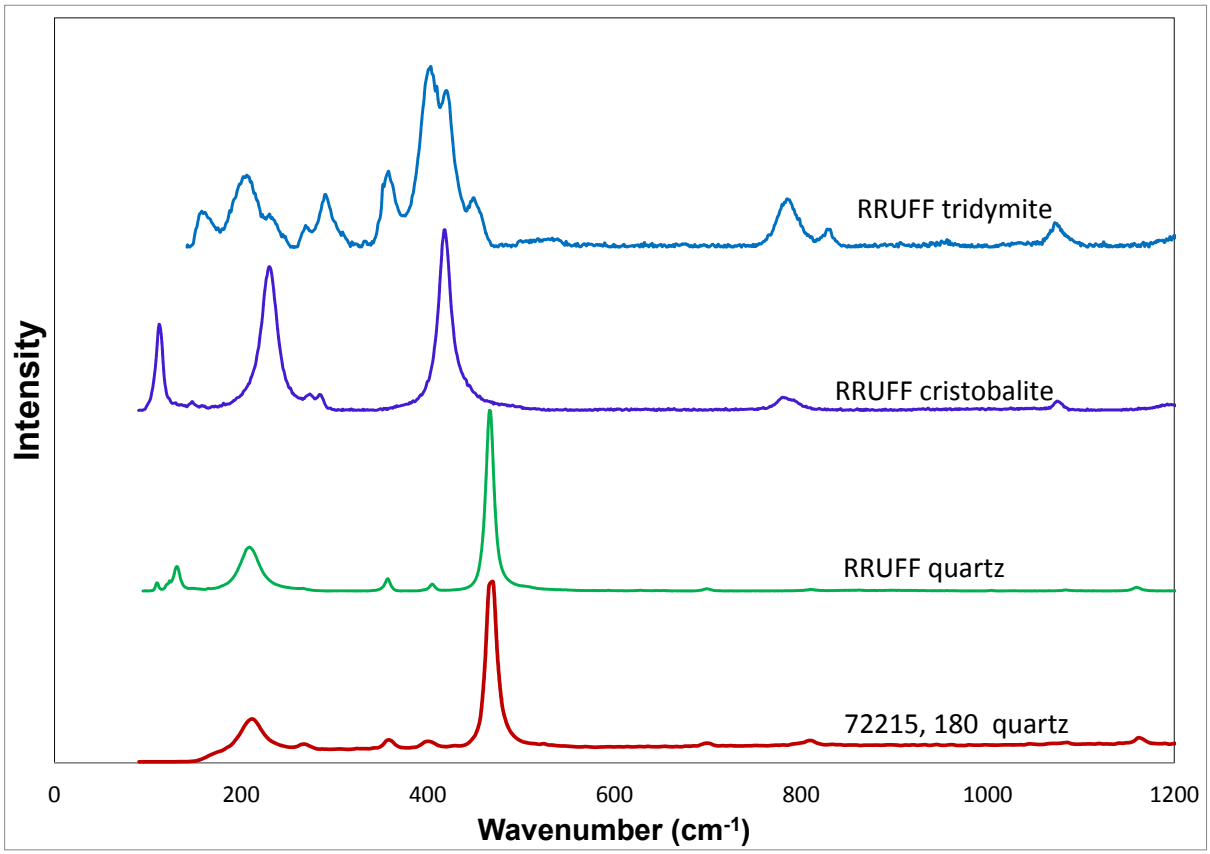

Figure 2.1. Representative Raman spectra of quartz in felsites compared to Raman spectra of quartz and other SiO_2 polymorphs from an online database. Intensity is in arbitrary units, and has been normalized to the maximum counts measured in 72215,180 quartz. After Robinson and Taylor (2011).

2.2. Methods

2.2.1. Raman spectroscopy.

Felsite samples in 19 thin sections were examined in a petrographic microscope. Silica polymorphs were identified by micro-Raman using the HIGP Wi-Tec confocal Raman microscope with 532 nm (green) laser. Raman spectroscopy is nondestructive when properly calibrated and can distinguish between minerals and their polymorphs. Prior to each session, the intensity of the laser was checked with a power meter and filters were added to ensure the power was not so high as to damage the samples. A few test spectra were made of a silicon wafer to calibrate peak locations. The position and intensity of the silicon peak were recorded; the peak position was always within 6 wavenumbers of the 520cm^{-1} silicon peak. The spectra obtained from lunar samples were compared with spectra from the online RRUFF database. If the signal was sufficiently strong, only one spectrum was taken. Otherwise multiple spectra were acquired over a short period (usually 5-10 acquisitions of 0.5s each) and then combined by the WiTec software into a single spectrum. The three silica polymorphs have distinctive spectra and are easily distinguished from one another visually (Fig. 2.1), as well as from other minerals (e.g. feldspars) and glass.

2.2.2. Ti Thermometry.

If a Ti-bearing phase is present in a sample containing quartz, the TitaniQ geothermometer (Wark and Watson 2006) for Ti in quartz can be used to calculate a formation temperature or the temperature at which Ti in quartz was in equilibrium with the Ti-bearing phase. Quartz in six felsites (72215,178, 72215,180; 14321,1029, 14321,1047; 73215,43; 77538,16) was measured for Ti abundance using the UH JEOL electron microprobe. The instrument was specially set up and calibrated for the Ti measurements using the procedures recommended by Wark and Watson (2006). Ti was measured on three spectrometers for 240 s with a 200 nA beam and a spot size of 10 μm. Al was also measured. Standards were sphene glass (Ti) and albite (Al). The data from the three spectrometers were combined into a single set, which was used for the Ti thermometry calculations. The Ti detection limit was ~ 14 ppm. We tried to position the electron beam at least 100 μm from any Ti-bearing phases during the measurements, as secondary fluorescence

generated by the electron beam can produce an artificially high measurement for Ti concentration (Wark and Watson 2006). Mixed analyses (e.g. too much Al from adjacent K-feldspar) or with low (< 98.5 wt%) or high (> 101.5 wt%) totals were discarded.

The TitaniQ geothermometer involves Ti^{4+} subsitution for Si^{4+} in quartz. The Ti content of quartz crystallizing in equilibrium with a Ti phase (e.g. rutile, TiO_2) will increase with T (Wark and Watson, 2006). A quartz crystal with higher Ti content thus equilibrated at a higher temperature than a quartz crystal with lower Ti content. Wark and Watson (2006) determined this relationship to be:

$$\log(X_{qtzTi}) = (5.69 \pm 0.02) - \frac{(3765 \pm 24)}{T} \quad \text{(eq.2.1)}$$

Where X is the ppm Ti in quartz, and T the temperature in Kelvin.

However, as Wark and Watson (2006) point out, this equation is only valid as-written if the Ti phase present is pure TiO_2 (rutile), which has an activity of 1. Ilmenite ($FeTiO_3$) is the Ti-bearing phase in most lunar samples, including the felsites measured here. Since ilmenite is an impure phase, we have to adjust the activity of TiO_2 in the equation in order to use the TitaniQ geothermometer (Wark and Watson 2006).

$$T\ (^{o}C) = \frac{-3765}{\log[\frac{X_{Ti}}{a_{TiO2}}] - 5.69} - 273 \quad \text{(eq. 2.2)}$$

Where X is ppm Ti in quartz and a is the activity $0 < a < 1$.

Activity is difficult to determine in a natural system without knowing the formation temperature from a separate geothermometer (not avaliable) and/or an accurate bulk composition for the samples (selection bias as sampled lunar felsites are usually less than 1mm across). Based on a case study of the Bishop Tuff described in Wark and Watson (2006), we take activity as $a = 0.6$. The Bishop Tuff is rhyolitic, which is compositionally similar to the felsites, and contains ilmenite rather than rutile (Wark and Watson, 2006), also like lunar felsites.

2.3. Results: Mineralogy and Petrology

2.3.1. Petrography and mineralogy of felsites and related rocks.

All felsites identified in the returned Apollo samples occur in breccias. The felsites and QMDs studied here have all been previously reported in several papers. Our samples and a key reference for each sample are listed in Table 2.1.

Table 2.1. Felsite samples studied in this paper.

Sample Number	Key References	Brief Description of felsite clasts
12033,547	Warren et al., 1987	Partially melted silicic soil fragment with residual quartz and fayalite
14001,7002	Morris et al., 1990	Partially impact-melted silicic fragment with residual quartz
14303,209	Warren et al., 1983	Relict granophyric intergrowths
14321,993; -,1029; -,1047	Warren et al., 1983	Largest unmodified lunar "granite" at 1.8 g; granophyric texture
14305,102; -,111	Shervais and Taylor, 1983	Small graphic intergrowths in breccia
14161,7069	Jolliff et al., 1999	Pyroxene-rich QMD fragment with large silica clasts and phosphates
14161,7373	Jolliff 1991	Phosphate-rich QMD fragment with exsolved, inverted pigeonites
72215,178; -,180; -,183	Ryder et al., 1975	Small graphic intergrowths in breccia
72235,9; -,58	Ryder et al., 1975	Small graphic intergrowths in breccia
72255,95	Ryder et al., 1975	Small graphic intergrowths in breccia
73215,43	James and Hammarstrom, 1977	Silica-rich edge along the edge of a breccia; Fe-rich phases nearby
77538,16; -,17	Warner et al., 1978	Graphic silicic and Fe-rich SLI pairs in breccia

There are four major petrographic types of felsites studied in this paper: small felsite clasts in breccias, a relatively coarse-grained, granophyric sample (14321), felsite-ferrobasalt silicate immiscibility (SLI) pairs, and felsite enclaves in QMDs. Representative BSE images of all but the felsite enclaves in QMDs are shown in Figure 2.2. Quartz was the only silica polymorph found in the felsites. Silica in the felsite enclaves in QMDs has an ambiguous Raman spectrum.

Small felsite clasts in breccias. These felsite clasts consist of intergrowths of quartz and K-rich feldspar, often with a distinctive barred texture (Fig. 2.2a,b; Fig.2.3). Quartz, rather than one of its polymorphs, was the only silica phase present. The felsite clasts are light-colored in plane polarized light and tend to be hundreds of μm across, though they can be smaller. The width of the quartz-K-feldspar bars varies from <10 μm to <50 μm. Mafic minerals are not present, although some felsites contain small grains of ilmenite, phosphates, zircon, and/or other high Z phases. The feldspars can be compositionally variable with K-feldspar, plagioclase, and even ternary compositions present (Fig. 2.4). K-feldspar is often Ba-rich; some are near pure barian K-feldspar (Ryder et al., 1975, James and Hammarstrom, 1977) or have Ba-rich rims on the edges of the grains. The majority of the felsites discussed in this paper are this type, including felsites in samples 72215, 72235, 72255, 14305, and 73215,43.

"Granites" 14321 and 14303. Despite brecciation by impacts, felsite clasts in 14321 preserve their original graphic intergrowths of quartz and unzoned, near-endmember orthoclase (Fig. 2.4, Warren et al, 1983). The quartz in these felsite clasts was identified optically by Warren et al., (1983), and we later confirmed this identification with Raman spectroscopy. This sample is much coarser grained than the small felsite clasts described above, with quartz and feldspar grain widths of 100-300 μm (Fig. 2.2c). The felsite clasts in 14303 are similar, with areas of quartz and K-feldspar intergrowth and more plagioclase than 14321 (Warren et al., 1983). The felsite in sample 14321 is extremely poor in mafic minerals including Fe-rich pyroxene and olivine (<1%), while the unbrecciated areas of 14303 are more mafic-rich (~12%, Warren et al., 1983). Apatite and ilmenite are also found in both samples (see Chapter 3 and Warren et al., 1983).

Felsite-ferrobasalt SLI pairs. Breccia 77538 contains many clasts of a unique lunar lithology including felsite intergrowths of quartz and K-feldspar coexisting with similar Fe-rich intergrowths of fayalite, augite, and amorphous silica with ilmenite, FeNi metal, and phosphates (Fig.2.2d). The felsite areas contain quartz, while Raman spectra of the silica in the ferrobasalt show that the material is amorphous, and EMPA analysis shows that it is nearly pure (~99%) SiO_2. Warner et al., (1978) and Taylor et al., (1980) proposed that these two lithologies represent

silicate liquid immiscibility pairs, generated when a melt spontaneously separates into Si-rich and Fe-rich liquids after extreme fractional crystallization of a KREEP-basaltic parent magma. Grain sizes are similar to the small felsite clasts found in other samples. Sample 12013 described in Quick et al., (1977), which consists of dark, Fe-rich patches and light Si-rich patches, might also represent a silicate liquid immiscibility pair. However, it is shock-melted and none of its original texture has been preserved (Quick et al., 1977). Felsite 12033,507 (Warren et al. 1987) is the only sample with intermediate FeO (7.6wt%) we have studied so far. It is a rapidly crystallized shock melt, but contains regions of apparently unmelted residues, which are graphic intergrowths of quartz and K-feldspar. The clast also contains fayalitic olivine and Fe-rich glass, suggesting that it could be a mixture of high-Si and high-Fe immiscible melts.

Felsite enclaves in quartz monzodiorites (QMDs). Like the felsites, the quartz monzodiorites are also produced through fractional crystallization of KREEP-basaltic magmas, and represent the magma intermediate between felsites and KREEP basalts (Ryder et al., 1975, Irving, 1977, Ryder and Martinez 1991). They contain more mafic material than the felsites, including exsolved pyroxenes, which indicates they formed in slow-cooled, intrusive environments (Ryder et al., 1975, Ryder and Martinez, 1991, Jolliff 1991, Jolliff et al, 1999). The QMDs also contain areas of silica and K-feldspar intergrowth, with felsite-like textures. However, the silica polymorph in the QMD samples studied here (14161,7373 and 14161,7069) is ambiguous. It appears largely amorphous, giving a broad Raman signal with no distinctive peaks. Jolliff et al., (1999) reports the presence of quartz, cristobalite, and amorphous silica, which should not be present in a slowly cooled, intrusive sample, and could thus represent a shock feature. Silica in 14161,7069 has a distinctive hackled texture not seen in the felsites, which could indicate transformation from one silica polymorph to another (Fig. 2.5. Jolliff et al., 1999, Seddio et al, 2013).

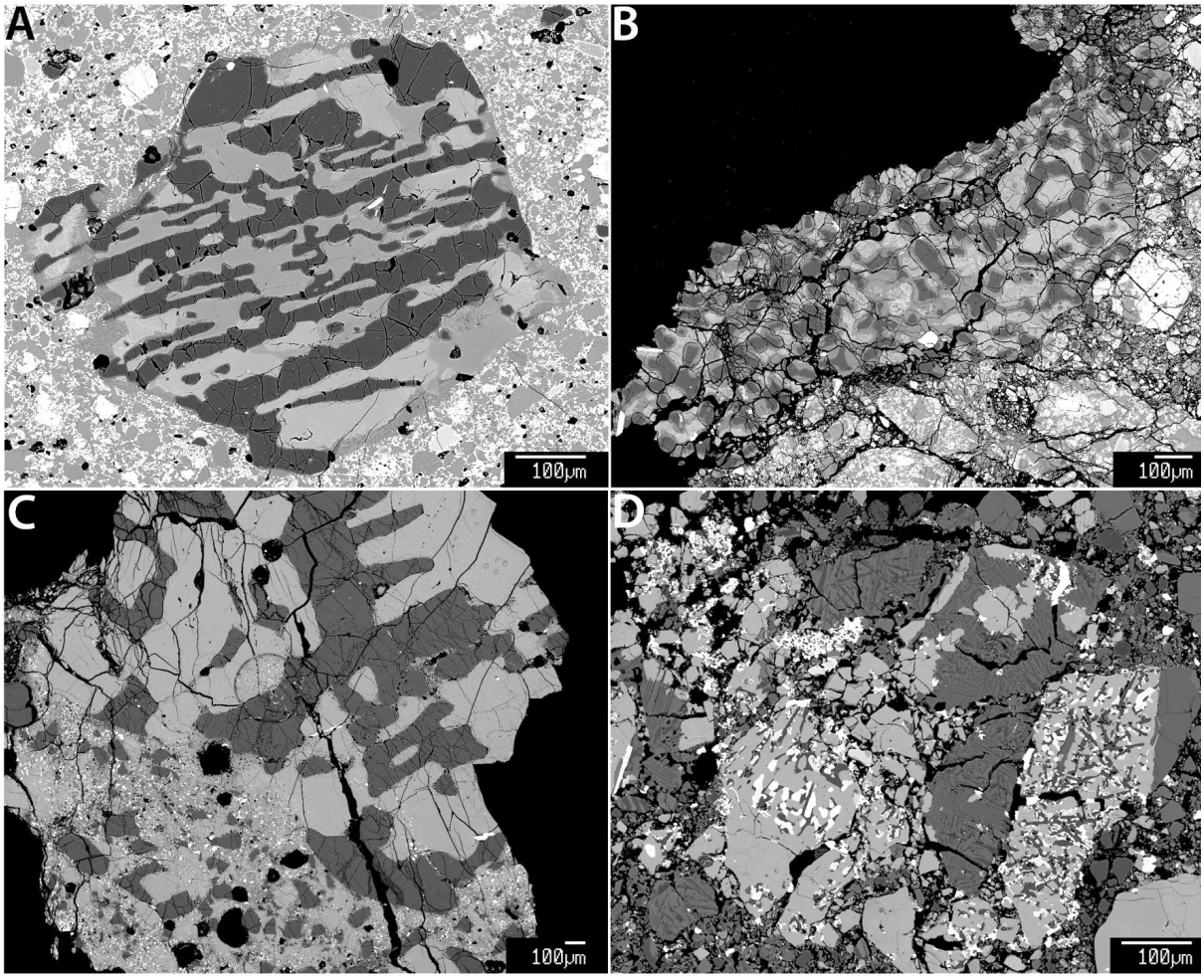

Figure 2.2. Representative BSE images of felsites illustrating the variety of observed textures. All felsite samples studied here exhibit the characteristic graphic intergrowth of quartz (dark gray) and K-feldspar (lighter gray). (A) Felsite clast in breccia 72215,180. (B) Felsite clast in 14305,102. (C) Felsite fragment in 14321,1047, the largest identified felsite. Note the coarse grain size and impact breccia around the edge of the felsite area. (D) Felsite-ferrobasalt silicate liquid immiscibility pair in unique sample 77538,16. The darker barred areas (felsites) are intergrown quartz and K-feldspar, while the brighter areas (ferrobasalts) are fayalite and augite, with ilmenite and FeS, as well as remnant silica glass (darkest gray).

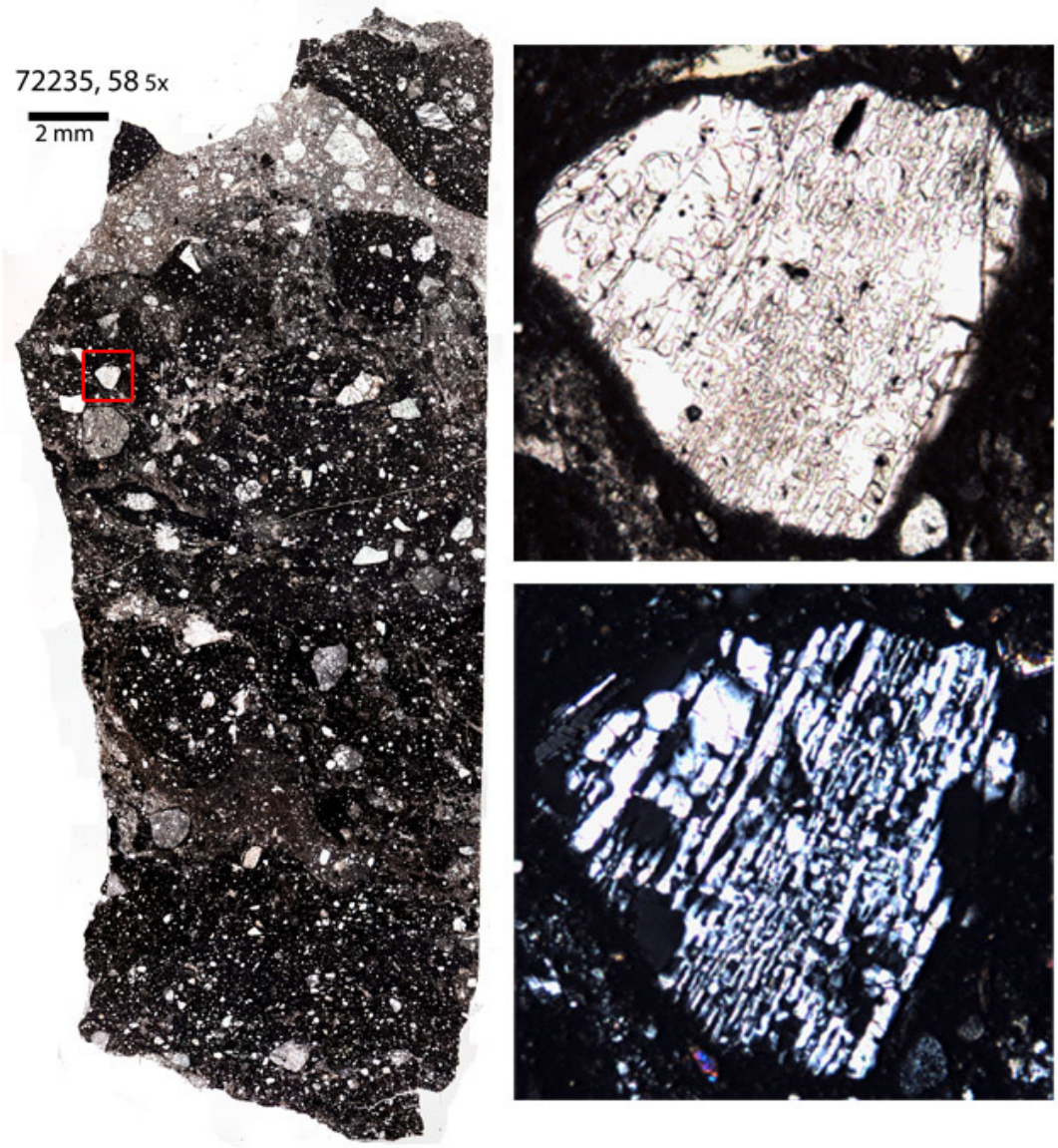

Figure 2.3. Optical images of a small felsite clast in breccia. A) Aphanitic impact melt breccia 72235,58 in plane polarized light. The felsite is located within the red box. Scale is 2 mm. B) Enlarged plane polarized light image of the felsite clast in breccia 72235,58. C) Cross polarized light image of the same felsites; note the intergrowth texture of quartz and K-feldspar.

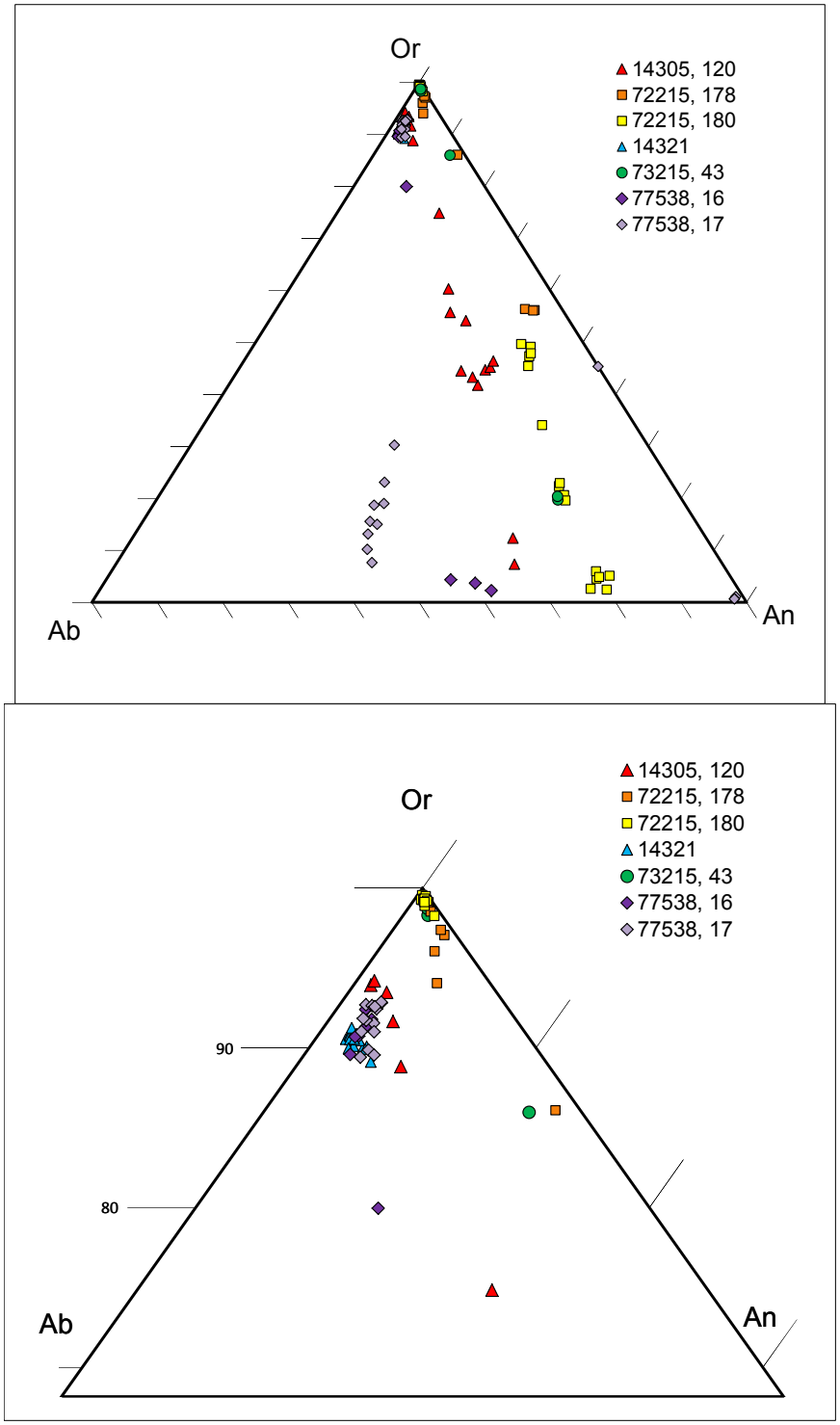

Figure 2.4. Feldspar compositions for selected felsites. Some felsites contain K-feldspar with unusual ternary compositions. Some also contain plagioclase feldspar.

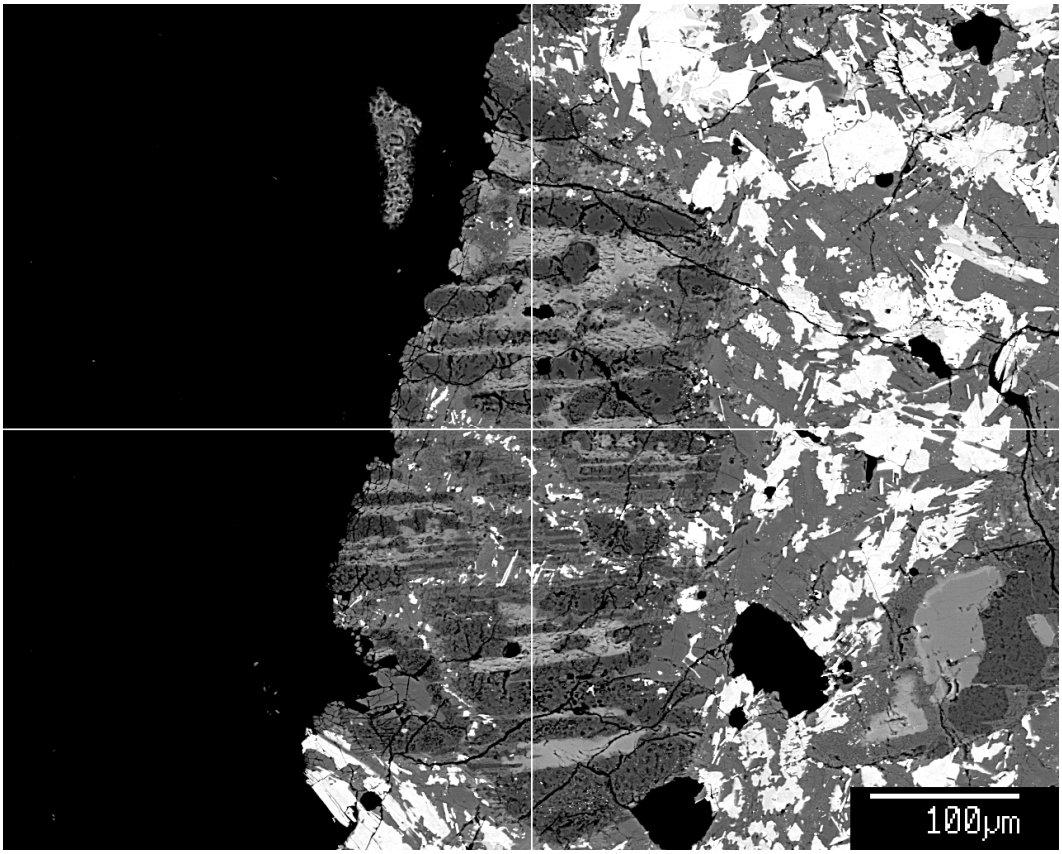

Figure 2.5. Felsite enclave in QMD 14161,7069. Quartz is the darkest gray, intergrown with lighter gray K-feldspar. Note the unusual hackled appearance of the quartz.

2.3.2. Ti concentrations in quartz.

Ti average abundances in felsite quartz are under 300 ppm except in one sample, 77538, which contains an average of 854 ppm (Table 2.2). Some points were discarded as they were found to be too close to ilmenite or other Ti-bearing phases (Figure 6). Sample 77538 contains by far the most Ti, with abundant ilmenite largely in the ferrobasalt coexisting with the felsite.

Table 2.2. Average Ti concentration in quartz for a representative group of felsites.

sample	Number of points	average ppm Ti	2-σ (ppm)	Temp (C)*
14321, 1047	4	213	7	930
73215, 43	4	264	7	960
14321, 1029	5	215	7	930
72215, 180	3	291	8	980
72215, 178	5	219	6	930
77538, 16	2	854	11	1200

*Equilibrium temperature calculated using TitaniQ (Wark and Watson, 2006).

When formation temperatures were calculated using the TitaniQ geothermometer (Eq. 2.2, Wark and Watson 2006), samples 14321, 73215, and 72215 gave temperatures 930-980 ºC (Table 2.2). These are well below the experimentally determined the silicate liquid immiscibility temperature range for KREEP basalts, 1014-1050 ºC (Hess et al., 1975, Hess et al., 1978, Hess et al., 1989), indicating some sub-solidus equilibration in these felsites, which we quantify below. The most Ti-rich sample, 77538, gave a temperature of ~1200 ºC, which is higher than the temperature at which silicate liquid immiscibility takes place in a fractionating KREEP basalt magma. In 77538, since quartz could not have formed at 1200 C, the high Ti abundance in its quartz actually reflects elemental partitioning from the 77538 parent melt into forming quartz. Using a literature distribution coefficient of 0.038 for Ti for quartz (Nash and Crecraft 1985), we calculated the Ti abundance of the felsite parent melt, 2.2 wt.%. The calculated Ti abundances of the 77538 parent melt is consistent with published analyses of melt Ti in both felsite and ferrobasalt melts formed during silicate liquid immiscibility experiments on KREEP basalts (2.4 wt.%, Hess et al. 1978, Rutherford et al. 1980).

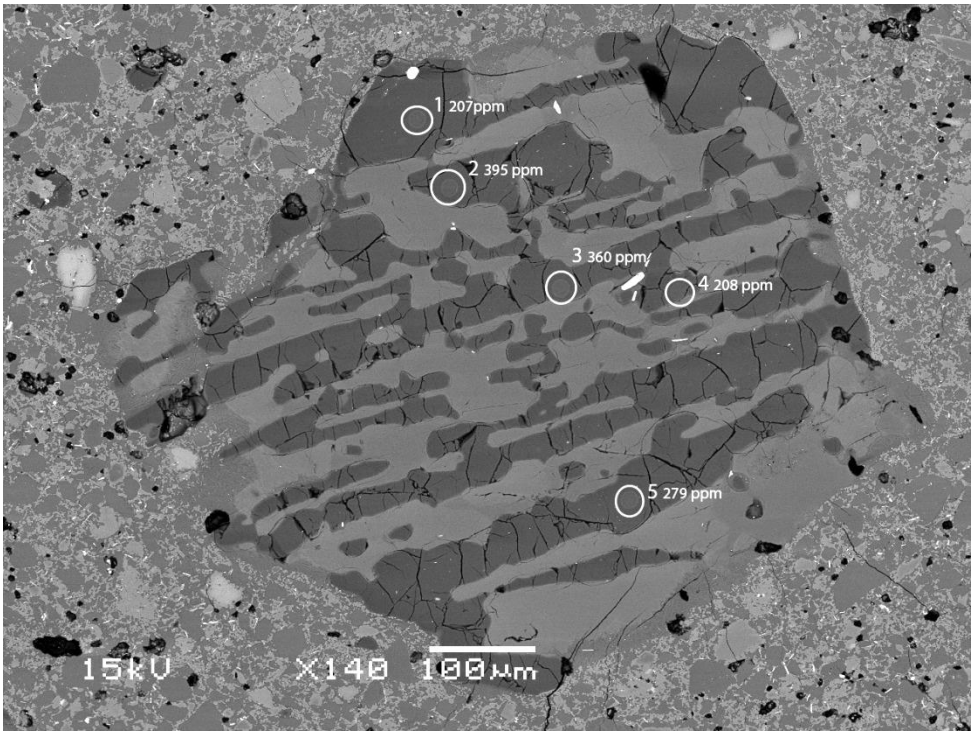

Figure 2.6. BSE image of felsite 1, 72215,180. White circles outline damage from the high current EMPA beam used for Ti analyses, while the numbers indicate the amount of Ti measured at those points. Points 3 and 4, closest to the bright white ilmenite grain, were discarded due to their proximity to the ilmenite.

2.4: Discussion: Thermometry, Cooling Rates, and Physical Setting for Felsite Formation

The magmatic fractionation leading to silicate liquid immiscibility would take place in an intrusive environment. Extrusive rocks, such as rhyolite flows, are more likely to contain cristobalite or tridymite, although quartz crystallized at depth could also be present. The presence of only quartz in felsites suggests that they are intrusive, consistent with their formation by fractionation of a KREEP basalt magma via silicate liquid immiscibility. Most importantly, the presence of quartz allows us to constrain the pressure (and therefore depth) of the intrusion by way of the silica phase diagram. Using Ti thermometry, quartz closure temperatures, and estimates of cooling rates, we can assess the size of felsite parental magma bodies.

Quartz in the graphic intergrowths in the felsites shows no textural evidence for transformation from tridymite or cristobalite, such as pervasive cracks developed due to the volume changes associated with the transformation. Although cracks are present in quartz in the felsites, they do not have the characteristic hackly texture found in quartz formed by transformation from tridymite (compare Figs. 2.5 and 2.6). This suggests that quartz might be a primary phase, and if so it could provide pressure information (Fig. 2.7), if we know the temperature of crystallization. During experiments on the crystallization of KREEP basalts (Hess et al., 1975, Hess et al., 1978, Hess et al., 1989), separation of high-Si and high-Fe melts took place at 1014 ºC (15386 starting composition), 1035 ºC (15382 starting composition), and 1050 ºC (14310 starting composition). We can therefore take this range as the felsite formation temperature, and assuming that quartz crystallizes promptly after the immiscibility takes place, we can consult the silica phase diagram to see where quartz (as the only silica phase present in the felsites) is stable. The range of 1014-1050 ºC is higher than the stability field for quartz at low pressure (Tuttle and Bowen, 1958). However, it is in the range for quartz crystallization at ~1 kbar (Figure 2.7). A magmatic intrusion with KREEP basaltic composition at a minimum of 0.85-1.05 kbar, could crystallize quartz directly (Figure 2.7). As pressure is related to crustal depth, and taking an average lunar crustal density of 2550 kg/m^3 (Wieczoreck et al., 2013), the felsites thus likely formed in small intrusions at least ~20-25 km deep.

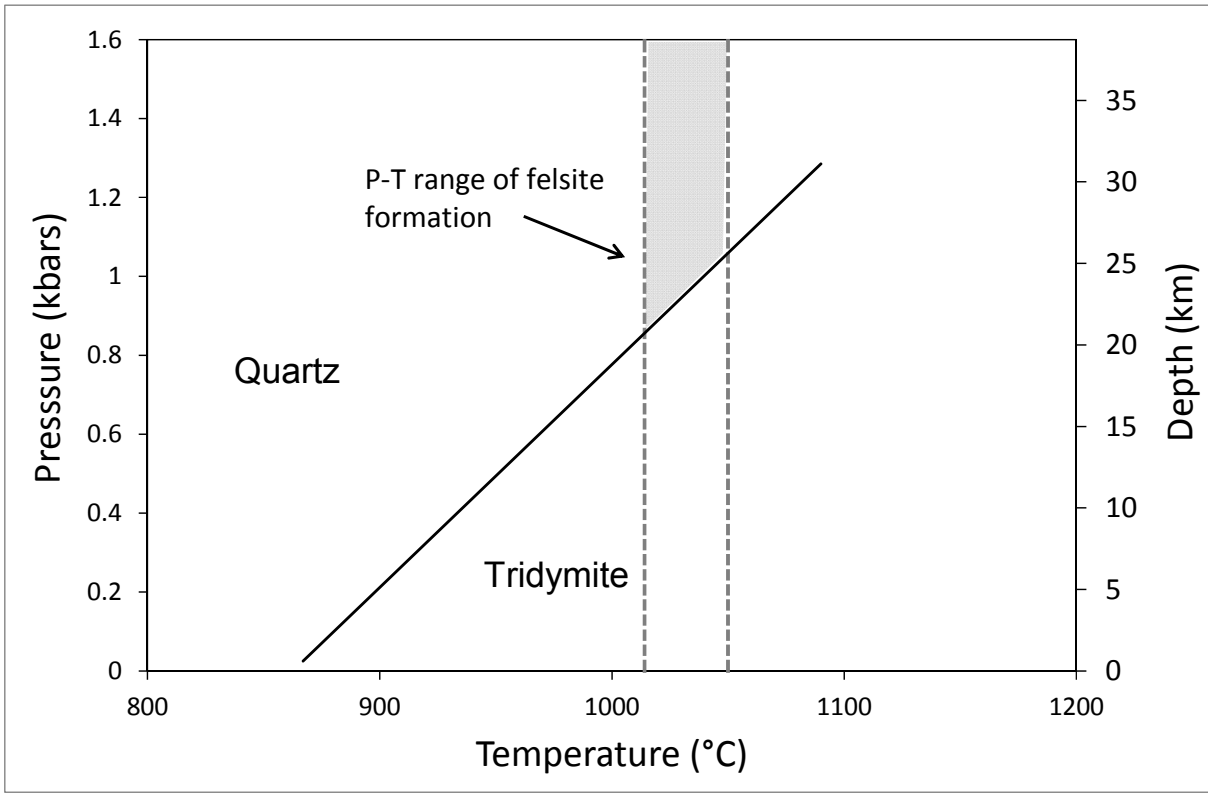

Figure 2.7. SiO_2 phase diagram showing the quartz-tridymite boundary between 800-1200ºC (Tuttle and Bowen, 1958). The shaded area represents the P-T range in which the felsites formed in order to crystallize quartz, based on the experimentally determined silicate liquid immiscibility temperatures for KREEP basalts 14310, 15382, and 15386 (Hess et al., 1975, Hess et al., 1978, Hess et al., 1989).

However, the depth of origin does not say anything about the size of the magmatic bodies that formed the felsites, though they must have been large enough to allow extensive fractional crystallization of magmas. We can use Ti in quartz thermometry and cooling rates to estimate the size of these parental intrusions. Our calculations for quartz-Ti thermometry yielded temperatures (Table 2.2) below the silicate liquid immiscibility temperature (1014-1050 ºC) in all but 77538, indicating there was some sub-solidus equilibration of Ti. In the felsite samples quartz-Ti thermometry can help constrain the size of the magmatic body from which each felsite originated. A magmatic intrusion crystallizes from the outside in as it cools, and this cooling rate is largely dependent on the size (width or diameter) of the intrusion. The closure temperature, the temperature at which Ti diffusion stops within a crystal, is also dependent on the cooling rate (Dodson 1973, eq. 2.3).

$$T_c = \frac{\frac{E}{R}}{\ln\left[\frac{GAT_c^2}{\frac{a^2 qE}{R}}\right]}$$

(eq. 2.3)

Equation 2.3 is one form of Dodson's equation. The closure temperature (T_c) is dependent on the cooling rate (q). Other terms include E=activation energy, A=pre-exponential factor in the diffusion coefficient, R=gas constant, a=grain radius, G=shape factor (which we assume is 27, for a cylinder, Zhang 2008). Diffusion data (providing E and A) have been measured experimentally and available from Cherniak et al. (2007).

We used Dodson's equation to calculate model Ti closure temperatures in quartz at several cooling rates and select grain sizes based on the grain sizes observed in the felsites (Figure 2.8). From the TitaniQ thermometry discussed above (Wark and Watson 2006), we know that the quartz crystals in the felsites studied here closed to diffusion between 930-980 ºC. The felsite cooling rate can then be estimated for a specific grain size, as it is constrained by the quartz closure temperature, by comparing the measured closure temperatures with the modeled closure temperatures (Figure 8). The parent intrusions for felsites in 72215, 14321, and 73215 would have crystallized at a rate between 0.2-100 K/yr.

Once a cooling rate has been determined for the felsite's parent intrusion, we can estimate the size of that intrusion (with some assumptions about emplacement details). Although the geometry of the magma bodies in which the felsites formed is not known, it is not unreasonable that they were roughly sill-like, so we used Equation 4-143 in Turcotte and Schubert (1982) to calculate the time to solidify a magmatic dike or sill. Eq. 2.4 shows that the solidification time, t_s, depends on the width and other thermal properties of the intrusion and country rock.

$$t_s = \frac{b^2}{4\kappa\lambda_2^2} \qquad \text{(eq. 2.4)}$$

where b is the half width of the intrusion and κ is the thermal diffusivity.

The constant λ_2 is defined by Eq. 2.5 (Turcotte and Schubert, 1982, 4-142):

$$\frac{L\sqrt{\pi}}{c(T_m - T_o)} = \frac{e^{-\lambda_2^2}}{\lambda_2(1 + erf\lambda_2)} \qquad \text{(eq. 2.5)}$$

where L is the latent heat of crystallization = 400 kJ/kg K, c =1 kJ/kg K (Turcotte and Schubert, 1982), T_m is the initial temperature of the melt and T_o is the temperature of the country rock.

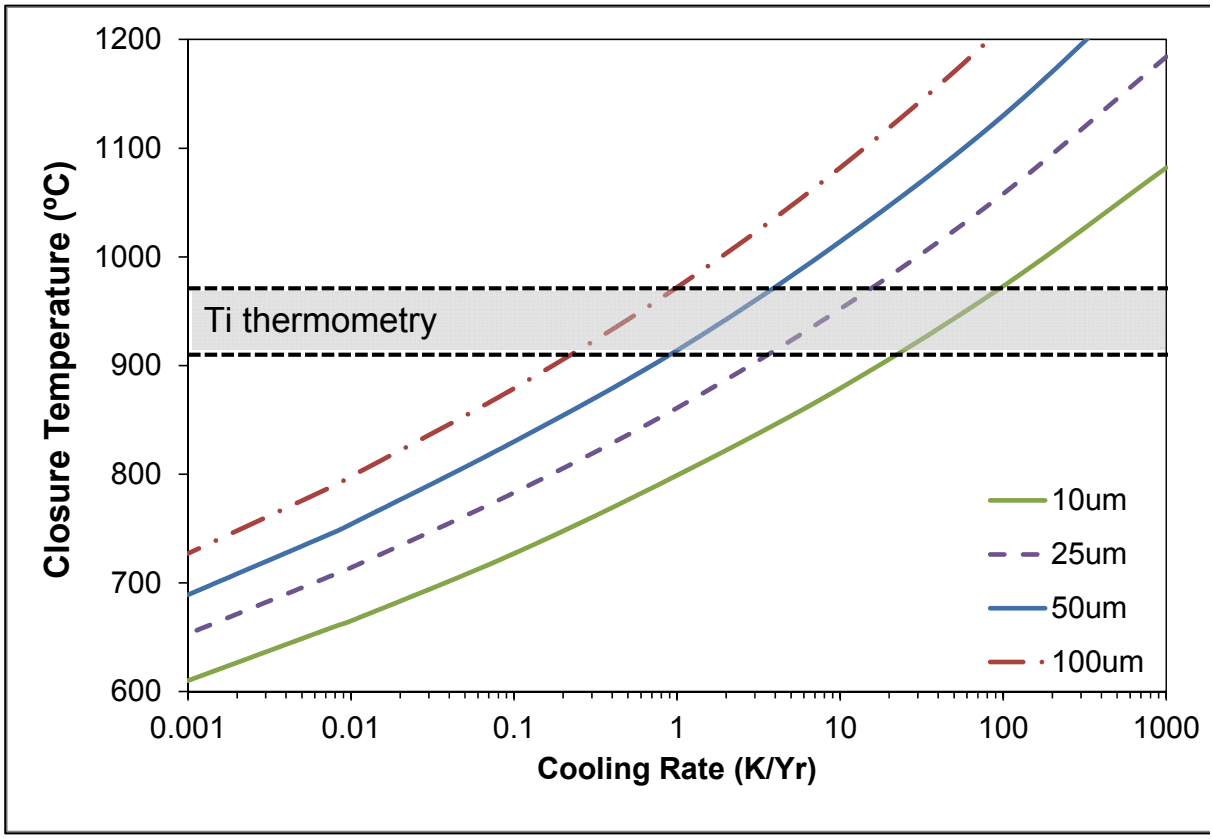

Figure 2.8. Felsite cooling rates based on Ti closure temperatures in quartz. Model closure temperatures were calculated for selected grain sizes at several cooling rates. The box labeled "Ti thermometry" shows the range of temperatures calculated from the TitaniQ geothermometer in felsites from 72215, 73215, and 14321. The cooling rate for a felsite with a given grain size will fall along the corresponding curve within in the gray box.

The initial temperature of the intrusion, a KREEP basaltic melt, is known from experimental petrology (1175 ºC, based on Hess et al., 1978), and we assume the temperature of the country rock at ~20 km depth to be 200 ºC. The calculation is not particularly sensitive to the temperature of the country rock; a T_o of 800ºC decreases the cooling rate by a factor of ~3. Once the solidification time for a given width is found, the average cooling rate for that dike can then be calculated:

$$CR = CI/t_s \quad \text{(eq. 2.6)}$$

where CR is the cooling rate, and CI is the temperature interval over which crystallization occurs, here taken to be 150 ºC. This provides an estimate of the average cooling rate in the center of a dike or sill of specified half width.

Once the cooling rates are known for a range of dike sizes, we can plot the cooling rate determined from the closure temperatures for Ti diffusion in quartz against the dike width to estimate the size of the felsite parent intrusions. Figure 2.9 shows the cooling rate versus dike half-width, with the cooling rates determined from the felsites outlined in two fields. Based on their cooling rates, the finer grained felsites in 72215, 73215, and 77538 likely formed in magmatic bodies 15-150 m wide (Fig. 2.9). Coarser-grained felsite 14321 formed in a larger intrusion about 300 m wide.

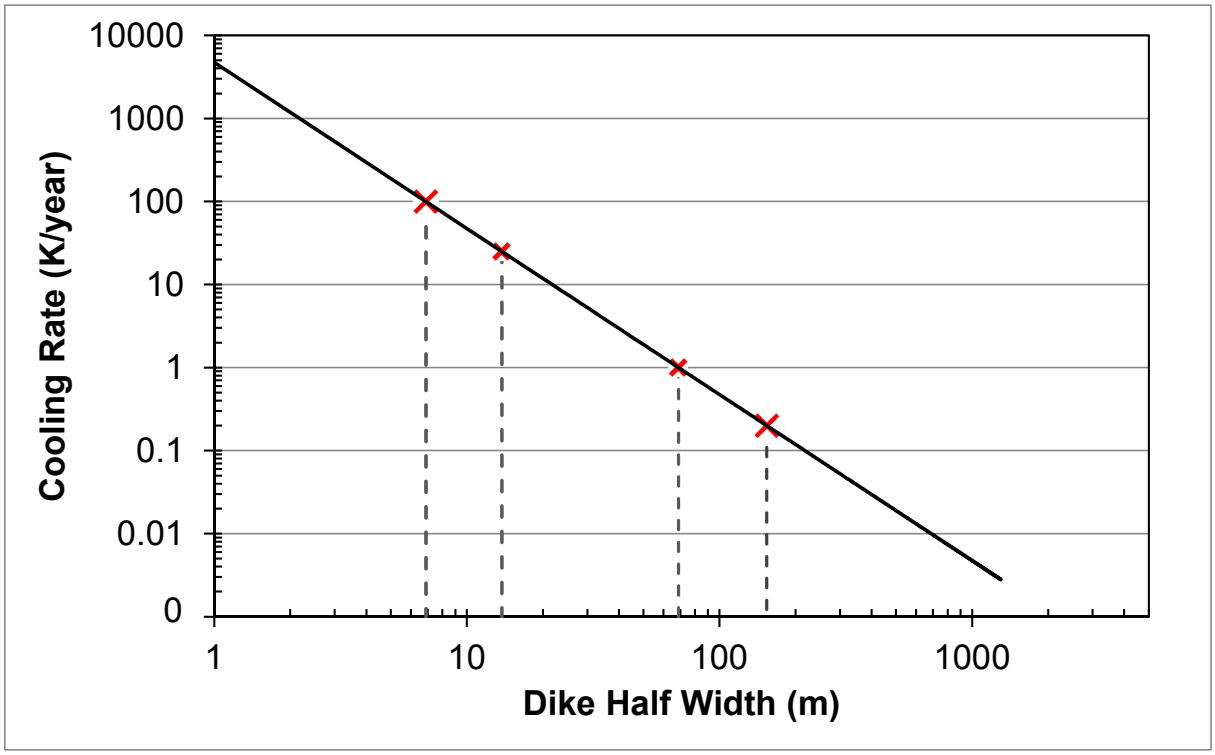

Figure 2.9. Calculation of felsite magmatic body size by calculated cooling rates. The crosses represent cooling rates calculated for selected widths (10, 25, 50, 100 μm) of felsite quartz observed in samples, including granophyric 14321 and fine-grained felsites from 73215 and 72215. The dashed lines then indicate the half-width of the dike.

These calculations show that the felsites studied here formed in small intrusions ~15-300 m wide, at ~20 km depth in the lunar crust. This supports petrographic observations (such as finely exsolved pyroxenes) that the felsites had an intrusive origin, and it provides quantitative estimates for the size and depth of formation of the felsite parental intrusions. The cooling rate, grain size, and dike size calculations plotted here might be useful for determining the depth and intrusion size for other felsites in the lunar sample collection.

However, this is only a small sampling of a relatively rare lithology on the Moon, and there is likely quite a bit of variation in intrusion size and burial depth among evolved, KREEP-related lithologies. For instance, quartz monzodiorite 14161,7373 contains quartz and relict cristobalite, and preserves a large-grained cumulate texture (Jolliff et al. 1999). Our Raman data for 14161,7373 also suggest a mixture of partly transformed quartz. This rock also contains exsolved, inverted pigeonite from which Jolliff et al. (1999) calculated a subsolidus cooling rate of 0.008ºC/y. The slow cooling seems inconsistent with the presence of cristobalite in addition to quartz. The cristobalite might reflect shock heating of the QMD clast, causing partial transformation of quartz to cristobalite, but still of sufficiently short duration to not alter the compositional zoning in pyroxene exsolution lamellae. Similar hackled textures in quartz in 14161,7373 are also seen in 14161,7069 (Jolliff 1991) and some Apollo 12 felsites (12033, discussed here, and 12032, Seddio et al., 2013), which could indicate a quartz-cristobalite inversion.

2.5. Implications for Silicic Domes

Many of the lunar red spots discussed above have long been associated with silicic volcanism on the Moon based on their rhyolite dome-like morphology (Head and McCord, 1978; Hawke et al., 2003; Wilson and Head, 2003) and more recently, their composition as determined from orbit (Hagerty et al., 2006, Glotch et al., 2010). While it is tempting to connect silicic lithologies in the lunar sample suite to the silicic domes observed from orbit (Glotch et al., 2010), the general intrusive character of the clasts we studied indicates that they are not samples of silicic domes, which ought to contain significant cristobalite or tridymite (e.g. the high-T silica polymorphs). The felsites studied here formed through silicate liquid immiscibility in relatively small, 15-300 m intrusions at depths around ~20 km in the lunar crust, while the silicic

domes are many km in size and were erupted onto the lunar surface. However, the felsites could be compositionally similar to the silicic domes, as they are very low in Fe and have evolved compositions (Hagerty et al., 2006, Glotch et al., 2010.)

The generation of silicic magma on the Moon has largely been attributed to silicate liquid immiscibility, but as silicate liquid immiscibility does not occur until the last 90-98% of crystallization (Roedder and Weiblen 1970, 1971), it seems impossible to generate a large enough volume of silicic magma to produce multi-km size domes (Hagerty et al. 2006). Intermediate compositions, such as quartz monzodiorites, are more voluminous in a fractionating KREEP basalt magma, but have FeO concentrations much larger than do the silicic domes, 13-18 wt.%, vs 4-7 wt.% in the domes. Basaltic underplating, in which a basaltic liquid near its liquidus temperature intrudes and partially melts existing crust, thus generating large quantities of rhyolitic melt, might be a better mechanism for producing the magma that formed the silicic domes (Hagerty et al., 2006). Underplating might also produce silicic magmas with appropriate Th and FeO content (4-8 wt. % FeO) (Hildreth 1981, Hagerty et al., 2006). We conclude that the felsites are not samples of the silicic domes, but that they are chemically similar to the dome lithology. The primary difference would be the silica phase in the dome lithology, at least on the surface accessible to orbital remote sensing, would be cristobalite or tridymite, consistent with an eruptive origin.

2.6. Implications for Retention of H species in Felsite Magmas

The intrusive origin of the felsites makes them ideal candidates to preserve magmatic water. The concentration of water in a magma is highly dependent on pressure; more water is soluble in a magma at higher pressure than at lower pressure (e.g. Dixon et al., 1995) Most of the lunar samples studied for water are erupted mare basalts, and Tartèse et al. (2013) showed that degassing can substantially alter the D/H ratio of water in a basalt by preferential H loss. The mare basalts were erupted into a low-pressure environment which favors water loss. The felsites were formed at depth and therefore pressure, which could have allowed them to avoid degassing, as water may have still been soluble in the melt.

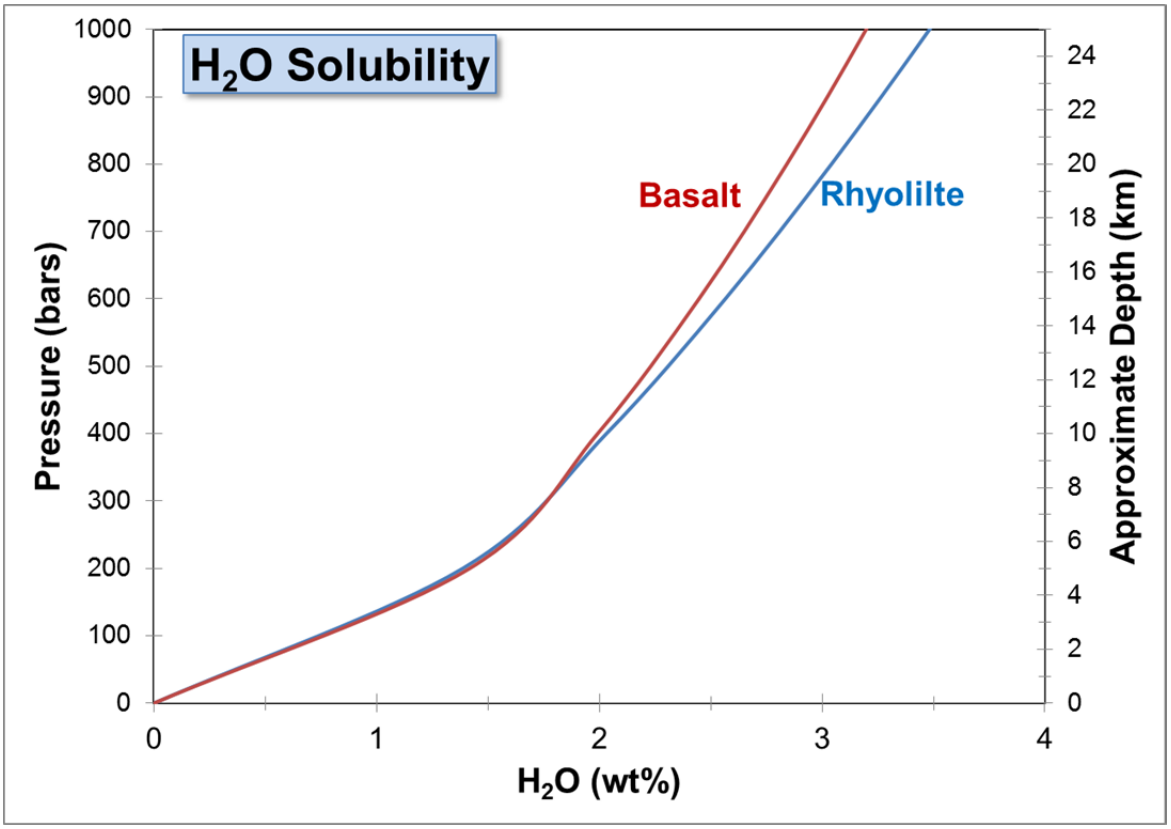

Figure 2.10. Curves showing the relationship between solubility of water in basaltic and rhyolitic magmas, and pressure (with approximate depth in the Moon shown on the right axis). (VolatileCalc, Newman and Lowenstern 2002)

Degassing almost certainly would have happened in even a thick lava flow, but our calculations and petrologic observations indicate the felsites are intrusive, originating at ~20 km depth. H_2O solubility in basalts (and rhyolite, which is chemically similar to the felsites) increases with pressure (Fig. 2.10). We used the program VolatileCalc (Newman and Lowenstern, 2002) to estimate how much water would be soluble in basaltic and rhyolitic melts at various pressures and their corresponding depths on the Moon. These curves are plotted on Figure 2.10. Over 1 wt.% H_2O is soluble in rhyolite at 2-4 km depth on the Moon, which is substantially shallower than the felsite origin depth. Water solubility at 1 kb, the possible felsite formation pressure based on the presence of quartz at the felsite formation temperature, is over 3 wt.%. It is extremely unlikely that any lunar magma contained that much water, as no hydrous phases indicative of such high water content like amphibole or mica have ever been identified in lunar samples.

We conclude that H_2O was not lost from the felsite parent magmas and, therefore, the D/H ratio was not fractionated by outgassing. Thus, the D/H of the felsites and other intrusive samples such as the quartz monzodiorites might be closer to that of the bulk Moon than that of erupted, degassed basalts, making them ideal candidates for determining the source of the Moon's water. We thoroughly assess this idea in Chapter 3 of this dissertation.

2.7. Conclusions

We conclude that the felsites are not samples of the silicic domes detected from lunar orbit. The presence of quartz in the felsites, along with thermal data from Ti measurements of the quartz, suggests that the felsites formed at a minimum depth of ~20-25 km in the lunar crust, in magmatic bodies 15-300 m wide as late-stage fractionation products of a melt with KREEP basalt composition. Since the felsites formed intrusively and at moderate pressure, they are good candidates for D/H measurements of their apatite grains. Water would have been soluble in the melt at the depth/pressure the felsites formed, which means hydrogen isotope fractionation due to degassing of the melt likely did not occur.

CHAPTER 3: WATER IN EVOLVED LUNAR ROCKS: EVIDENCE FOR MULTIPLE RESERVOIRS

In preparation for publication in *Geochimica et Cosmochimica Acta* as Robinson, K.L., Barnes, J.J., Nagashima, K., Thomen, A., Franchi, I.A., Huss, G.R., Anand, M., and Taylor, G.J. Water in evolved lunar rocks: Evidence for multiple reservoirs.

Abstract.

We have measured apatite in several KREEP-rich lithologies, including felsites, quartz monzodiorites (QMDs), a troctolite, and an alkali anorthosite. Apatite in all of these intrusive rocks contains < 267 ppm H_2O, which is quite low compared to the majority of studied mare basalts (200 to ~6500+ ppm H_2O). Unless degassing occurred before apatite formation and given similar contents of F and Cl in their parent melts, the KREEP-rich parent magmas to the felsites, QMDs, alkali anorthosite, and troctolite contained substantially less water than the mare basalts. However, degassing was less likely to have occurred in intrusive lithologies, as they formed at pressures great enough that water was soluble in the melt during crystallization. Additional measurements of residual glass in a KREEP basalt independently show that the KREEP basaltic magmas were low in water, and that the source of 15358 contained ~10ppm H_2O. This is an order of magnitude lower than the source of the Apollo 17 pyroclastic glass beads. The H-isotope data from apatite provide additional evidence for multiple H reservoirs in the lunar interior. Apatite measurements from some KREEP-rich intrusive rocks are moderately elevated in D, while others fall into the δD range of the terrestrial upper mantle. Apatite in quartz monzodiorite 15403,71 has the lowest apatite δDs measured from the Moon (-749‰) so far, and could potentially represent a low D reservoir in the lunar interior.

3.1. Introduction

The detection of water in lunar volcanic glasses, apatites, and melt inclusions has implications for planetary accretion, the source of water to the Earth-Moon system, and the role of water in lunar evolution (Saal et al., 2008; McCubbin et al., 2010a; Boyce et al., 2010; Greenwood et al., 2011; Hauri et al., 2011; Tartèse et al., 2013, 2014; Barnes et al., 2013, 2014). Recent work shows that apatites in mare basalts are richer in water than previously thought, and

generally are enriched in deuterium (^{2}H, or D) with respect to Earth, possibly due to the addition of D-rich material early in the Moon's history (Greenwood et al., 2011) or to the loss of H preferentially to D during degassing (e.g., Tartèse et al, 2013). As the final fractionate of the global lunar magma ocean, the KREEP component, so named for its enrichment in K, Rare Earth Elements, and P (e.g., Warren and Wasson 1979) is highly enriched in incompatible elements compared to other lunar materials. Because water behaves like an incompatible element (Koga et al., 2003; Aubaud et al., 2004; Grant et al. 2007) , KREEP-rich rocks ought to be enriched in water relative to other lunar rocks. Many KREEP-rich lithologies consist of evolved compositions that formed intrusively, which means they (unlike mare basalts) would have avoided or at least minimized water loss and potential hydrogen isotope fractionation due to magmatic degassing. This makes them attractive samples for studying water in the lunar interior as they should be water-rich, and they may possess a more representative isotopic composition of lunar interior water than degassed samples such as the mare basalts or pyroclastic beads.

The mineral apatite [$Ca_5(PO_4)_3(F,Cl,OH)$] incorporates water as OH into its crystal structure, making it a potential recorder of the concentration of OH in magma at the time of apatite crystallization. The OH in apatite is resistant to exchanging O or H with adsorbed terrestrial water on thin section surfaces (Greenwood et al., 2011), hence it is useful for H isotopic measurements by secondary ion mass spectrometry (SIMS). The D/H ratio, expressed as δD (‰) = $([D/H]_{sample}/[D/H]_{standard} - 1) \times 1000$, relative to Vienna Standard Mean Ocean Water (V-SMOW), is important for identifying the source of the Moon's water and the extent of water loss during magmatic processing (Greenwood et al., 2011; Elkins-Tanton and Grove, 2011, Tartèse et al., 2013). Previous studies have hinted that the water content of lunar apatite varies by rock type. Apatites in mare basalts have the highest H_2O content (up to ~0.8wt.%) and D/H ratios (+390 to +1100‰) (McCubbin et al., 2010a; Greenwoood et al., 2011; Barnes et al., 2013, Tartèse et al., 2014) , while apatites in many more evolved, KREEP-related rocks have very little H_2O (<0.03wt%) and lower D/H values (+231 to +791‰, Robinson et al., 2013, Robinson and Taylor, 2014). However, the degree of water loss from the mare basalts during and after eruption appears to have been substantial (Tartèse et al., 2013).

Though it was initially thought that apatite water contents could be used to infer initial magmatic water abundances (McCubbin et al., 2010a; Boyce et al., 2010; Tartèse et al, 2013, 2014; Barnes et al. 2014), Boyce et al. (2014) demonstrated that the F-Cl-OH partitioning into apatite is not well-described by a simple apatite-melt partition coefficient. Apatite water contents thus cannot be used to quantitatively determine the amount of water in a magma, but the D/H ratios are still valid and useful.

Rocks formed intrusively could minimize D-H fractionation and water loss because they form at pressures where water is far more soluble in silicate melt than at low pressures near or on the surface (e.g., Dixon et al., 1995). Water solubility in magmas decreases with decreasing pressure, so when a hydrous magma approaches a planetary surface, the melt degasses and water is lost. Diffusion modelling of water loss from volcanic lunar pyroclastic glasses indicates that they lost up to 98% of their initial water content (Saal et al., 2008). Mare basalts would also have degassed during eruption onto the lunar surface, and low-Ti mare basalts could have lost 85 to 99% of their pre-eruptive water contents (Tartèse et al., 2013). The degassing of hydrogen from a magma or lava also fractionates lighter H from heavier D, especially if H_2 is lost rather than H_2O. The erupted mare basalts have the highest δD values (up to ~1100‰) found in lunar rocks so far (Greenwood et al., 2011; Barnes et al., 2013; Tartèse et al., 2013). Apatite in intrusive rocks may thus represent a less modified sampling of the lunar interior water than the water bound in mare basalt apatites (Robinson et al., 2013, Robinson and Taylor 2014, Barnes et al., 2014).

If water was present in the lunar magma ocean, it should be highly concentrated in KREEP-rich materials, assuming no significant loss during magma ocean crystallization and subsequent cumulate overturn (Tartèse et al., 2014). Anything KREEP-rich or derived from KREEP basaltic magmas should also be enriched in water, although it is not a simple path from late-stage magma ocean products to KREEP-rich secondary magmas. KREEP-related magmas formed by either assimilation of the KREEP component by rising magnesian magmas, or by partial melting of hybrid mantle sources formed by sinking KREEP (and other dense components such as ilmenite-clinopyroxene cumulates) mixing with magnesian olivine-orthopyroxene cumulates (Shearer and Floss, 1999; Shearer and Papike, 2005; Elardo et al, 2011). These magmas gave rise to KREEP basalts and the norites and troctolites of the Mg-suite. Fractional crystallization of

magmas resembling KREEP basalts led to evolved rocks such as quartz monzodiorites, even involving silicate liquid immiscibility in the case of felsites (e.g., Snyder et al., 1995; Ryder and Martinez, 1991). Most importantly, all this petrologic processing took place inside the Moon at pressures high enough to inhibit water loss from magmas or mantle rocks.

3.2. Samples

The felsites and quartz monzodiorites (QMDs) are both intrusive late-stage fractionates of KREEP-basaltic magmas (Ryder et al., 1975; Ryder and Martinez, 1991). The felsite suite consists of evolved Si-rich (~70wt% SiO_2) rocks with graphic intergrowths of quartz and K-feldspar (Robinson and Taylor, 2011). Silica-rich compositions can be generated by partial melting, but extensive fractional crystallization also produces silica-rich melt through the process of silicate liquid immiscibility (e.g. Rutherford et al., 1974). After 90-98% crystallization of a basaltic magma, the remaining liquid will spontaneously separate into Si-rich and Fe-rich liquids (Roedder and Weiblen, 1971, Hess et al., 1975). The Si-rich end member is called felsite, while the Fe-rich end member is called ferrobasalt (Rutherford et al., 1974). Based on felsite texture and the presence of quartz rather than another silica polymorph, Robinson and Taylor (2011) argued that the felsites and their corresponding Fe-rich phases formed in small intrusive bodies through silicate liquid immiscibility of an evolving magma of KREEP-basalt composition.

Felsite sample 14321,1047 is well-known (Warren et al., 1983), consisting of clasts of graphically-intergrown quartz and K-feldspar in impact breccia 14321 (Fig. 3.1a). Sample 77538,16 is unique in that it preserves both silicate liquid immiscibility end-members in co-existing felsite and ferrobasalt areas (Warner et al. 1978; Fig. 3.1b). We found apatite in both the Si-rich and Fe-rich end members; it is enclosed in clinopyroxene in the Fe-rich regions and in quartz in the Si-rich portions, suggesting that it was a liquidus phase.

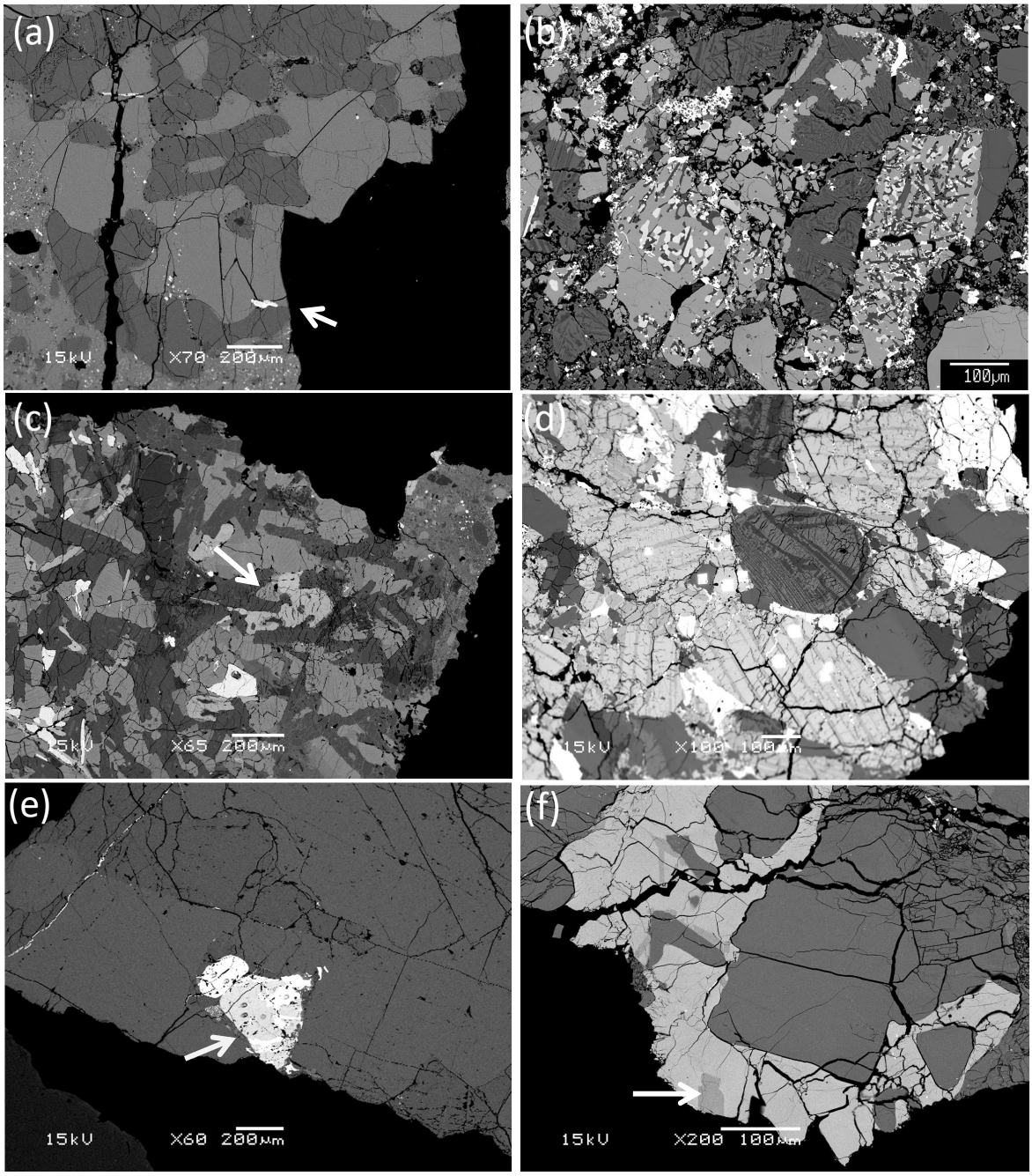

Figure 3.1. Representative backscattered electron (BSE) images of samples described in this work. Apatites are denoted by arrows. (a) Graphic intergrowth of quartz (dark gray) and K-feldspar (light gray) in 14321,1047. (b) Felsite-ferrobasalt SLI pair in 77538,16. Darker intergrowth is quartz and K-feldspar, while the bright areas are Fe-rich olivine, pyroxene, and amorphous silica. Fe-Ni metal and ilmenite are also present. (c) Portion of QMD15404,55. (d) Portion of QMD14161,7373. The exsolved phase is inverted pigeonite, while the brightest phase is whitlockite. The bleb near the center of the image is intergrown silica and K-feldspar. Bright squares are ion microprobe analysis pits. (e) Apatite-whitlockite intergrowth surrounded by plagioclase in troctolite 76353,56. The darkest phase is olivine. Note the large grain size. (f) Apatite-whitlockite intergrowth in an alkali anorthosite clast in breccia 14305,656. The bright gray is whitlockite, the darker intergrowths are apatite. Darkest gray is plagioclase.

The quartz monzodiorites (QMDs) are similarly evolved rocks. They exhibit a cumulate texture and are probably fractional crystallization products of KREEP basalts (Ryder and Martinez, 1991; Jolliff 1991), though not quite as extreme fractionates as the felsites. Many have exsolved pyroxenes, indicating they formed in a slow-cooling, intrusive environment. Both 14161,7069 (fig. 3.1d) and -,7373 were classified as QMDs (Jolliff 1991). Section 14161,7373 is particularly notable for its inverted, exsolved pyroxenes and high phosphate content, mostly in the form of whitlockite (Jolliff 1991); strictly speaking, this anhydrous phosphate is more properly called merrillite (Hughes et al., 2008). In a strict chemical sense the quartz monzodiorites are probably more accurately described as monzogabbros, but we use monzodiorites here to maintain consistency with previously published literature.

We studied three QMDs from soil sample 15400, which was likely derived from the large boulder (sampled as 15405) on top of which it was found. Sample 15403,71 is a single fragment from the 2-4mm fraction of 15400. It is roughly half impact melt and half shocked QMD. The QMD contains large phosphates, including a single >500μm apatite grain. Sample 15404,51 and ,-55 come from the 4-10mm size fraction. Apatite in QMD 15404, 51 was studied previously by McCubbin et al., 2010a. Sample 15404, 55 (Fig. 3.1c) is also a QMD, from the same chip and lithology as 15404, 51. Pyroxene in all three A15 sections is finely exsolved, indicating an intrusive origin, and the samples' enrichment in rare earth elements relative to Apollo 15 KREEP basalt shows it probably formed via fractional crystallization of an Apollo 15 KREEP-like basalt.

Alkali anorthosite clasts we studied are found in breccia 14305,656 (Fig. 3.1f). The alkali anorthosites are also products of fractional crystallization of a KREEP-rich basaltic magma, thought to form as flotation cumulates in intrusive magma bodies (Shervais and McGee, 1999). Whitlockite was reported in other alkali anorthosite sections of 14305 (Shervais and McGee, 1999), and this section seems to be particularly rich in whitlockite. Apatite is intergrown with whitlockite in 14305,656.

Troctolite 76535 is coarse-grained and shows signs of slow subsolidus annealing, leading to the interpretation that it could have formed at a depth of tens of kilometers in the crust, significantly inhibiting water loss (Gooley et al., 1974; Dymek et al., 1975; Schwartz and

McCallum, 1999). We measured apatites in two sections, 76535,52 and -,56 (Fig. 3.1e). It is not directly derived from KREEP basalt like the felsites or QMDs, but it has a high KREEP content as revealed by trace element analyses of mineral grains (Shearer and Floss, 1999). However, 76535 could have been affected by metasomatism (Elardo et al. 2012). The intrusive origin of the felsites, quartz monzodiorites, and troctolite suggests that they probably did not lose water through degassing, hence did not fractionate their D/H ratio in the process of degassing, and their KREEP-rich source magmas imply they could be some of the most water-rich lunar rocks.

We also examined two KREEP basalt fragments in impact melt breccia 15358,6 as a comparison with the KREEP-derived rocks. These KREEP basalts have intersertal to intergranular textures and abundant yellow glass that is interpreted to be the last 11-18% of a KREEP basaltic melt, which quenched instead of crystallizing (Ryder 1988, Taylor et al. 2012). Apatite large enough for SIMS analysis was not identified in either fragment, but we measured H and D in the glass.

3.3. Methods

3.3.1. Secondary Ion Mass Spectrometry (SIMS) protocols.

3.3.1.1. University of Hawaii (UH). Our protocol for measuring H isotopes in apatite was developed for use with both martian and lunar materials. Hallis et al. (2012) and supplemental materials also detail the UH protocol described here. Lunar apatites were analyzed in situ with the UH ims 1280 secondary-ion mass spectrometer in four separate rounds of measurements in May and November 2011, August 2012, and July 2014. We used a 2 nA Cs^+ primary beam (4 nA in August 2012) accelerated to 10keV. The secondary-ion mass spectrometer was operated at 10 keV (giving a 20 keV impact energy) with a 50 eV energy window. The mass resolving power was ~1900, sufficient to separate any interfering molecules. A normal-incidence electron flood gun was used for charge compensation of the analyzed area.

Using a rastered beam, a 25 × 25 μm^2 area was sputtered for 300 s to remove the carbon coat and any surface contaminants before the actual measurement took place. During the presputtering, we monitored the H ion image to avoid possible terrestrial contamination. In the H ion image, H-rich material such as epoxy or small cracks appears very bright. The beam was then repositioned (when possible) to avoid H-rich areas. The measurement was aborted if no

"clean" area could be identified. $^{1}H^{-}$, $^{2}D^{-}$, and $^{18}O^{-}$ were then measured sequentially on an electron multiplier in monocollection mode from a reduced rastered area of 15 x 15 μm^2. For glass measurements, we collected $^{30}Si^{-}$, instead of $^{18}O^{-}$. An electronic gate was used to exclude counts from all but the inner ~8 x 8 μm^2 of this area to avoid the edges of the sputtered pit and H creep across the sample surface. If contamination appeared during the course of a measurement, the affected cycles were eliminated during data reduction.

Each measurement consisted of 40 cycles. ^{1}H was counted for 3 s, D for 40 s, and ^{18}O (or ^{30}Si for glasses) for 2 s in each cycle. The primary beam was blanked for the first 10 and final 5 cycles in order to measure background H and D signals (mainly contributed by the electron gun). The background counts were subtracted from the measured isotope signal, which was collected between cycles 11 and 35 while the beam was positioned on the sample. We made appropriate corrections in data analysis to account for the electronic gate and deadtime of the electron multiplier (Hallis et al., 2012).

Hydrogen isotopes of lunar glasses were measured on the same instrument in March 2012 using the same conditions, with a single difference. After measuring the first few sets of apatites, we found that increasing the primary beam current from 2 nA to 4 nA resulted in ~10x decrease in the detection limit. The KREEP basalt glasses were measured at 4 nA current, but all other analytical conditions (presputtering time, raster sizes, counting times) were the same as for the apatite measurements.

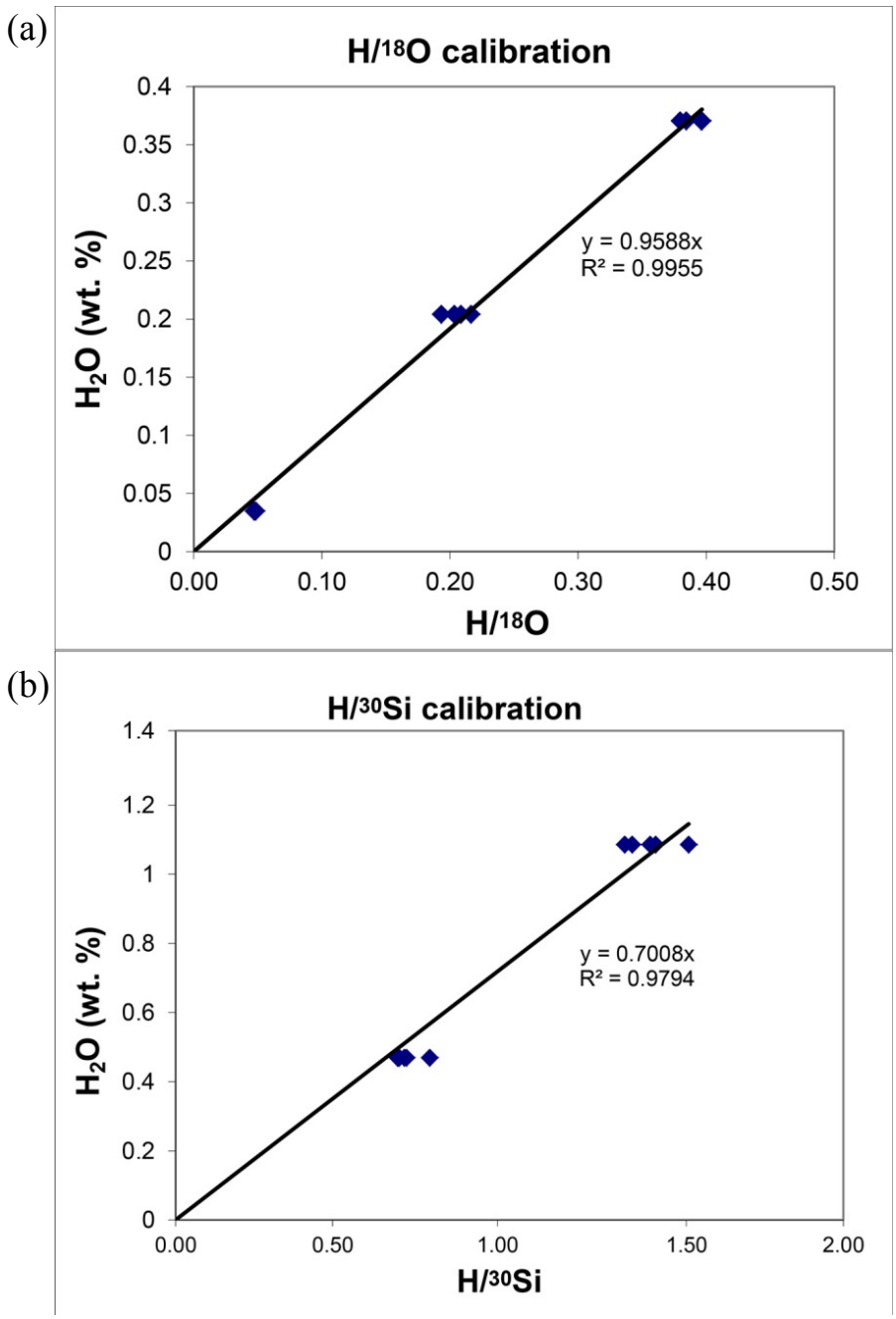

Figure 3.2. Sample calibration curves for ims-1280 analysis. (a) Calibration curve for H_2O in apatite and (b) calibration curve for H_2O in basaltic glass. Similar calibration curves were used to calibrate NanoSIMS data.

The SIMS measurements were calibrated prior to lunar apatite measurements using 3 natural terrestrial apatites provided by F. M. McCubbin (University of New Mexico). The apatite standards were characterized by continuous-flow mass spectrometry and are described in McCubbin et al. (2012). We originally received 5 apatite standards, but over the course of our measurements, we found that the three best behaved were Ap003 Durango, Ap018 Russia, and Ap005 Crystal Lode. Ap018 and Ap005 were also used for instrumental fractionation correction of measured D/H ratios. H_2O content of lunar apatite samples was determined from their measured $^{1}H/^{18}O$ ratios and a calibration curve of H_2O (wt.%) vs. $^{1}H/^{18}O$ determined using the 3 apatite standards with different H_2O abundances (Fig. 3.2a). The curve was forced through the origin as in McCubbin et al. (2012).

For the KREEP glass measurements, we used two basaltic glass standards (D52-5 and D51-3) with published D/H ratios (Hauri et al., 2002). The H_2O contents of our specific pieces of these two standards were determined by Rhea Workman using FTIR at Caltech. H_2O content of KREEP glass was calculated using a similar calibration curve (Fig. 3.2b) for H_2O (wt.%) vs. $^{1}H/^{30}Si$. That curve was also forced through the origin. The reported errors on water contents and δD values include both the internal precision of an individual analysis and the external reproducibility (standard deviation) for standard measurements during a given analytical session.

The detection limit for H_2O content was estimated by measuring anhydrous minerals such as olivine and pyroxene present in the same sections, and San Carlos olivine standard in a separate mount. Samples were stored in a 60 °C vacuum oven to minimize the adsorption of water on section surfaces. As shown in Table 3.1, measurements with 2 nA primary beam resulted in a detection limit of ~100 ppm. The detection limit was later significantly improved (decreased by up to 10x) by using a 4 nA primary beam. This improvement is probably due to more efficient removal of H ions creeping along the sample surface in the outer part of the rastered region before they could enter the 8 x 8 μm^2 data collection region. Yurimoto et al. (1989) also reported use of intense primary beam efficiently improves the detection limit of hydrogen measurement.

3.3.1.2 The Open University (OU). The Cameca NanoSIMS 50L at the OU was used for determining the OH contents and H isotopic composition of apatites following the protocol

described in details in Barnes et al. (2013, 2014) and Tartèse et al. (2013). A Cs+ primary beam of ~ 260 pA current was used and negative secondary ions of ^{1}H, D, ^{12}C, and ^{18}O were collected simultaneously on electron multipliers. Electronic gating was used to restrict counting secondary ions from the inner 25 % of the sputtered area. Before analysis, pre-sputtering was performed over a 20 μm x 20 μm area using a ~ 600 pA primary beam for 1 minute to clean the sample surface and to locate the apatite using real time isotope (RTI) imaging, then further pre-sputtering was performed at a reduced area (analysis area) using the same beam conditions. An electron gun was used to provide charge compensation. Due to the variation of apatite grain size within and between samples, and the need to avoid cracks or inclusions, the analysis areas varied from 8 μm x 8 μm to 5 μm x 5 μm. The vacuum in the analysis chamber during analyses was ~ 6.0×10^{-10} Torr.

RTI imaging was also carried out during the pre-sputtering to monitor ^{1}H and ^{12}C in order to identify cracks and hotspots. Occasionally, during an analysis, a crack or hotspot appeared; in such a case, only the signal corresponding to analysis of the pristine sample was considered. This signal was isolated using the NanoSIMS DataEditor, software developed by Frank Gyngard (Washington University). Data inclusion was based on the ^{12}C signal, which is very low in lunar apatites but is several orders of magnitude higher for material filling the cracks. No discernible differences in D/H and $^{1}H/^{18}O$ ratios have been observed when subsets of the data are compared to the ~ 20 minute integration for the reference apatites, which ensure that standardization to ~20 minute long analyses remained valid.

Three terrestrial apatite standards (Ap003, Ap004, and Ap018 described in McCubbin et al., 2012) pressed in indium were used for calibration along with a “dry” San Carlos olivine crystal. This dry olivine was used to monitor instrumental OH background which ranged between 13 and 24 ppm H_2O for the different analytical sessions. To ensure that this measure is adequate for epoxy-mounted samples, analyses were also carried out under our routine analytical conditions in two plagioclase crystals in sample 15404. Two analyses of plagioclase yielded between 19 and 33 ppm OH, which is considered background OH assuming that the crystals are indeed dry. Overall, the calculated background OH contents for indium-pressed dry olivine and epoxy-

mounted nominally anhydrous plagioclase were similar. Background OH was then subtracted from the measured values of the unknown apatites.

3.3.2. Cosmic Ray Exposure.

Exposure to cosmic rays on the surface of the Moon can produce D and H in situ, which can alter the apparent D/H ratio of lunar materials. Saal et al. (2013), Barnes et al., (2014), and Robinson and Taylor (2014) demonstrate the importance of correcting for spallogenic D, especially in materials with low H_2O content. Spallation-produced D will have a proportionally larger effect on the D/H ratio in samples with low water (H) content than in samples with high water content (Saal et al. 2013) and in samples with old cosmic ray exposure ages. Since the apatites and glasses we measured have very low water contents (<267ppm), this correction is important.

We calculate the correction after Saal et al. (2013), determining the amount of spallation-produced D with the D production rate (4.6×10^{-11} mol / 100 Myr, Merlivat et al., 1976) and cosmic ray exposure (CRE) age of the sample, then subtracting that contribution from the measured D abundance and recalculating the D/H ratio. The reported uncertainty includes the uncertainty in the D production rate (~50%, Saal et al., 2013) and our 2σ analytical uncertainties. Unlike Saal et al. (2013), we do not correct for spallogenically produced H, because correcting for H has little effect on the overall D/H ratio. For example, the typical spallation correction for H expressed as H_2O is only ~1 ppm (Saal et al., 2013).

Cosmic ray exposure age data were available for samples 14321 (23.8 Ma, Lugmair and Marti, 1972; and 24 Ma, Burnett et al., 1972), 14161 (363 Ma, Kirsten et al. 1972), 76535 (195 Ma, Bogard et al. 1975; 211 Ma, Crozaz et al. 1974; 233 Ma, Lugmair et al. 1976). When multiple ages were available, we averaged the ages. Since the error on the correction for cosmogenic D is dominated by the large uncertainty in the D production rate, we did not factor errors on the cosmic ray exposure ages into the total uncertainty of the corrected values. As the cosmic ray exposure (CRE) age of sample 15403/15404 has not been determined, the CRE age of 11 ± 1.1 Ma for sample 15405 was used. Soil sample 15400 was collected from on top of 15405, and is classified as an immature soil.

Sample 77538 does not have a measured cosmic ray exposure age. However, it was collected at Station 7 as a rake sample with lunar soil that was designated mature (Meyer, 2013). According to Morris (1978), it takes 100 Myr of exposure time to develop a mature soil. Therefore, we take 100 Myr as the exposure age of 77538 for the purposes of spallogenic D correction, but this is only meant to be a rough estimate.

Table 3.1. δD and H_2O abundances of lunar apatites and glasses. Corrected δD is the estimated δD of the apatite after correcting for the contribution of spallation-produced D after Saal et al. 2013. Italic font denotes measurements below our detection limit. *n.d.* indicates not determined, for points that were below detection limit. Analytical errors are 2σ.

Sample	ppm H_2O	δD	Corrected δD	detection limit (ppm H_2O)	Instrument
77538,16 apt1	175±55	335±74	304*±74	100	ims-1280
77538,16 apt2	188±55	411±74	383*±74	100	ims-1280
14321, 1047 apt1	*<100*	*n.d.*	*n.d.*	100	ims-1280
14321,1047apt1	*<100*	*n.d.*	*n.d.*	100	ims-1280
14161,7069 triapt1	162±49	231±55	114±66	110	ims-1280
14161,7069 triapt2	189±57	265±56	165±62	110	ims-1280
14161,7373 apt3	174±52	432±56	323±70	110	ims-1280
14161,7373 apt2	*<110*	*n.d.*	*n.d.*	110	ims-1280
14161,7373 apt1	*<110*	*n.d.*	*n.d.*	110	ims-1280
76535,52 apt1	75±7	791±66	639±93	22	ims-1280
76535,56 bigapt 1	62±6	572±79	388±106	22	ims-1280
76535,56 bigapt2	86±8	475±110	342±103	22	ims-1280
76535, 56 bigapt3	*<22*	*n.d.*	*n.d.*	22	ims-1280
15358,6 c4 gls1	95±11	698±71	566±88	10	ims-1280
15358,6 c4 gls2	95±11	610±71	477±86	10	ims-1280
15358,6 c1 gls1	58±7	789±84	572±124	10	ims-1280
15358,6 c1 gls2	64±8	830±83	634±117	10	ims-1280
15404,51 Apt6 -1	58±6	-428±135	-438±138	6	ims-1280
15404,51 Apt6-2	46±5	-640±80	-653±82	6	ims-1280
15403,71 apt1 -1	77±9	-589±78	-597±79	6	ims-1280
15403,71 apt1-2	181±20	-721±48	-724±48	6	ims-1280
15403,71 apt 1-3	129±14	-749±56	-754±57	6	ims-1280

Table 3.1 (Continued). δD and H_2O abundances of lunar apatites and glasses.

Sample	ppm H_2O	δD	Corrected δD	detection limit (ppm H_2O)	Instrument
14321,1047_Ap6#1	66±2	943±356	925±356	24	NanoSIMS
14321,1047_Ap6#2	76±2	806±317	790±317	24	NanoSIMS
14321,1047_Ap5#1	*<24*	*n.d.*	*n.d.*	*24*	NanoSIMS
14321,1047_Ap1#1	82±2	247±415	231±415	24	NanoSIMS
14321,1047_Ap4#1	93±2	-313±439	-327±439	24	NanoSIMS
14321,1047_Ap2#1	*<24*	*n.d.*	*n.d.*	*24*	NanoSIMS
14321,1047_Ap2#2	137±3	-108±364	-118±364	24	NanoSIMS
Ap1_14305,656	23±1	799±650	735±652	13	NanoSIMS
Ap3#2_14305,656	136±4	491±320	481±320	13	NanoSIMS
Ap3#3_14305,656	41±1	-28±528	-65±528	13	NanoSIMS
Ap3#4_14305,656	37±1	973±513	934±514	13	NanoSIMS
Ap4#1_14305,656	49±2	-76±458	-107±459	13	NanoSIMS
Ap5#1_14305,656	54±2	-6±481	-34±481	13	NanoSIMS
Ap6#1_14305,656	36±1	649±417	608±418	13	NanoSIMS
Ap7#1_14305,656	53±2	-139±420	-168±420	13	NanoSIMS
Ap1#1_15404,55	134±4	-587±432	-592±432	13	NanoSIMS
Ap1#2_15404,55	267±9	-344±319	-346±319	13	NanoSIMS
Ap2#1_15404,55	76±2	-344±492	-352±492	13	NanoSIMS
Ap2#2_15404,55	99±3	-683±491	-689±491	13	NanoSIMS
Ap2#3_15404,55	99±3	-541±491	-547±491	13	NanoSIMS
Ap2#4_15404,55	69±2	-505±523	-514±523	13	NanoSIMS

*Exposure ages have not been determined for this sample, which is reported to be from "very mature" regolith (Morris, 1978), so we take 100Myr, consistent with exposure ages of other material from the Apollo 17 site.

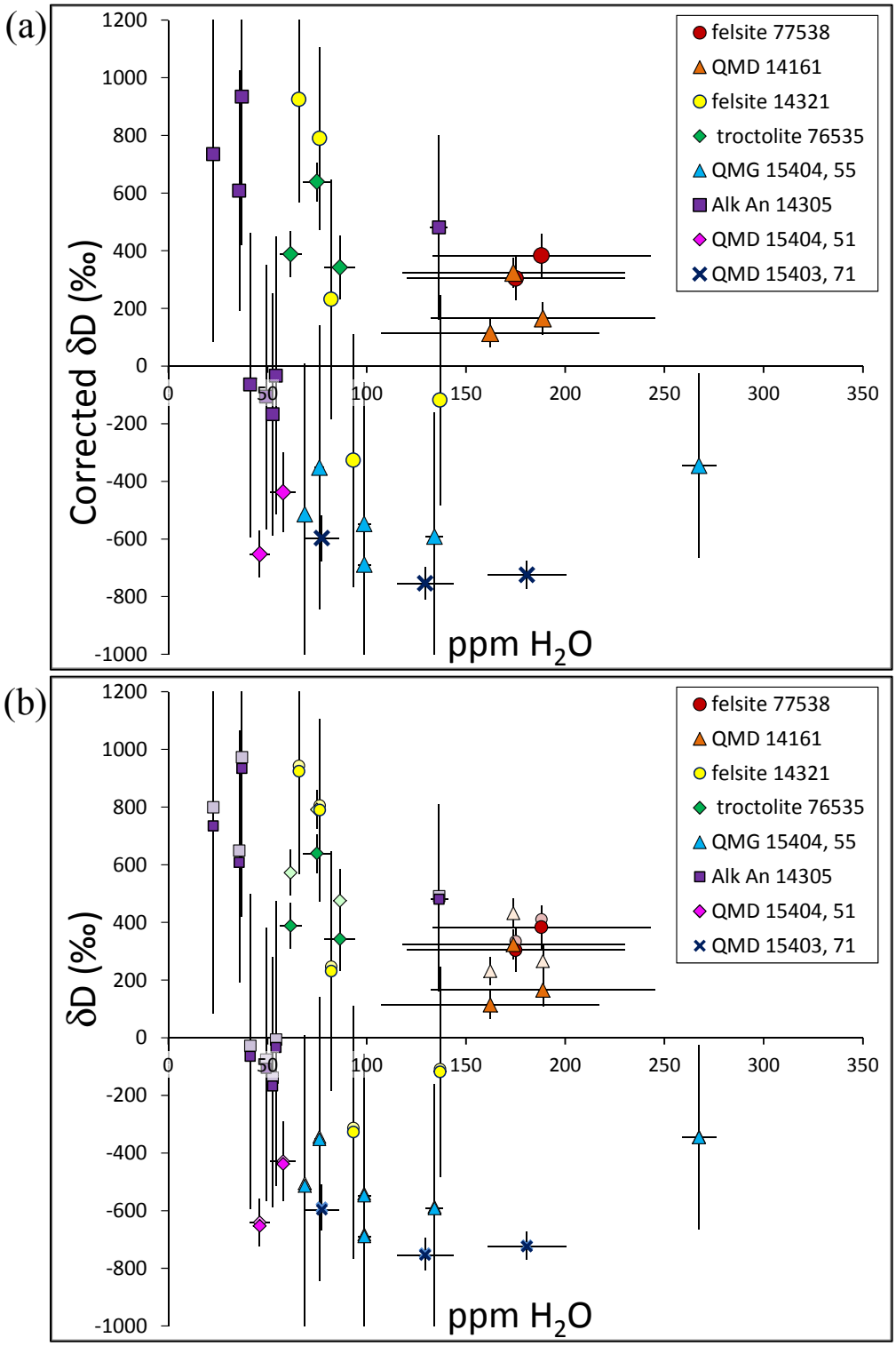

Figure 3.3. Apatite data for KREEP-rich intrusive samples. a) Measured data for all samples, with 2σ error bars. b) Spallation corrected data (bright colors) shown with uncorrected data (pale colors). The spallation correction can lower the δD of apatite by >100‰ in samples with high exposure ages.

3.4. Results

Although we measure H, we report its concentration as H_2O equivalent. In the lunar literature, "water" has been used to describe the presence of H, OH, or H_2O collectively. As explained in Robinson and Taylor (2014), in magma "water" is present largely as OH until the total concentration reaches ~3.5 wt.%, at which point H_2O becomes the dominant molecular species (Dixon et al., 1995). No lunar magmatic water concentrations reach such high levels, implying that it is present dominantly as OH. However, under the reducing conditions prevailing in lunar magmas, "water" probably consists of a combination of OH and H, with the proportion of H rising with decreasing fO_2 (Elkins-Tanton and Grove, 2010; Hirschman et al., 2012). To avoid confusion because of the uncertainty in how much of each species is present, we report our results as H_2O (see Chapter 3 for more discussion). This approach is similar to reporting total Fe as FeO in electron microprobe analyses. We use the word "water" as a shorthand way of describing the total amount of $H+OH+H_2O$, bearing in mind that this does not imply the presence of liquid H_2O.

We performed analyses with the UH ims-1280 on a total of 18 points among 11 apatite grains in eight thin sections of intrusive rocks to determine their D/H ratios and water contents. We also made four measurements of residual glass in two KREEP basalt clasts in sample 15358,6 using the same instrument. Many apatite grains are too small (<30μm) or too cracked to be measured with the ims-1280, so they were analyzed with the NanoSIMS 50L ion microprobe at the Open University. A total of 19 points among 13 apatite grains in three thin sections were measured using the NanoSIMS. All δD values, water contents, and their associated uncertainties are listed in Table 1. Apatite data are plotted on Fig. 3.3 and compared with literature apatite data in Fig. 3.4. Some of the data obtained with the ims-1280 was first reported in Robinson et al. (2012, 2013) and Robinson and Taylor (2014).

The low H_2O content measured in KREEP-related materials (ranging from 23-267 ppm) is in stark contrast to apatite in most mare basalts, which contain ~1000-7500 ppm H_2O (Fig. 3.4). One apatite in felsite 14321,1047 and two apatites in QMD 14161,7373 had H_2O content below

our detection limits. The KREEP basalt residual glass was similarly found to be water-poor, containing 58-95 ppm H_2O with elevated δD of +610 to +830‰ (Table 3.1).

The range in δD values for apatite in intrusive samples measured here is astoundingly large, varying from ultralow (-749‰) to quite elevated (+973‰). There are substantial (2σ from 317-650‰) uncertainties on the NanoSIMS measurements due to poor counting statistics (the price paid for much better spatial resolution) and low water abundances in the apatite, but these data are consistent with lower uncertainty measurements of the same sample (14321,1047 apt1) taken with the ims-1280. Correction for spallogenic D decreases δD by up to 184‰, yet many lunar apatites with detectable water show δD higher than in the Earth, -140 to +60‰ (Hallis et al. 2012 and references therein). The δDs of other apatites fall near or somewhat below the terrestrial range. However, the δD of apatite in 15403,71 (as low as -749±56‰) is by far the lowest yet reported from the moon, indicating that there could be a low D source in the lunar interior.

3.5. Discussion

All δD values, water contents, and their associated uncertainties listed in Table 3.1 are compared with literature apatite data in Fig. 3.4. The low H_2O content measured in KREEP-related materials (maximum 267 ppm) is in stark contrast to apatite in most mare basalts, which contain ~1000-7500 ppm H_2O (Fig. 3.4). If the F and Cl abundances of their respective parent magmas were roughly similar, so that partitioning of H is proportional to total F+Cl+OH, these data suggest that the felsites, QMD, and troctolite parent magmas contained substantially less H_2O than did the mare basalt and pyroclastic-glass magmas. Published data suggest that F and Cl concentration ranges and F/Cl ratios are similar in mare and KREEP basalts (Wanke et al., 1975, 1976; Bouchet et al., 1971; Morrisson et al.,1971; Wanke et al., 1971; Compston et al., 1971, Jovanovic and Reed, 1975). Thus, the low H_2O contents of apatite in KREEP-derived samples suggest that their parent magmas contain substantially less water than those of mare basalts, based on previous studies of apatite in mare basalts (Greenwood et al., 2011, McCubbin et al., 2011; Barnes et al., 2013, 2014; Tartèse., 2013, 2014). Though we might not be able to quantitatively infer the water abundances of parental magmas based on apatite OH (Boyce et al. 2014) as was previously thought (McCubbin et al., 2010a, Boyce et al., 2010, Barnes et al., 2014,

Tartèse et al. 2013, 2014, Robinson et al., 2013), this difference is striking. The melt inclusion and glass bead data are less ambiguous. The pyroclastic glass beads and melt inclusions trapped in olivine grains within them indicate that the Apollo 17 orange glass magma had MORB levels of H_2O (Saal et al., 2013), on the order of 1000 ppm. Measurements of quenched glass from KREEP basalt clasts in 15358 suggest that their magmas contained less than 100 ppm H_2O. As we discuss in detail below, based on water content alone, there seem to be at least two different reservoirs in the lunar interior, one with MORB-like levels of water and one with much less.

The δD data from apatite provides even stronger evidence for multiple H reservoirs in the lunar interior. Apatite in mare basalts and some alkali suite and magnesian suite rocks is elevated in D with respect to Earth (Fig. 3.4). The KREEP basalts range in δD is offset to lower values than the mare basalts (Fig. 3.4, Tartèse et al. 2014), and some evolved samples, such as norite 78235 (Barnes et al., 2014), fall into the δD range of the terrestrial upper mantle. Apatite in samples 15403 and 15404 has the lowest δDs reported in lunar apatite so far, and could potentially represent a low D reservoir in the lunar interior. There seem to be at least three different H geochemical reservoirs based on δD inside the Moon.

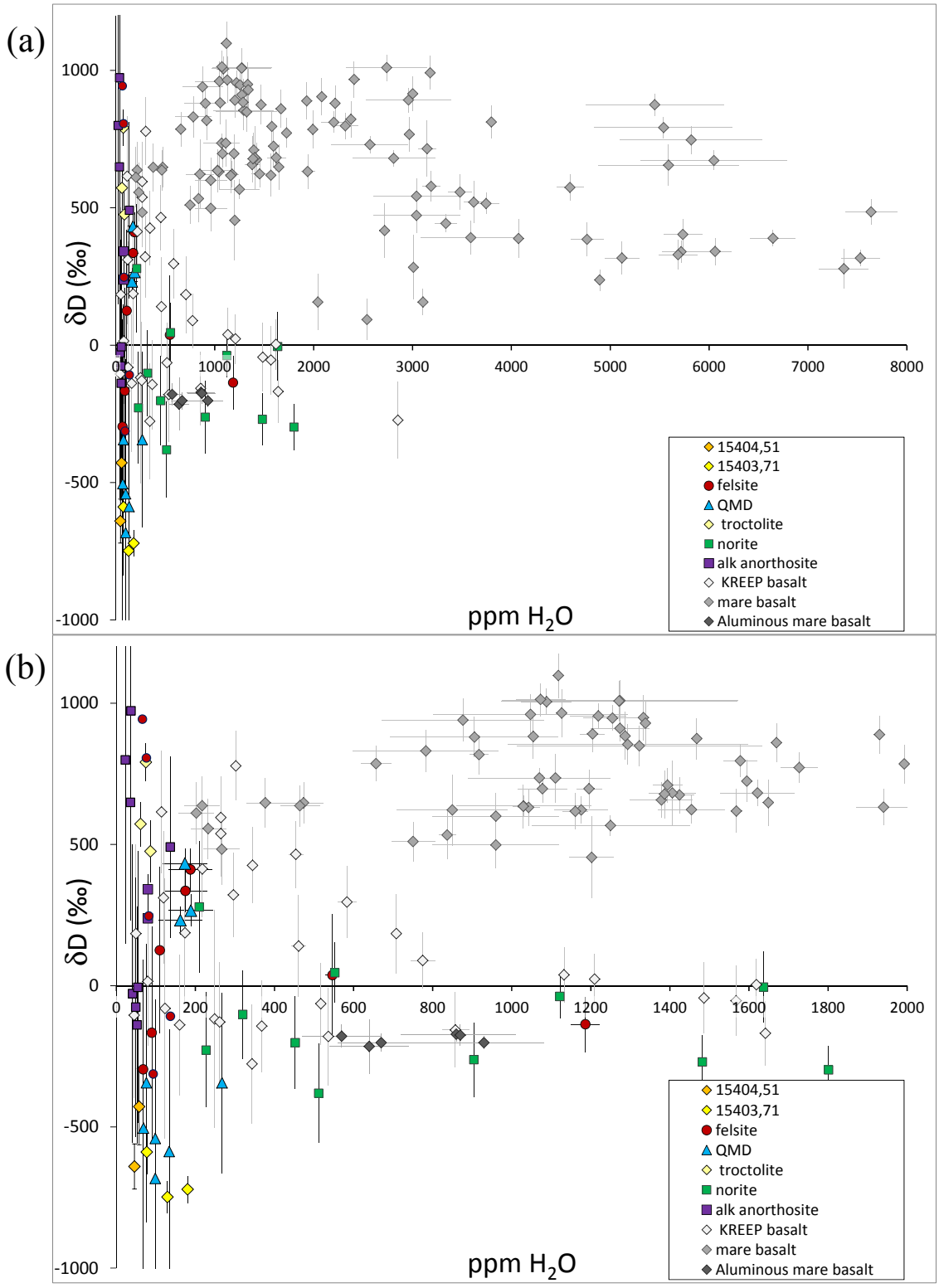

Figure 3.4. Plots showing δD value (normalized to V-SMOW) versus ppm H_2O of (a) our measurements compared with literature apatite data (Greenwood et al. 2011; Tartèse et al. 2013, 2014, Barnes et al. 2013, 2014). (b) Enlargement of figure (a), to show the spread in low water measurements.

3.5.1 Heterogeneous Water Concentrations

Since H_2O in low abundances acts like an incompatible element in a magma, to first order, apatite H_2O contents should be high in KREEP basalt magmas. By the time a fractionating KREEP magma had crystallized enough for silicate-liquid immiscibility (such as during the formation of the felsites) to occur (90-98%) (Roedder and Weiblen, 1971; Hess et al., 1975), H_2O should have been enriched in the melt, yet the maximum amount of H_2O we detected was ~180 ppm in apatites in 77538 and ~267 ppm in QMD 15404,55. H_2O was undetectable in some apatite crystals in 14321 and 14161 (Table 1), and it is low in both the felsite and ferrobasalt of the felsite-ferrobasalt pairs. Apatites in troctolite 76535 and alkali anorthosite 14305 are also very dry (Table 3.1).

In contrast, H_2O in apatite in mare basalts contains up to 0.8 wt.%. The volatile content of the apatite reflects the volatile content of the magma from which it crystallized, although partitioning of F, Cl, and OH into apatite is more complicated than previously thought (Boyce et al. 2014). The timing of apatite crystallization is also important, as F, Cl, and H are incompatible in major lunar minerals, but F and to some extent Cl are very compatible in apatite (Boyce et al., 2014). Once apatite crystallization begins, these elements are rapidly depleted in the melt (Boyce et al., 2014). Petrographic observations indicate that apatite is a liquidus phase in felsites and complementary ferrobasalts. Apatite is found surrounded by quartz and/or K-feldspar in felsites and surrounded by Ca-rich pyroxene or Fe-rich olivine in ferrobasalts, indicating relatively early crystallization. By the time apatite was crystallizing, F,Cl, and OH would have all been concentrated in the melt. Most of these KREEP-rich rocks were formed through extensive fractional crystallization, and simple partition coefficients cannot be used to back calculate how much water was present in the melts before apatite began to crystallize (Boyce et al., 2014). Nevertheless, it is possible to make broad comparisons of relative apatite water contents, especially if halogen concentrations and F/Cl are similar in two rocks being compared.

Mare basalt apatites (Greenwood et al., 2010, Tartèse et al., 2013, Barnes et al., 2013, McCubbin et al., 2010a, Boyce et al., 2010) contain ~10 to >50 times more H_2O than apatites in the KREEP-rich intrusive rocks (Figure 3.4). Apatites in KREEP basalts themselves (Tartèse et al., 2014) contain ~4 to10 times less H_2O than mare basalt apatites. As noted above, it seems

reasonable that if the parental melts had similar F and Cl contents, differences in the H_2O content of the apatites should reflect different water contents in their parent melts. While we cannot quantify exactly how much water was in these parental melts from apatite H_2O, the KREEP-rich intrusive rocks seem to have formed from a much drier source than the mare basalts.

While estimating the water content of a magma from apatite H_2O might not be possible, the H_2O concentration of residual glass in KREEP basalts in rock 15358 can be used to estimate the initial concentration in the magma before crystallization and loss occurred (Fig. 3.5). The glass contains between 58 and 95 ppm H_2O and represents the last ~20% of magma remaining, as determined by modal analyses (Taylor et al., 2012). Thus, if no loss of H_2O occurred, the parent magma would have contained between 12 and 19 ppm H_2O. Its high δD (average of 732‰) suggests that the magma might have lost water. To assess the initial water content, we calculate the amount of water loss for the major members of the suite of samples we analyzed. We assumed conditions reducing enough that a significant fraction of molecular H was present and calculated water loss and initial magma H_2O for three cases: initial δD like that of Earth (-62.5‰), QMDs (230‰), and felsites (400‰) to reach a final δD of 732‰. Based on these calculations, we estimate the parent magma of the 15358 KREEP basalts contained between 29 to 160 ppm H_2O (Fig. 3.5b), depending on the initial δD of the magma. As the KREEP-rich intrusives were derived from KREEP basalt, this low water content in the KREEP basalt parent magma is consistent with the low water content of apatite in the KREEP-rich intrusive rocks, affirming that the water content of apatite is a useful indication of relative magmatic water contents, if F and Cl contents are similar in the magmas being compared.

Taking 100 ppm H_2O as a typical concentration in KREEP basaltic magmas, and assuming 10% partial melting of the mantle source regions and no assimilation of H_2O before eruption, we estimate that the KREEP basaltic magma mantle sources contained ~10 ppm H_2O. In contrast, the sources of mare volcanic glasses contained ~100 ppm. This dichotomy indicates that water is heterogeneously distributed in the lunar interior, which supports the conclusions of McCubbin et al., (2011). A fundamental question is whether this heterogeneous distribution is due to primary heterogeneities, lunar formation or early addition, or reflects water loss from KREEP-related samples.

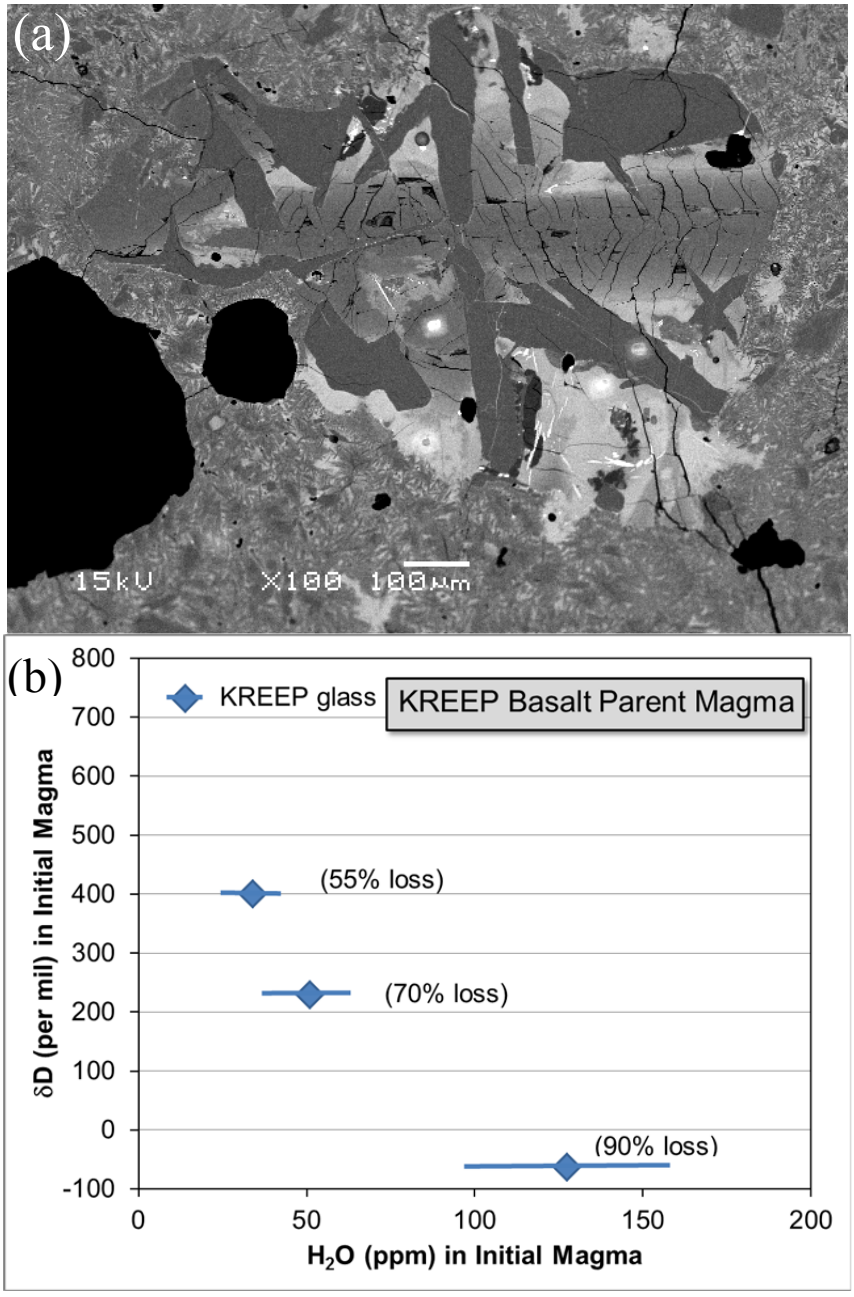

Figure 3.5. KREEP basalt 15358 (a) BSE image of a KREEP basalt fragment containing quenched residual glass in 15358,6. Plagioclase is dark gray, pyroxene is medium gray, and the bright gray material with wavy edges is the Fe-rich quenched glass. The bright white squares are pits from ion microprobe analysis. (b) Calculation of degree of water loss required to obtain δD measured in 15358 KREEP basalt glass starting with observed terrestrial, QMD, and felsite δD and H_2O abundances. Limits represent the range of measured H_2O content in 15358 glasses. For example, if KREEP basalt 15538 began with δD similar to the QMD, it would need to have lost 70% of its initial H_2O to fractionate D from H enough to reach the average KREEP glass δD of 732‰. This calculation assumes that loss is dominated by loss of H, which maximizes D/H fractionation.

3. 5.1.1. Loss from Intrusions. There are several ways that the intrusive KREEP-related rocks could have lost water at some point in their histories, leading to apparent low water contents for their parent magmas. In principal, the magmas might have lost H_2O as they crystallized. We tried to avoid the problem of water loss by selecting intrusive samples, but the felsites, ferrobasalts, QMDs, and troctolites have complex igneous histories. Water could have been lost at several steps during the formation of these rocks, from magma ocean crystallization and fractionation to loss in intrusions in the crust. However, all processes that formed these rocks occurred at depth, and therefore relatively high pressure, where water solubility is high (e.g., ~3 wt. % at 1 kbar, Newman and Lowenstern, 2002; Dixon et al., 1995). Water would probably have been soluble in the melt throughout the formation of the parent magmas of the intrusive rocks.

This assumes that water loss was dominated by outgassing of H_2O, but under reducing conditions like those on the Moon, ~ IW-1 (Wadhwa, 2008), a significant amount of hydrogen would have been in the form of H_2 (Elkins-Tanton and Grove, 2011; Hischmann et al., 2012; Sharp et al., 2013) and the escaping gas was most likely dominated by H_2 (Tartèse et al., 2013). It is conceivable that molecular hydrogen was lost from KREEP-related magmas, in spite of their emplacement in intrusions. Loss of H during crystallization of the intruded magma has not been modeled in detail, so it is not known if H loss would be a few percent of the initial H_2O or all but a few percent. However, at elevated pressures, even H is quite soluble. For example, Sharp et al. (2013) calculate that at an oxygen fugacity of IW-1 and pressure of 3 kbar the maximum solubility of H would be 950 ppm. We suggest that the intrusive origin of the suites of rocks we studied likely precludes significant loss of H or H_2O.

3.5.1.2. Loss from the Magma Ocean. It seems unlikely that water was lost from the magma ocean, even late in its crystallization when urKREEP formed. As the last 2% of the lunar magma ocean, the urKREEP layer would have resided beneath 40 km of feldspathic crust (Wieczorek et al., 2013). The pressure (~2 kbar) would have been sufficient for H_2O to remain soluble in the remaining melt and not degas, unless the concentration was greater than H_2O solubility (~5 wt.%). A low initial water content in the magma ocean (hence possibly in the bulk Moon) or a higher one followed by extensive loss (most likely as H_2) from the magma ocean are

both consistent with our data indicating that KREEP-related magmas, hence most likely urKREEP, had low water contents. Hui et al. (2013) used FTIR spectroscopy to measure water in plagioclase in an anorthosite (a direct product of magma ocean crystallization) and concluded that the magma ocean contained 320 ppm H_2O initially and 1.4 wt.% in urKREEP. This interpretation is inconsistent with our observations, perhaps indicating significant loss of H from the last 1-2% of the magma ocean. It seems most likely that our data, published data on mare basalts and pyroclastic glasses, and Hui et al. (2013)'s measurement on an anorthosite show that water was not uniformly distributed during magma ocean crystallization.

3.5.1.3. Loss by Impact Heating. Impact heating might be a possible mechanism for post-crystallization water loss, as all samples were found in breccias or as fragments in the regolith. None of the samples we analyzed showed any evidence of high shock pressures (deformation, transformation of plagioclase into maskelynite, etc.). All sampled mare basalts are also regolith fragments, and thus would have been similarly exposed to impacts or in the case of lunar meteorites even ejected from the Moon via impacts, yet they retained high water abundances (Tartèse et al 2013). Intrusive rocks of the Mg-suite were excavated from deep in the crust, so would be expected to be highly shocked. In fact, most norites have been heavily shocked, yet contain easily measureable amounts of water (Barnes et al., 2014). In contrast, troctolite 76535 appears to be unshocked, so its low water content is a primary feature of the rock. Minitti et al. (2008) show that while water can be lost during impact, it can also be *added* by impacts. In addition, they show that shock can fractionate H isotopes, but by less than 100‰, which is not enough to explain the high δD of the mare basalts without some other factor at work (Minitti et al., 2008). Impact heating is not likely to have affected the H_2O concentrations in the samples studied.

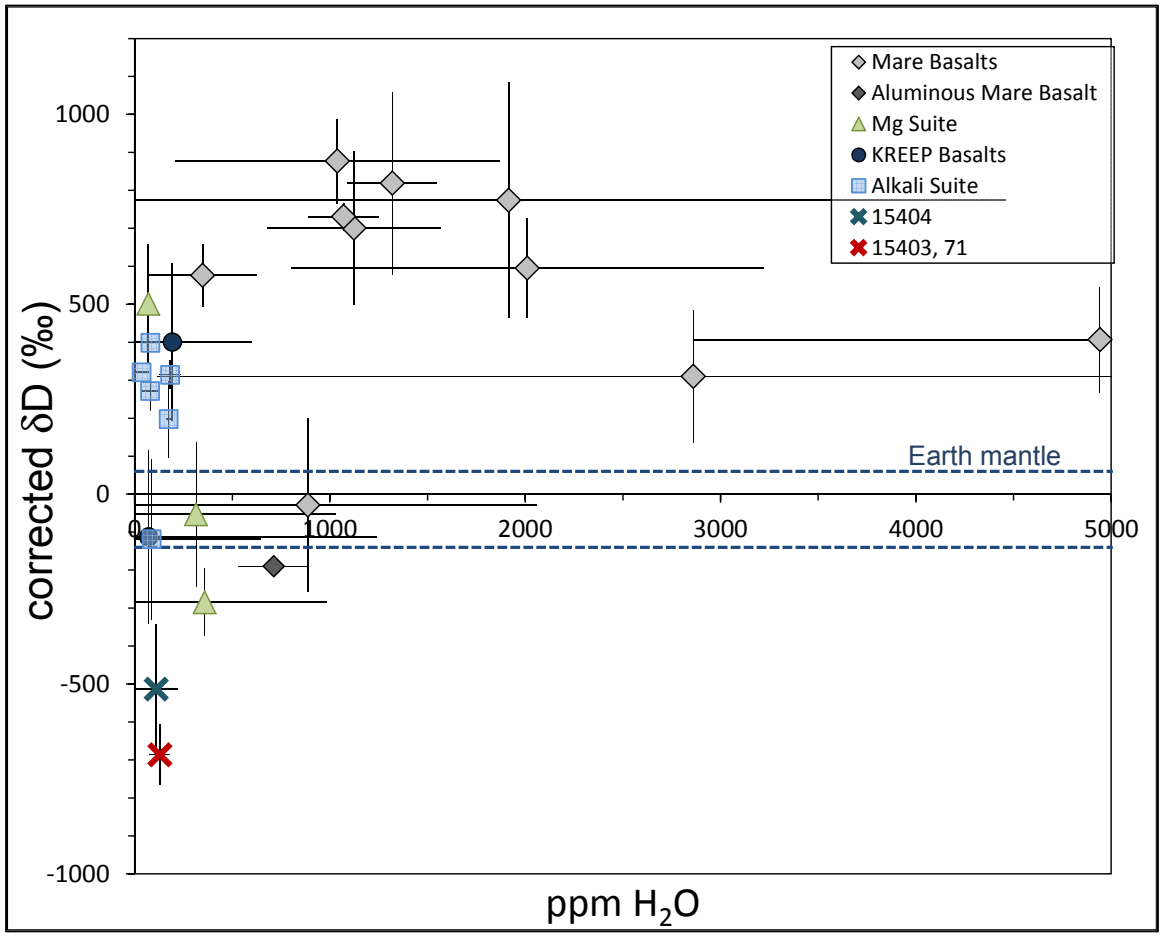

Figure 3.6. All apatite analyses for each sample weighted according to their uncertainties and averaged, after Robinson and Taylor, 2014. The δD range of Earth's mantle is also shown. There appear to be at least three H reservoirs in the lunar interior: an Earth-like reservoir, a moderately elevated reservoir, and a very low D reservoir. The mare basalts would have had an initial unfractionated δD near the Earth range, ~100‰ (Tartèse and Anand 2013). Error bars represent one half of the range of the data for each sample.

3.5.2 Hydrogen isotopic composition: Multiple Reservoirs

Apatites in our sample suite vary widely in δD (Table 1, Fig. 3.3), ranging from -749 ‰ to +947‰. Apatite in individual samples can also vary by 100s ‰ (Fig. 3.3). To evaluate broad variations among δD and H_2O content of many samples (and reducing the clutter on the δD/H_2O plot), we calculated averages for all data for individual samples (Fig. 3.6), weighting each data point by its analytical uncertainty (after Robinson and Taylor, 2014). Averaging all data for a sample also may help even out local variations in H_2O caused by lack of connection between individual pockets of mesostasis (Pernet-Fisher, et al., 2014) and may provide more representative values for the sample as a whole. Our goal is to present an overview of the broad variations in the samples, hence in the Moon. Averaging does, however, remove important trends in the data for an individual rock, such as evidence for degassing during crystallization, but only one such case has been reported (Tartèse et al., 2014). The data seem to cluster into groups with similar δD and water concentrations. These clusters could represent different reservoirs in the lunar interior, which we evaluate below.

3.5.2.1. Earth-like reservoir. The δD range of Earth's present day upper mantle is -140 to +60‰ (Hallis et al., 2012 and references therein, Shaw et al., 2012), shown by dashed lines on Fig. 3.6. Several samples, including a KREEP basalt, three KREEP-rich intrusive rocks, and two mare basalts, fall in or near this δD range. As we argue above, the KREEP-rich intrusive rocks formed at depth and pressure, so are unlikely to have degassed fractionated D from H. These rocks could thus retain their original (or close to their original) δD ratios, which are essentially Earth-like (Barnes et al., 2014). All of this evidence indicates that there is at least one reservoir in the lunar interior that has a δD value like the terrestrial mantle. Tartèse et al. (2014) argue that KREEP basalt 72275 did not degas before apatite crystallization, implying that its δD reflects a source with a terrestrial-like hydrogen isotopic composition. These data are consistent with the calculation done above for water loss from KREEP basaltic glass (sample 15358), suggesting that at least one KREEP basalt source had an Earthlike δD.

Despite the high δD values observed in mare basalt apatites, the mare basalt source may also fall into the Earth-like δD reservoir. Calculations by Tartèse and Anand (2013) show that the entire range of elevated δD values seen in mare basalt apatite can be produced by degassing

of 85-99% of the hydrogen from a melt with chondritic δD of ~100‰, (Alexander et al. 2012). While the water content of the mare basalts appears to be greater than the KREEPy intrusive rocks, they both could have had similar initial δD values, which are in or near the range of the terrestrial mantle.

3.5.2.2. Moderately elevated D reservoir. Another cluster of points on Fig. 3.6 appears between ~200-400‰. All appear to have low water contents. Five of these samples are alkali suite rocks, formed intrusively though extensive fractional crystallization of KREEP basaltic magmas. There is also a magnesian suite sample (troctolite 76535) that plots near this moderately elevated δD range. The alkali suite rocks, the norite, and the troctolite, however, formed intrusively and thus did not degas, or degassed little compared to eruptive samples. They could represent a reservoir inside the Moon with an inherent moderately elevated δD.

3.5.2.3. Low D reservoir. A third reservoir, with very low δD, is represented by 15404,51, and -,55, and 15403, 71. Apatite in these samples has an average δD of -630‰, which is far below the range of the terrestrial mantle and of other δD values reported from the Moon (Fig. 3.4, 3.6). We believe this extremely low δD reflects the magma from which the sample formed. REE abundances for 15404,36 (the parent chip of 15404, 51 and -,55) is elevated with respect to those of Apollo 15 KREEP basalt (D. Mittlefehldt, personal communication), which is consistent with formation from a KREEP basaltic magma, and its texture indicates that it formed intrusively, thus avoiding H fractionation due to degassing. Even if the source of these Apollo 15 QMDs had degassed, degassing elevates δD, which means that their source would have had an even *lower* initial δD.

Solar wind is also extremely depleted in D (< -998‰, Huss et al., 2012) and the δD range of solar wind in agglutinate glasses from the regolith (Liu et al. 2012) is strikingly similar to the range seen in apatites from the Apollo 15 QMDs. However, there is no clear mechanism for introducing solar wind H into fragments of intrusive rocks residing inside an impact melt. The Apollo 15 QMDs were formed at depth, in a shallow intrusion in the lunar crust, far deeper than D-depleted solar wind could have penetrated. It was brought to the lunar surface by impact, where it was exposed to solar wind and cosmic rays for ~11Myr (Drozd et al., 1976). Direct implantation of solar wind H into these apatite grains is unlikely, as solar wind penetrates less

than 1μm into the surface of a grain and ambient lunar surface temperatures are too low to allow diffusion of H farther than ~10^{-5}μm into an apatite during the 11 million years of exposure on the surface (calculated using diffusion rate from Cherniak 2010).

In order for apatite in the Apollo 15 QMDs to be contaminated with solar wind, H from solar wind would have had to have been incorporated into their source impact melt breccia and then somehow diffused into the apatite grains. These samples were collected from on top of a three-meter boulder, sampled as 15405 (Meyer, 2013). This boulder, an impact melt breccia, was probably formed and thrown to the A15 site by impact that formed Aristillus crater (Ryder, 1976; Ryder and Martinez, 1991; Ryder et al., 1991; Taylor et al., 2012). Drozd et al. (1976) measured Ne, Kr, and Xe isotopes in 15405 and Bernatowicz et al. (1978) measured Ar isotopes in 15405 (matrix and a QMD clast) as part of their Ar-Ar dating. Both papers state that the rock contains no measurable solar wind component. Given the size of Aristillus crater (55km), we calculate that very little regolith contaminated by solar wind (depth of ~5m) would have been incorporated into the impact melt. We calculate that the contribution of solar wind H from this regolith would be undetectably low, < 0.3 ppm in apatite, even if it were all incorporated into apatite. The more likely situation is that the Aristillus target contained rocks that had H in them from a distinctive isotopic reservoir in the Moon. This is supported by δD data from relict apatite grains in the impact melt of 15405, which have preserved low δDs similar to those measured in 15403 and 15404 (Barnes et al. 2014b). Even if they were re-equilibrated while in the impact melt as it rapidly cooled, the Aristillus target had low δD material.

The presence of a very low D reservoir in the lunar interior has interesting implications for potentially degassed samples with low δDs, such as the two basalts (NWA 773 and 14053) that have δD in the terrestrial range. Both of these samples have had their low δD values explained by lack of degassing (NWA 773, Tartèse et al., 2014) or incorporation of low D solar wind during impact heating (14053, Greenwood et al., 2011). However, if a very low D reservoir existed in the Moon perhaps these samples owe their low δD to formation in a mantle source with inherently low δD. We calculate that if they had started with δD of -500‰, similar to the average δD of 15404, 55, the average δD values of both 14053 and NWA 773 could be

obtained with >85% H loss. This did not necessarily occur for these samples, but it is an intriguing possibility.

3.5.3 Implications for the lunar interior

The Moon appears to have several H reservoirs. This is not unlike the Earth, where there are large H isotopic variations between the upper mantle (-140 to +60‰, Hallis et al., 2012, Shaw et al., 2012, Lécuyer et al., 1998) and surface reservoirs such as ice sheets (-400 to -300‰, Lécuyer et al., 1998). There also appear to be distinctive isotopic reservoirs (H, He, and other isotopes; Stuart et al., 2003; Starkey et al., 2009; Jackson et al., 2010; Hilton et al., 1999; Hallis et al., 2014), within the Earth's mantle, although the total range of δD values seen in terrestrial rocks is much less than that observed in lunar materials. Earth's mantle water contents also vary (MORB sources versus oceanic volcanic arcs (Grove et al., 2012)). Similar to the Moon, these reservoirs reflect both initial compositions and later processing during the evolution of the Earth. The recycling of water during subduction could lead to some homogenization of H isotopes inside the Earth, but as shown by MORBs and other reservoirs, not necessarily its water concentrations.

The primary goal of all measurements of water in volcanic glasses, melt inclusions, and apatites is to determine the bulk water content and H isotopic composition of water in the Moon. The observed heterogeneities in water abundance and δD in the lunar interior present a major problem, as it is unclear which samples, if any, are the most representative of the Moon as a whole. The most reliable H_2O abundance measurements for determining pre-eruptive water content of lunar magmas come from the melt inclusions in olivine in pyroclastic glass beads, which indicates that at least one part of the lunar interior contains as much water as MORBs (Hauri et al., 2011). These melt inclusions did not lose much water when they formed, which means their δD values are minimally fractionated (Saal et al., 2013). After correction for spallation, the δD of the A17 melt inclusions ranges +187 to +327 ‰ (Saal et al., 2013). To the extent that H loss did happen, the original δD would have been lower. This is near the Earth range, but it is also near the range of the moderately-enriched δD reservoir discussed above, which primarily consists of KREEP-rich, intrusive rocks. We argue above that it is unlikely these intrusive samples degassed, so their apatite may also record unfractionated δD values

(Barnes et al., 2014, Robinson and Taylor, 2014). However, apatite in the KREEP-rich intrusives is very water-poor, which likely means that the parent melt was very dry, but we cannot estimate the water content from apatite data or evaluate possible water loss from these samples.

Füri et al., (2014) reported data suggesting that the source of the Apollo 17 orange glass (74002) had an initial δD of -100, which is within the δD range of the terrestrial mantle. Could this source be somehow related to a terrestrial mantle source? Füri et al., (2014) point out that δD of -100 is within the range of carbonaceous chondrites, and could indicate the delivery of at least some water to the Earth-Moon system by impacts. However, if this water was not added after lunar formation through an addition to the Earth-Moon system, then lunar formation allowed for some regions to contain substantial water, with Earthlike δD (Saal et al., 2013; Barnes et al., 2014; Füri et al., 2014).

Greenwood et al. (2011) were the first to measure δD in lunar samples, showing that mare basalt apatite had high δD. They suggested that the Moon accreted dry, and water was added later from a source, such as comets, that had high δD. This seems unlikely for several reasons. First, the mare basalts almost certainly lost water when erupted, so their δD values are high due to H isotope fractionation. As discussed in detail above, Tartèse and Anand (2013) calculate that pre-eruptive mare basalt magmas could have had δD of ~100‰, but lost 85-99% of their water. Thus, there is no compelling need for a source with high δD. Second, the mare basalts and pyroclastic glasses are derived from source regions between 200 and 500 km deep (Longhi, 1992). Thus, water-bearing projectiles would have had to penetrate through hundreds of kilometers of crustal and mantle rock to in order to deposit water up to 500 km deep, which seems extremely unlikely.

The dry regions of the lunar interior vary in δD from moderately enriched to extremely depleted. The regions moderately enriched compared to Earth may reflect fractionation in the protolunar disk after the Moon-forming impact (Desch and Taylor, 2012). Fractionation of D from H (preferential loss of lighter H) is consistent with the presence of heavy Zn isotopes in lunar samples (Paniello et al., 2012). H loss from the disk needs to be modelled thoroughly, but if H loss was high (~90%) during lunar formation, D/H fractionation could have been sufficient

to change δD from -140 (the lower range of mantle values) to the range shown by the moderately enriched lunar reservoir (+200 to 400). Alternatively, the dry interior regions with δD in the terrestrial range might reflect moon-forming materials that lost water, but did not fractionate D from H. This could happen if much of the H was lost as H_2O, where Raleigh fractionation is not efficient. The regions with Earthlike δD could also have formed by extensive fractionation of D from H during lunar formation, but began with a low δD like we observe in the Apollo 15 QMDs. This implies that the primitive Earth could have a much lower δD that we observe for the present-day upper mantle. In fact, primitive mantle sources have been identified and at least some contain low δD, as low as -225‰ (Hallis et al., 2014).

Given the complexities in water abundances and δD in lunar samples, it is clear that existing data do not allow an unambiguous assessment of the primary lunar δD or bulk water content. The bulk H_2O concentration of the Moon is much less than bulk water in the Earth (Robinson and Taylor, 2014). Current data indicate that the most water-rich mantle sources are those of the pyroclastic glasses, which contain about the amount in MORB sources in the Earth (Hauri et al., 2011, Saal et al., 2013), which are the driest parts of the terrestrial mantle. Whatever the details, the apparent heterogeneous distribution of water and substantial variation in δD in the Moon must be explained by models for lunar origin, differentiation, and possibly early bombardment.

3.6. Conclusions.

Water is heterogeneous in the Moon, varying in both concentration and hydrogen isotopic composition. We have identified several distinct reservoirs whose formation, although not known in detail, likely reflect a combination of lunar formation and differentiation. Bulk lunar water concentration is difficult to constrain, but is clearly much lower than in the bulk Earth.

CHAPTER 4: HETEROGENEOUS DISTRIBUTION OF WATER IN THE MOON

Published in its present form as Robinson, K.L. and Taylor G.J. Heterogeneous distribution of water in the Moon. *Nature Geoscience* **7**, 401-408 (2014).

Abstract

Initial analyses of lunar samples returned by the Apollo missions indicated that the Moon was essentially devoid of water. However, improved analytical techniques have revealed that pyroclastic glass beads in Apollo samples contain measureable amounts of water. Taking into account volatile loss during eruption of the glass beads onto the surface, the pre-eruption magma could have contained water on the order of 100 ppm by weight, concentrations that are similar to the mantle sources of mid-ocean ridge basalts on Earth. Lava flows from vast basaltic plains—the lunar maria—also contain appreciable amounts of water, as shown by analyses of apatite in mare basalt samples. The hydrogen isotopic composition of lunar samples is relatively similar to that of the Earth's interior, but the deuterium to hydrogen ratios obtained from lunar samples seem to have a larger range than found in the Earth's mantle. Thus, measurements of water concentration and hydrogen isotopic composition suggest that water is heterogeneously distributed in the Moon and varies in isotopic composition. The variability in the Moon's water may reflect heterogeneity in accretion processes, redistribution during differentiation or later additions by volatile-rich impactors.

4.1. Introduction

Beginning with the first glimpses of lunar basalts returned by the Apollo 11 mission in 1969, the conventional wisdom was that the Moon was essentially anhydrous. Although this view was based on sound reasoning (Appendix 1), it turned out to be incorrect, as shown by discoveries of water in volcanic glass beads (Saal et al, 2008) and in apatite in lunar basalts (McCubbin et al., 2010a).

These discoveries provide a new tool to unravel processes involved in lunar origin, differentiation, and bombardment. The current consensus is that the Moon formed as the result of a giant impact of an approximately Mars-sized planetesimal with the proto-Earth (Hartmann and Davis, 1975; Cameron and Ward, 1976; Canup, 2004). A chief geochemical virtue of this model

is that the hot conditions led to loss of volatile elements, explaining the strong depletion of volatile elements in the Moon compared to Earth. One might assume that all water would be lost during such an event, but this is not correct (Desch and Taylor, 2011; Desch and Taylor, 2013). The water in the Moon is a tracer of the processes that operated in the hot, partly silicate gas, partly magma disk surrounding the Earth after the impact. (See Appendix 2 for a discussion of what "water" means.)

Water could have been redistributed during lunar differentiation. The Moon's differentiation began with a global magma ocean at least hundreds of kilometers deep. Crystallization produced a cumulate crust a few tens of kilometers deep, dominated by anorthosite. Overturn of the magnesian, low-density early cumulates (dominated by olivine and orthopyroxene) produced hybrid sources that when heated by long-lived radioisotopes produced other igneous lithologies, including the mare basalts that make up the dark regions of the lunar nearside. Any of these processes could alter the distribution of water in the Moon (Warren and Taylor, 2014; Shearer et al., 2006).

The Moon was also bombarded by numerous large planetesimals, making the large impact basins and craters that decorate its surface. It is conceivable that water was added by such impactors (Bottke et al., 2010). If so, then at least some of Earth's water might also have been added after it essentially finished accreting. Water in the lunar interior might thus be a tracer for addition of water to the Earth.

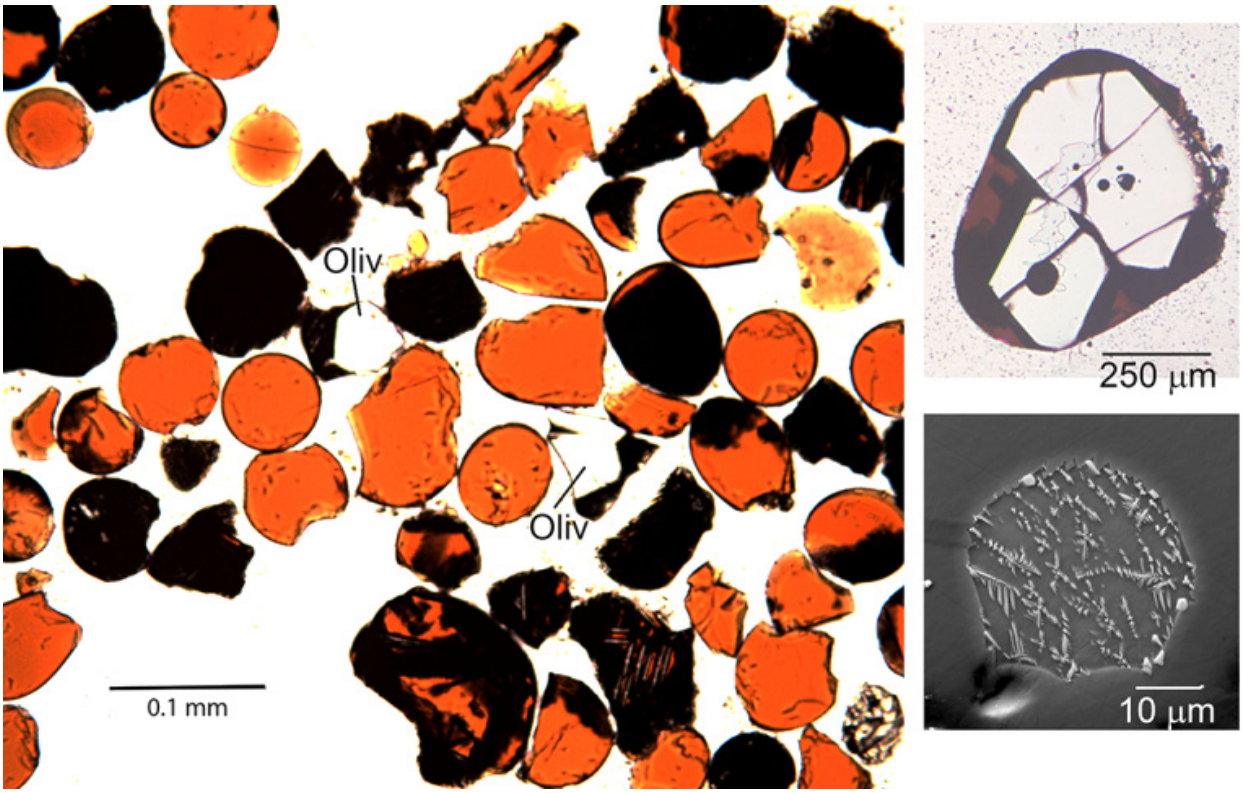

Figure 4.1. Microscopic views of lunar volcanic glass. (Left) Thin section of orange glass. Note the olivine microphenocrysts (oliv) inside some glass beads (none has a melt inclusion visible in the photograph). (Right, top) A few olivine crystals contain inclusions of trapped melt, which are often partially crystallized, as shown in the scanning electron microscope image on the bottom right (courtesy of Eric Hauri; Hauri et al., 2011).

4.2. Water in glassy volcanic deposits

The first report of water inside lunar materials came at the Lunar and Planetary Science Conference in 2007 (Saal et al., 2007), soon followed by detailed analyses of H, C, F, S, and Cl in lunar volcanic glasses (Saal et al., 2008). The abundances were small, but detectable, in sensitive measurement techniques honed for measuring volatile contents in volcanic glasses from the sea floor (Hauri, 2002; Hauri et al., 2002; Saal et al., 2002; Hauri et al., 2006). Lunar volcanic glass deposits (Fig. 4.1) were formed by volatile-driven fire fountains and are distinguishable from glass particles produced by impacts (Delano, 1986). They contain a huge amount of information about the lunar interior, in part because of the wide range in their chemical compositions. This compositional difference shows up in the colors of the glasses: red have the highest titanium (~15 wt.% TiO_2) and green the lowest (< 1 wt.% TiO_2).

The glass beads contain up to 45 ppm H_2O with most in the range 10-30 ppm (Fig. 4.2), comfortably above detection limits and the < 1 ppm expected from conventional wisdom (Saal et al., 2008). These low water contents represent lower limits as significant amounts of H_2O would have been lost by degassing during eruption (Saal et al., 2008). Consistent with loss, the concentrations of H_2O, Cl, F, and S decrease from the interiors to the surfaces of glass beads. Diffusion calculations show the initial magma had an H_2O concentration of 260-745 ppm (Saal et al., 2008), not significantly different from those measured in nondegassed mid-ocean ridge basalt (MORB) glasses. In other words, the water contents were Earthlike. This does not mean that the Moon contains as much water as Earth because the MORBs originate in the driest part of the terrestrial mantle. For example, pre-eruptive magmas produced in terrestrial subduction zones have percent-levels of H_2O (Grove et al., 2012). Nevertheless, water contents similar to MORBs are highly significant.

The water contents of melt inclusions trapped inside olivine microphenocrysts in orange glass beads (Fig. 4.1) confirm the diffusion calculations. The melt inclusions contain 615-1200 ppm H_2O (Hauri et al., 2011, Fig. 4.2). These data clearly show that the mantle source regions for the volcanic glasses contained on the order of 100 ppm H_2O (assuming 10% partial melting and that H_2O strongly concentrates in the melt), which is similar to the mantle sources for MORB (Saal et al., 2002).

The isotopic composition of hydrogen is as important as its total abundance. The deuterium/hydrogen ratio, δD (Saal et al., 2013, Appendix 2), is higher in three types of lunar volcanic glass (green, yellow, and orange) than in the trapped melt inside olivine crystals in orange glass (Fig. 4.3a, Saal et al., 2013). The high δD in the glasses reflects H-D fractionation from the droplets of lava when erupted. The measured δD of the melt inclusions ranges from +187 to +327 ‰, higher than the terrestrial mantle (-140 - +60 ‰) (Boettcher and O'Neil, 1980; Michael, 1988; Ahrens, 1989; Deloule et al., 1991; Bell and Rossman, 1992; Thompson, 1992; Graham et al., 1994; Jambon, 1994; Wagner et al., 1996; Xia et al., 2002). The D and H concentrations must be corrected for cosmic ray production (Appendix 2). The orange glass deposit sampled at the Apollo 17 site was exposed only about 30 Ma ago (Eugster, 1977), making the correction in δD trivial for the melt inclusions. A thorough analysis of H and noble gas isotopic compositions in orange volcanic glasses (Füri et al., 2014) indicates δD of -100 ‰, lower and more terrestrial-like than the melt inclusion data. It appears that δD of the mantle source region for the orange glass magma is similar to that of the terrestrial mantle. Diffusive re-equilibration during magma ascent (Gaetani et al., 2012) cannot be ruled out, but even if it happened, the equilibration appears to have been with a reservoir like that of the Earth.

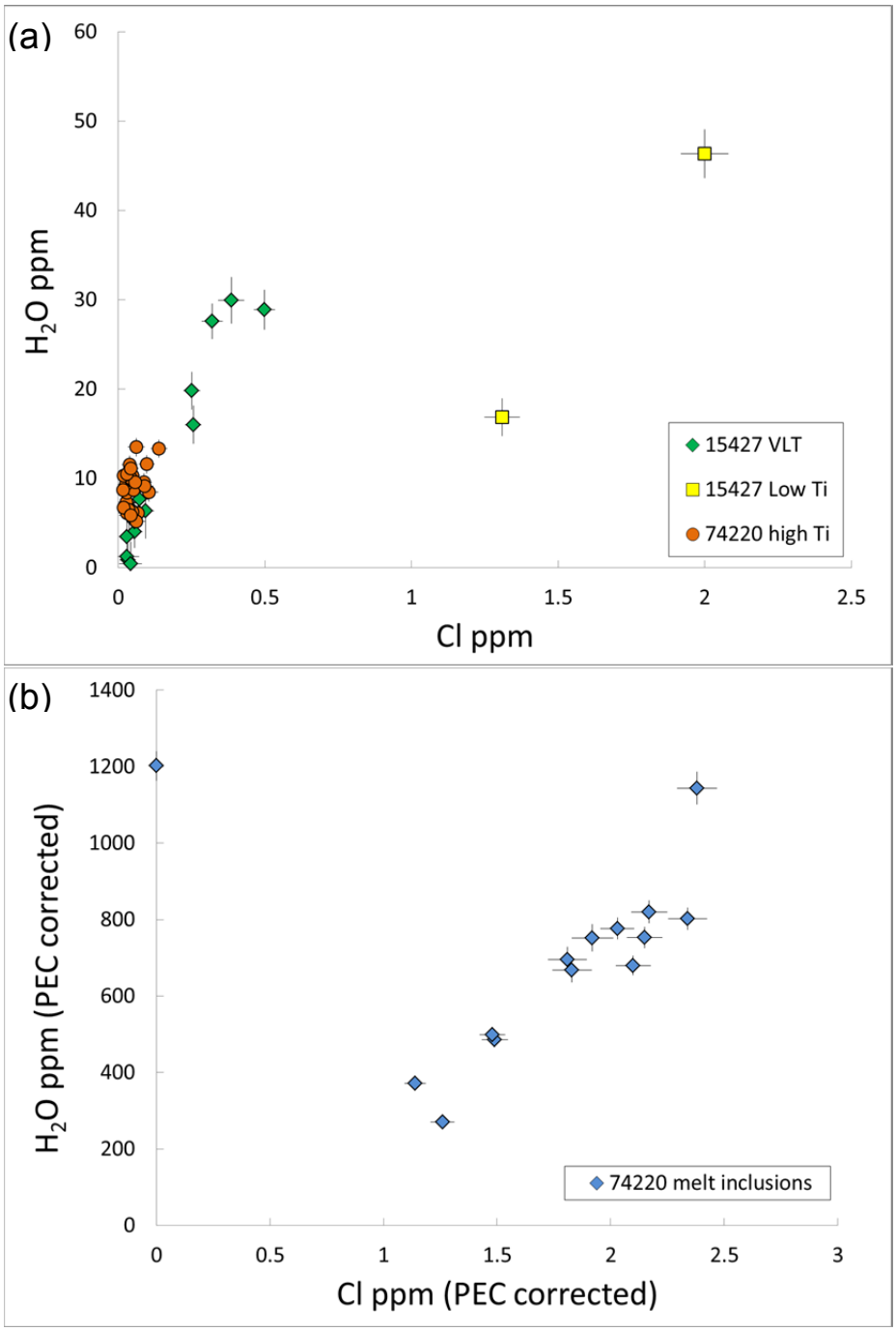

Figure 4.2. Volatiles in orange glass beads. (a) H_2O concentration in lunar orange and green glassy volcanic spheres, plotted against another volatile element, Cl (Saal et al., 2008) (b) H_2O concentrations in melt inclusions in olivine crystals suspended in volcanic glass, corrected for crystallization in the inclusions (Hauri et al., 2011). H_2O concentrations range from 200 to 1200 ppm, similar to concentrations in melt inclusions in terrestrial Mid-Ocean Ridge Basalts (Saal et al., 2002). Note the difference in the H_2O scale between (a) and (b). Error bars are 2-σ analytical uncertainties.

4.3. Water in Lava Flows from the Lunar Maria

The lavas that make up the lunar maria are volumetrically much more abundant than the volcanic glasses and were derived from diverse mantle source regions. While water-bearing minerals such as amphibole or micas are absent on the Moon, the common igneous mineral apatite [$Ca_5(PO_4)_3(F,Cl,OH)$] can also incorporate OH into its crystal structure. Apatite is useful for studying the volatile content of magma because it records the volatile content of the melt at the time of apatite crystallization. Apatite has been used effectively to study volatiles in Martian magmas (Watson et al., 1994; Boctor et al., 2003; Greenwood et al., 2008; Hallis et al., 2012), particularly for hydrogen isotopic composition, and has now been studied in lunar samples. While OH cannot be directly detected by electron microprobe analysis, apparent stoichiometric vacancies in the F+Cl+OH site in lunar apatite suggest its presence (McCubbin et al., 2007; McCubbin et al., 2011) and secondary ion mass spectrometry (SIMS) data confirms it (McCubbin et al., 2010a; McCubbin et al., 2010b; Boyce et al., 2010; Greenwood et al., 2010; Greenwood et al., 2011; Barnes et al., 2013; Tartèse and Anand, 2013; Tartèse et al., 2013;, Fig. 4.3b). Water contents in mare basalt apatite crystals are high, ranging from 650 to ~7500 ppm. Like volcanic glasses, the mare basalt lavas must have lost substantial amounts of water, so it is not straightforward to estimate the H_2O concentrations in the pre-eruptive magmas, let alone in their mantle source regions (Appendix 3). Recent work also suggests F-Cl-OH partitioning behavior between apatite and melt is not well understood, which may confound efforts to use apatite OH measurements to estimate pre-eruptive H_2O content in samples which have undergone fractional crystallization (Boyce et al., 2014; Appendix 3). The uncertainty stems largely from hydrogen incorporation into the F+Cl+OH site, which is governed by the apatite stoichiometric requirement that F+Cl+OH sum to 1, exchange reactions with the melt, and the strong decrease in F during fractional crystallization (Boyce et al., 2014). A potential way around this problem is to use the lowest water measurement (Boyce et al., 2014) of apatite in each rock to assess relative abundances of water in mare basalts. The lowest published mare basalt apatite water contents in individual rocks range from ~200-3500 ppm (Greenwood et al., 2010; Greenwood et al., 2011; Barnes et al., 2013; Tartèse and Anand, 2013; Tartèse et al., 2013), implying a large range in magmatic water content *if* F and Cl were roughly similar in each magma. The mantle source regions for mare basalts would have been similarly variable.

Mare basalts have high δD (Fig. 4.3b), which is almost certainly caused by magmatic degassing and loss of H_2, rather than reflecting the mare basalt source region (Greenwood et al., 2011; Barnes et al., 2013; Tartèse and Anand, 2013; Tartèse et al., 2013). Extensive degassing occurs when a magma moves from high to low pressure, and as the mare basalts were erupted they undoubtedly degassed. Lighter H will escape while heavier D stays behind preferentially, enriching the melt in D. The δD of the mare basalt source region in the lunar interior would thus be much lower than is observed in the apatite crystals in mare basalts. However, it is not known how much degassing and loss occurred. Experiments and calculations (Hirschmann et al., 2012) indicate that at the H_2O concentrations in mare basalt lavas 10-20% of the total H would be in the form of molecular hydrogen. Taking into account the H species in both lava and the escaping gas, estimates of the initial δD can be made. These calculations indicate that pre-eruptive δD could have been ~100‰ (Tartèse et al., 2013).

4.4. Drier Nonmare Rocks

Mare volcanic deposits make up only ~1 volume % of the lunar crust. Lunar rocks rich in a chemical signature called KREEP (an abbreviation for **K**, **R**are **E**arth **E**lements, and **P**) are also important because they are related to the final fractionate of the lunar magma ocean, the last ~2% of the magma ocean. This final melt was highly enriched in K, P, rare earth, and other elements not readily incorporated in major minerals, the so-called incompatible elements. H_2O behaves like an incompatible element when in low abundances (Koga et al., 2003; Aubaud et al., 2004; Grant et al., 2007), so if the lunar magma ocean contained water, these KREEP-rich rocks could also be enriched in water. At the very least, they represent a geochemically distinctive reservoir compared to other lunar rock suites, so the abundance and isotopic composition of water in them is an important part of the global water inventory.

The KREEP rocks are classified into three major groups: KREEP basalts, and intrusive rocks composing the magnesian and alkali suites. Besides sampling a distinctive geochemical reservoir, the magnesian and alkali rocks are intrusive, hence they crystallized at higher pressure than did the mare volcanics. The solubility of water increases with pressure, so rocks formed at depth might have avoided most or all of the degassing experienced by mare basalt lavas. The δD

of intrusive rocks could thus be more representative of a primordial interior reservoir of lunar water than the water in mare basalts. On the other hand, not all the H components are oxidized under the low fO_2 of lunar magmas (Hirschmann et al., 2012; Sharp et al, 2013), so it is possible that H_2 is lost by diffusion from the magma. As H_2 is lost, the reducing buffer (probably metallic iron, Sharp et al., 2013) converts additional H_2O or OH to H_2. However, loss of molecular hydrogen is less likely if its concentration is below its solubility, which is 950 ppm at a pressure of 3 kbars (Sharp et al., 2013). This pressure corresponds approximately to the base of the crust and would be less for intrusions into the crust. Nevertheless, intrusions are more favorable to water retention and may minimize isotopic fractionation, but they are not necessarily tightly sealed containers. KREEP basalts, of course, are subject to extensive water loss during eruption and emplacement as lava flows.

The nonmare rocks are distinctly lower in water than the mare basalts (Robinson et al., 2012; Robinson et al., 2013; Tartèse et al., 2014; Barnes et al., 2014; Fig. 4.3b). Except for a magnesian suite norite (Barnes et al., 2014), apatite in the intrusive KREEP-related rocks have much lower H_2O (< 200 ppm) than the apatite in mare basalts (Tartèse et al., 2014). If the apatite water contents reflect proportionally lower magma water contents than in mare basalt magmas, the KREEP-related magmas contained substantially less water. Apatite in the magnesian suite norite has up to 1500 ppm and the KREEP basalts have several hundred ppm (Fig. 4.3b), implying water contents in the lower range of those in mare basalts. Additionally, the δD of water in these rocks is generally lower than in mare basalts, except for one troctolite (rock 76535). Some samples have low δD, ranging from about -100‰ to -381‰. Others have higher values, clustering in the +200 to +400‰ range (Fig. 4.3b).

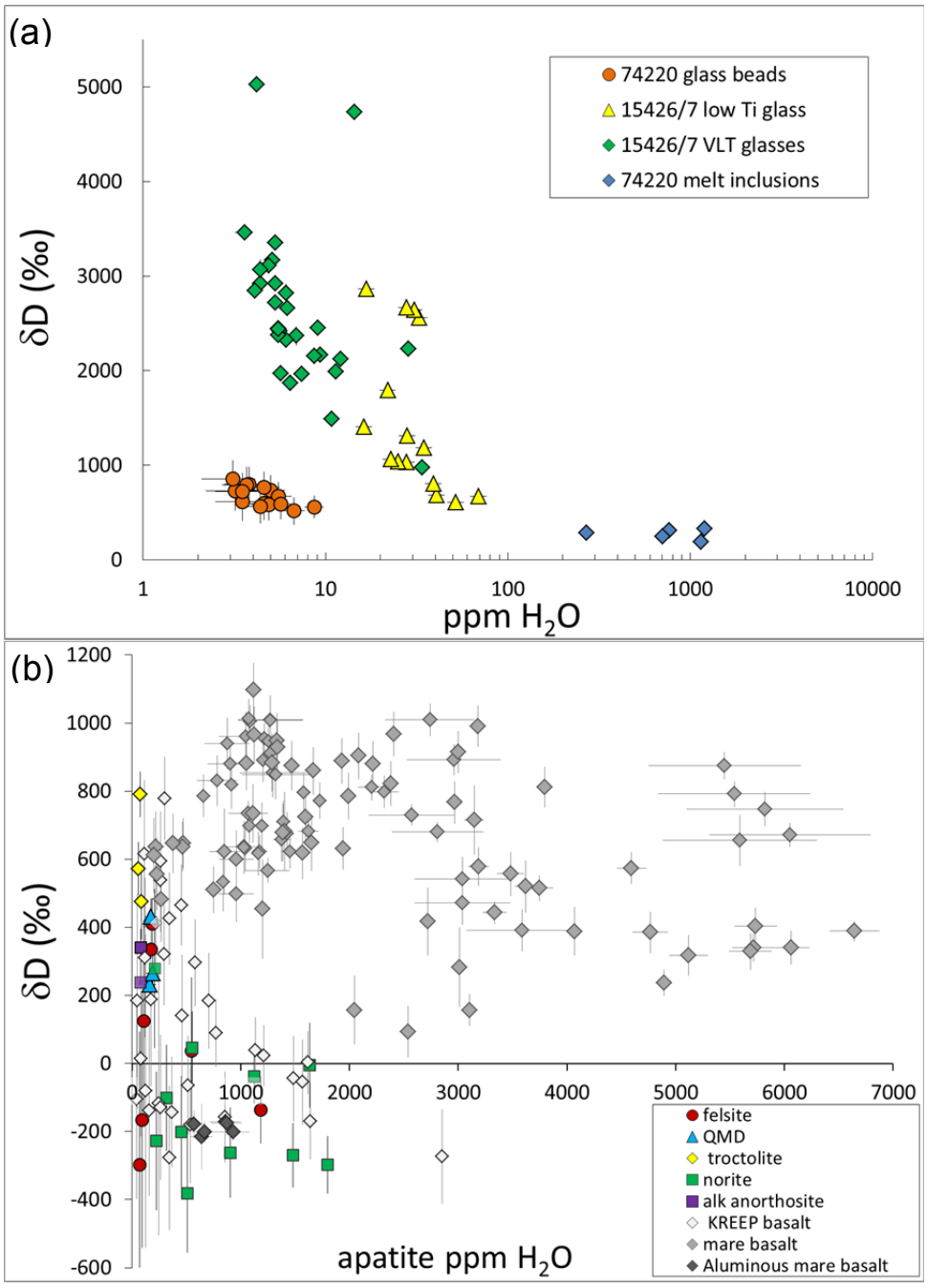

Figure 4.3. Hydrogen isotopic composition and water contents of lunar materials**.** a) Hydrogen isotopic composition plotted against H_2O concentration for glasses and melt inclusions (Saal et al., 2013). Note the logarithmic scale on the x-axis. The melt inclusions have uniformly low δD, only slightly higher than in the terrestrial mantle, whereas the glasses have high δD, almost certainly due to fractionation during loss of H during eruption. b**)** δD versus wt.% H_2O plot for apatite in KREEP basalts and KREEP-related intrusive Mg-suite and alkali-suite rocks compared to apatite data from mare basalts (McCubbin et al., 2010a; Greenwood et al., 2010, 2011; Barnes et al., 2013, 2014; Tartèse et al., 2013, 2014; Robinson et al., 2012, 2013). Error bars are 2-σ analytical uncertainties; data have not been corrected for D and H produced by cosmic rays.

A speculative implication from the apparent low water abundances in KREEP-related samples is that the magma ocean had very low water content, perhaps only a few ppm, if the KREEP component retained water along with incompatible trace elements during petrogenesis of the KREEP-related rocks. In contrast to this interpretation, direct measurements by FTIR spectroscopy of plagioclase in lunar ferroan anorthosites (rocks 15415 and 60015) suggest that the magma ocean could have contained ~320 ppm at the time plagioclase began to crystallize (Hui et al., 2013). The plagioclase contains ~6 ppm H_2O, which is likely to be present as OH (Hui et al., 2013) . (The detection limit was ~0.5 ppm.)

Another contrasting study is based on remote spectral observations of the central peak of Bullialdus Crater, a crater 61 km in diameter in Mare Nubium on the eastern nearside of the Moon (Klima et al., 2013). Central peaks are composed of igneous rocks brought up from depth and have steep slopes that prevent regolith buildup, hence they are unlikely to have been contaminated with surficial H from the solar wind or other external sources. The data show the presence of OH bands around 2800-3000 nm, distinctly different in character from those exhibited by most of the surface bombarded by solar wind. In addition, the central peak of Bulliadus is enriched in Th, so is probably also enriched in other incompatible elements associated with KREEP. The remote sensing connection between KREEP and detectable OH is different from observations of KREEP-related samples, indicating more complexity in the distribution of water in the Moon. The complexity is shown further by spectra of the crater Aristillus (located north of the Apollo 15 landing site). This crater has a strong Th signature, yet has no detectable OH band (Klima et al., 2013). Similar spectral features are found in the Compton-Belkovich volcanic complex (Bhattacharya et al., 2013), thought to be a site of Th-rich silicic volcanism (Jolliff et al., 2011). These interesting remote observations need to be tested by data from other instruments (all are based on the Moon Mineralogical Mapper on the Chandrayaan-1 mission), with close attention paid to artifacts introduced by sun angles, slopes, and calibration of the concentrations present.

Appearing to support the low water contents found in KREEP-related samples are measurements of chlorine isotopes (Sharp et al., 2010). The Cl isotopic measurements show a large range in $\delta^{37}Cl$, from -1 to +24‰ ($\delta^{37}Cl$ is the $^{37}Cl/^{35}Cl$ ratio normalized to the mean Cl

isotopic composition in terrestrial oceans, in parts per thousand). This contrasts sharply with terrestrial samples, which vary in $\delta^{37}Cl$ by only about 1‰. This difference could be caused by low water contents in lunar magma, leading to fractionation due to volatilization of metal halides, but not necessarily low H_2 (Sharp et al., 2013). Molecular hydrogen produced in magmas at low lunar oxygen fugacity would be lost by diffusion much faster than Cl, changing the Cl/H ratio and driving Cl isotopic fractionation. Whether sufficient H_2 is lost in intrusions has not been modeled in detail.

4.5. Heterogeneous Distribution of Water in the Moon

The fundamentally important conclusion from the spurt of measurements of water in lunar samples is that the lunar interior contains water. This discovery changes our whole view of volatiles inside the Moon. Nevertheless, outstanding questions abound about the total amount of water in the Moon, its distribution, and its isotopic composition.

The data show that water is heterogeneously distributed inside the Moon (McCubbin et al., 2011). Both mare volcanic glasses and mare basalts came from deep sources (200-500 km, Longhi, 1992) in the lunar mantle. Based on estimated magmatic H_2O contents, the volcanic glass sources could have contained up to 100 ppm (Saal et al., 2008; McCubbin et al. 2012), similar to terrestrial MORB sources. On the other hand, water in intrusive rocks related to KREEP and KREEP basalt magmas appear to contain less H_2O than did other lunar magmas, either implying significant loss of H during their protracted petrogenesis (cumulate formation, partial melting, and crystallization in intrusions) or that their source regions were inherently low in water. Because the KREEP component formed as a late-stage magma ocean product and H_2O behaves as an incompatible element, these low H_2O contents imply that the magma ocean contained little water (assuming no extensive loss during their petrogenesis). This intriguing story faces a thorny, possibly insurmountable problem from measurements of OH in plagioclase in anorthosites (Hui et al., 2013), which formed from the magma ocean. The measurements suggest the magma ocean might have contained a few hundred ppm H_2O when plagioclase crystallized. Remote sensing measurements indicating the presence of readily detectable OH coupled with high Th concentrations (Klima et al., 2013; Bhattacharya et al., 2013) in some

locations, as well as uncertainties in OH partitioning behavior in apatite (Boyce et al., 2014) further complicate the story. Nevertheless, the basic observation is correct: lunar samples range significantly in H_2O content and KREEP-rich samples appear to contain less than volcanic samples from the maria.

If some regions of the lunar interior are much wetter than others, what caused this heterogeneous distribution? Assuming the giant impact model is correct, one possibility is that the Moon accreted from the proto-lunar disk sequentially from wetter to drier materials. Considerable modeling of disk processes is required to account for this heterogeneous accretion. Another possibility is that the Moon formed relatively dry, perhaps because the hot proto-lunar disk lost most of the water it inherited from the Earth and the impactor. In this case, water must have been added from impacting hydrous planetesimals to form water-enriched regions such as those giving rise to volatile-rich volcanic glasses. If plagioclase-rich crust had already formed, then the impactors would have had to blast through a fully-formed anorthosite crust tens of kilometers thick (Wieczorek et al., 2013) to deposit H_2O as deep as 500 km (Longhi, 1992). The feasibility of such impact deposition deep into the solid Moon is problematic. These ideas need thorough analysis, but only after we have established the extent to which water is heterogeneously distributed in the Moon and how the water varies in hydrogen isotopic composition.

The overall impression from Fig. 4.3 is that δD is elevated conspicuously in lunar samples compared to terrestrial rocks (-140 to +60 ‰). However, all lava flows and the glass beads are likely to have lost a significant fraction of their initial water when erupted, which would likely enrich the remaining water in deuterium. To evaluate overall variations in H_2O and δD we averaged the analyses for each rock that has been studied (Fig. 4.4a). Average values are useful because in lunar basalts the variation in H_2O may be a local effect caused by a lack of communication among pockets of mesostasis (Pernet-Fisher et al., 2014). A thin section samples a very small volume (~ 1 cm^3) of magma. Large differences in pre-crystallization H_2O in such a small volume are unlikely, indicating that local variations emerge during crystallization.

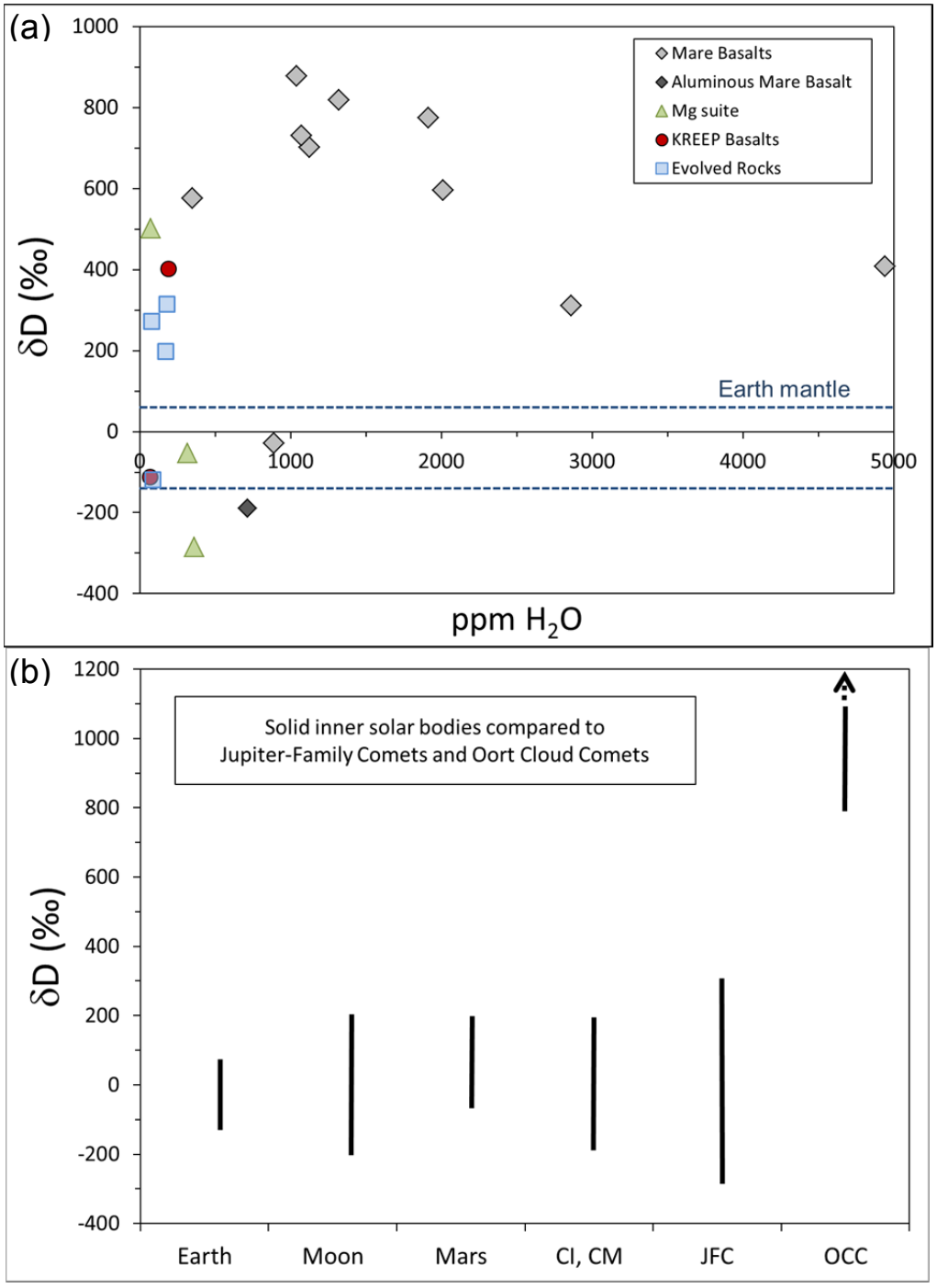

Figure 4.4. Broad view of hydrogen isotopic composition. (a) Averages weighted by measurement uncertainties of δD and H_2O in all rocks for which published data are available (sources in Fig. 4.3), with δD corrected for spallation. Blue lines show δD in Earth's mantle. Elevated δD in mare basalts are caused by H loss from lavas; initial δD are likely ~100‰ (Tartèse et al., 2013). (b) δD values for solar system objects. JFC, Jupiter Family Comets (Hartogh et al., 2011); OCC, Oort Cloud Comets (Eberhardt et al., 1995; Bockelee-Morvan et al., 1998; Meier et al., 1998). Earth's mantle (Boettcher and O'Neil, 1980; Michael, 1988; Ahrens, 1989; Deloule et al., 1991; Bell and Rossman, 1992; Thompson, 1992; Graham et al., 1994; Jambon, 1994; Wagner et al., 1996; Xia et al., 2002); Moon (see Fig. 4.3); Mars' mantle (Hallis et al., 2012); CI, CM chondrites (Alexander et al., 2012).

The high δD in mare basalts can be modeled by 85 to 99% H loss from lava that erupted with a δD of +100‰ (Tartèse et al., 2013). The exceptions are aluminous mare basalt 14053 (-190‰) and NWA 773, a breccia composed of very low Ti mare basalt fractionation products. Both exceptions have δD in or close to the terrestrial mantle range and are enriched in REE compared to typical mare basalts. Any loss from their parent magmas would have caused an increase in δD, implying even lower initial values than measured. Melt inclusions and detailed analysis of orange glasses[19,31] indicate an initial magma δD of -100‰, similar to the terrestrial mantle (Saal et al., 2013, Füri et al., 2014). Two of three Mg-suite rocks plot in the terrestrial range, along with a KREEP basalt clast in breccia 72275 and a felsite in breccia 14303 (Fig. 4.4a). On the other hand, three felsites have low H contents and elevated δD, 200–315‰, and intrusive troctolite 76535 has a δD of 500‰. More data are needed to determine the extent to which δD and total H vary inside the Moon and how any definitive variations correlate with other chemical properties such as the abundances of incompatible trace elements or highly volatile elements (e.g., Tl, Bi, Cd).

Hydrogen isotopic data are presented in Fig. 4.4b for the solid portions of Earth, Moon, Mars, carbonaceous chondrites, a Jupiter family comet, and Oort Cloud comets. All the inner solar system objects are relatively uniform. These data suggest a similar source of water to all the bodies in the inner solar system for which we have data. The Moon appears to have a larger range than does the Earth. This may be due to more extensive loss of H rather than OH or H_2O, though more data are needed to test this. A higher δD in the Moon could reflect loss of H and isotopic fractionation during igneous processing inside the Moon and during its primary differentiation, or in the proto-lunar disk (Desch and Taylor, 2013). Fractionation of hydrogen isotopes in the proto-lunar disk is consistent with the presence of heavy Zn isotopes in lunar samples (Paniello et al., 2012).

4.6. Conclusions

The conventional wisdom that the Moon is virtually anhydrous has been overturned. Even with the uncertainties in interpreting the H_2O contents of apatite, it is unambiguously clear that the mantle source regions for the volcanic glasses contain as much water as do the terrestrial mantle sources for Mid-Ocean Ridge basalts (MORBs). However, the striking similarity in the water contents of MORBs and lunar volcanic glasses should not lead one to conclude that the Moon has Earthlike water abundances. The MORB mantle represents the driest region of the terrestrial mantle. The terrestrial oceans alone represent about 230 ppm of the bulk Earth's water (Mottl et al., 2007), more than double what has been estimated for the volcanic glass source regions (Saal et al., 2008). In addition, the KREEP-related rock source regions seem to contain considerably less water than the mantle sources for the volcanic glasses, possibly only a few ppm. Even if the Moon did have a bulk water content like those of the volcanic glass source regions, it would not raise questions about the validity of the giant impact model for the Moon's origin, as some have proposed (Boyce et al., 2014). The giant impact and the processes associated with forming the Moon, such as the extent of volatile loss from the protolunar disk hypothesized to have formed around the post-impact Earth, are not understood quantitatively. Even if it is shown eventually that the giant impact would have led to quantitative loss of water, it is possible that water could have been added after the Moon formed. Studies of water in the lunar interior are just beginning, and it is clear that more data are needed. The important point is that water concentration and hydrogen isotopic composition vary inside the Moon, and these variations might be useful tracers of lunar formation, differentiation, and early bombardment.

CHAPTER 5: CONCLUSIONS

After detailed petrographic study, we have shown that the felsites are likely not samples of the silicic domes observed from lunar orbit. The presence of quartz in the felsites allowed us to estimate the felsites formed intrusively at minimum pressures between 0.8 and 1.1 kbar, corresponding to a depth of ~20-25 km in the lunar crust, which is consistent with previous work showing that they formed through extensive fractionation of a KREEP basaltic magma. Thermal data from quartz-Ti thermometry lets us estimate the possible size of the studied felsites' parental magmatic bodies as 15-300 m wide. Given the felsites' formation at depth and moderate pressure, they are good candidates for D/H measurements of their apatite grains. A substantial amount (~3 wt. %) of H_2O would have been soluble in the melt at the depth/pressure the felsites formed, which means water loss and hydrogen isotope fractionation due to degassing of the melt would have been unlikely.

While water would have been soluble in the parental felsites' melt, it was not necessarily present. Our measurements of apatite grains in evolved, KREEP-related rocks such as the felsites and quartz monzodiorites indicates that their parental melts were water-poor compared to those of the mare basalts, although studies show that apatite is not a reliable indicator of magma water content. Likewise, our measurements of glass in a KREEP basalt, which circumvents the problems with apatite-OH partitioning, indicate that its parental melt contained ~10x less water than mare basalt sources. At least two reservoirs, one MORB-like and one about ~10x lower, exist in the lunar interior. The hydrogen isotopic composition of apatite is not affected by the same issues as the OH content, and our measurements of the evolved rocks indicate that there are also at least three distinct reservoirs based on D/H ratios (Earth-like, moderately elevated, and very low D).

The formation of these diverse reservoirs likely reflects a combination of lunar formation and differentiation, with asteroidal or cometary additions early in the Moon's history. Several authors have suggested that Earth and Moon (meaning regions of the Moon with Earthlike D/H) have D/H similar to carbonaceous chondrites. If correct, the similarity of the interior of Mars to Earth (Hallis et al., 2012) and Vesta (the HED meteorite parent body) to Earth (Sarafian et al., 2014) suggests a widespread addition of carbonaceous chondrite material to the inner solar

system. However, many lunar samples have D/H much higher or lower than in bulk Earth and carbonaceous chondrites (Fig. 5.1). Figure 1 displays the lowest δD analysis from a given rock, Given the large range in measured δD within some samples and substantial uncertainties for some analyses, using the lowest δD measurement for each sample may not be the best way to represent the data. However, plotting the average δD for each rock is subject to the same issues, while using the lowest δD has the advantage of minimizing the effect of fractionation due to H loss.

Almost all of the samples with high δD are mare basalts, but a few intrusive rocks, such as troctolite 76535, also have high values. Some analyses, as reported in Chapter 2, have exceptionally low δD values, approaching the value of the protoplanetary disk (-865‰, Geiss and Gloecker, 1998). This raises the possibility that this low D/H reservoir in the Moon represents the D/H of the primitive, still-accreting Earth, and that most of the hydrogen in the Earth when the Moon formed derived from adsorbed water on dust grains (Drake, 2005).

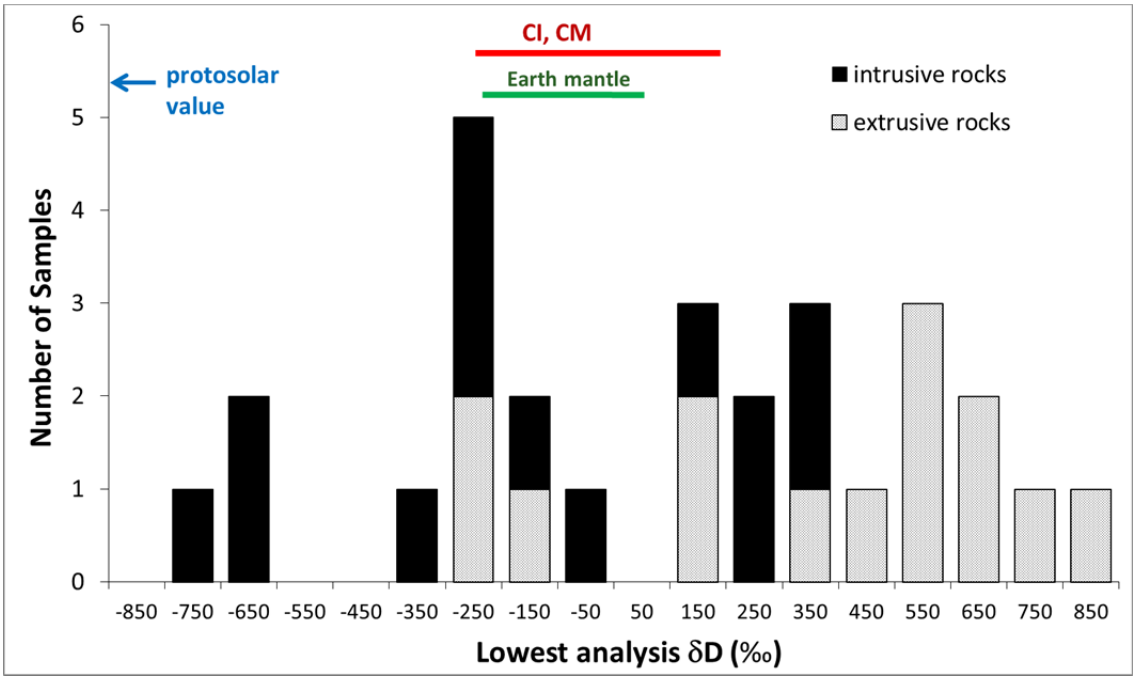

Figure 5.1. Histogram of the lowest analyzed δD from lunar samples (Taylor and Robinson, 2015). The extrusive samples tend to have the highest δD, while the intrusive rocks have lower δD. Also shown are the δD ranges of Earth mantle, carbonaceous chondrites, and the protosolar δD (Alexander et al. 2012, Hallis et al., 2014, Geiss and Gloecker, 1998).

In short, water is heterogeneous in the Moon, varying in both concentration and hydrogen isotopic composition. Our re-analysis of all published data from various sources (pyroclastic glasses, melt inclusions, and apatite), further supports the idea of water reservoir heterogeneity in the lunar interior. The bulk lunar water concentration is difficult to constrain, but is clearly much lower than in the bulk Earth, as the wettest reservoir measured on the Moon so far is as dry as the driest (depleted MORB) reservoir on Earth.

Future Work

There are still many questions to be answered about water in the lunar interior. While we have observed two reservoirs based on water abundance and at least three reservoirs based on D/H ratios, it is possible that there could be a continuum of reservoirs without definite delineations. More analyses of all kinds, particularly of melt inclusions (which are the most reliable samples for measuring pre-eruptive water content and δD), are needed from a variety of lunar rock types in order to determine how many water reservoirs are present in the lunar interior. Determining the number of reservoirs is an important first step in figuring out how these reservoirs formed, and their relationship to early lunar differentiation and/or the protolunar disk.

Other volatile elements and species must be taken into account as well. Though data are sparse, highly volatile elements such as Tl have near Earth-like abundances in lunar pyroclastic glasses, but are severely depleted in the mare and KREEP basalts (Figure 2, Taylor and Robinson 2015). This indicates there is likely heterogeneity of other volatiles in the lunar interior. Understanding the variation of these volatile elements inside the Moon and their relation (if any) with water could be helpful in determining the number of reservoirs in the lunar interior and tracing the sources of the Moon's volatiles.

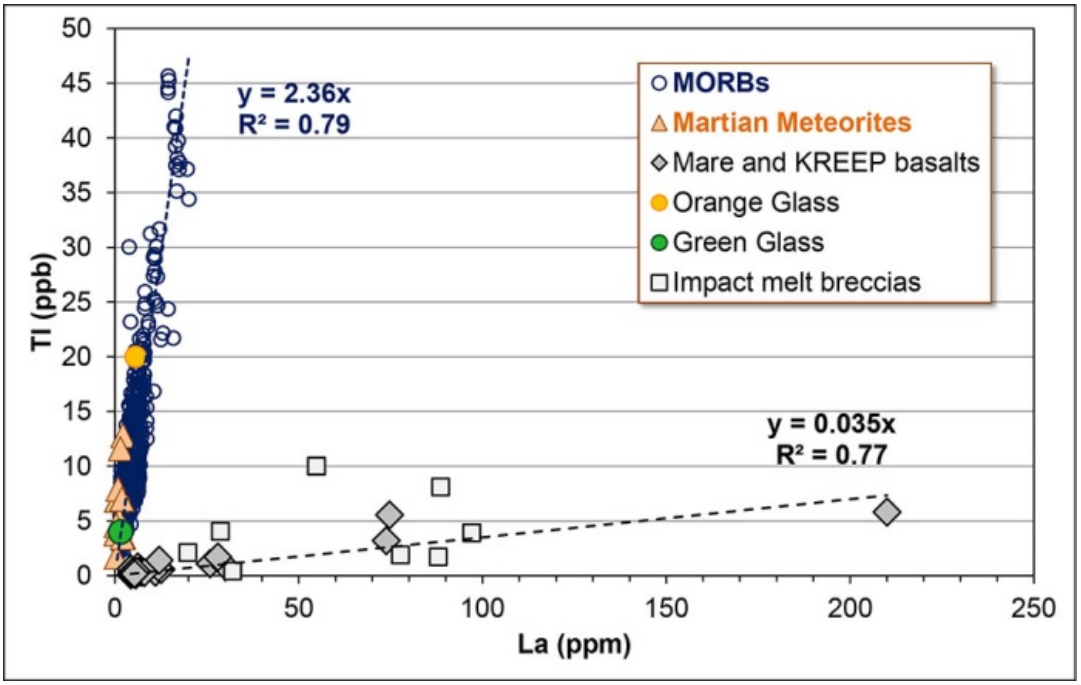

Figure 5.2. Tl vs. La plot from Taylor and Robinson (2015). The orange and green glasses plot along the terrestrial line, while the Tl/La of mare and KREEP basalts is ~75x lower.

Understanding the behavior of H isotopes during lunar accretion and differentiation is also crucial for understanding the distribution of water in the lunar interior. H isotopes have the potential to help indicate solar system water sources, but they can also be altered by degassing and H loss from hot magmas in low-pressure environments. Being able to quantify how much degassing occurred for a sample and understanding H loss from lava flows, intrusions, and melt inclusions is vital for determining the initial δD of lunar rocks, and therefore, their parental sources.

APPENDIX 1: WHY LUNAR SCIENTISTS THOUGHT THE MOON WAS DRY

The long-held belief of a nearly anhydrous Moon was based on sound reasoning. Weathering products were conspicuously absent in lunar basalts, suggesting that water did not flow across the surface or leak out to alter the original igneous rocks. The basalts did not contain any water-bearing minerals, but more importantly, neither did intrusive rocks. Intrusive rocks crystallize at depth, where higher pressure increases the solubility of water in magmas (Dixon et al., 1995). If water is present it would be expected to lead to the formation of hydrous minerals such as amphibole at least some of the time, yet no such hydrous minerals were found. Bulk chemical analyses of lunar basalts indicated H_2O concentrations of < 100 ppm (Maxwell et al., 1970), compared to 1000–3000 ppm H_2O in Hawaiian basalts (BVSP, 1981). (Analytical techniques with low detection limits to measure water contents in individual mineral grains were not available.) Furthermore, the dry Moon hypothesis was consistent with low contents of elements such as Cd and Bi,which are volatile, but less so than H_2O and H_2 (Wolf and Anders, 1980).

Another driver of the dry-Moon hypothesis was the surprisingly weak attenuation of seismic waves as measured by seismometers left by the Apollo missions (Latham et al., 1970). Seismic attenuation is expressed by the inverse of the "quality factor," Q; the higher the value of Q, the less attenuation. The upper crust of the Moon has a Q of 3000–5000, compared to terrestrial values of at least ten times smaller (Latham et al., 1970; Toksoz et al., 1974). Experiments showed that seismic Q increases in rocks under high vacuum (as low as ~10^{-9} Pa) and low water contents (Tittmann et al., 1980). For example, in the laboratory, lunar sample 70215 (a mare basalt) had a Q of 60 in air, but in high vacuum and after repeated heating to outgas adsorbed water, Q rose to 4800 (Tittmann et al., 1977). Thus, the seismic properties of the lunar crust fortified the idea that the Moon has a much lower water content than Earth.

A few measurements did suggest that water was present in lunar samples, but all were rejected as terrestrial contamination. One study crushed samples of lunar basalt from both exterior surfaces and the rock's interior to <250 μm, and measured the gases released from each sample while they were heated from 25 to 1400ºC (Gibson and Johnson, 1971). A sharp peak in H_2O for the surface sample and release over a broad range of temperatures for H_2O for the interior sample was observed, similar to the release from measurements on lunar soils. The

investigators concluded that that the water in the surface sample was probably adsorbed from the terrestrial atmosphere (Gibson and Johnson, 1971). D/H and oxygen isotopes were also measured in regolith samples (Epstein and Taylor, 1974). The solar wind, like the Sun, has low δD (~ -1000‰, Huss et al., 2012), compared to the bulk Earth (-62.5‰, Lécuyer et al., 1998). The water released by heating the regolith has δD of -100‰, in the range of air samples in Pasadena, California, where the samples were measured, leading lunar scientists to conclude that the water was terrestrial contamination (Epstein and Taylor, 1974). Of course, at the time we did not know the δD of lunar interior water. (The δD nomenclature is described in Appendix 2.) Evidence for lunar water was also reported from "rusty rock," an impact melt breccia from the Apollo 16 site (Taylor et al., 1973; Taylor et al., 1974). The "rust" is distributed throughout the rock. Analyses of the small amounts of water in 66095 indicated terrestrial contamination (δD in -80 to -120 ‰ range, Epstein and Taylor 1974).

APPENDIX 2: WATER JARGON, ISOTOPES, AND COSMIC RAY CORRECTIONS

In the lunar literature, "water" has been used to describe the presence of H_2, OH, or H_2O collectively, sometimes leading to ambiguity. In SIMS analyses, investigators usually measure ^1H and ^2H (also denoted D, for deuterium) when aiming to determine the isotopic composition of the hydrogen in a sample. In terrestrial basalts, "water" is present largely as OH until the total concentration reaches ~3.5 wt.%, at which point H_2O becomes significant (Dixon et al., 1995). No lunar magmatic water concentrations reach such high levels, implying that it is present dominantly as OH. However, under the reducing conditions prevailing in lunar magmas, "water" probably consists of a combination of OH and H_2, with the proportion of H_2 rising with decreasing oxygen fugacity (Hirschmann et al., 2012; Elkins-Tanton and Grove, 2011). To avoid confusion because of the uncertainty in how much of each species is present, many results are reported as H_2O, in spite of measuring H only or knowing that in apatite the H is present as OH. We use the word "water" as a short hand way of describing the total amount of H_2+OH+H_2O.It may be preferable to refer to the collection of H species as the H-component (Zhang, 2011).

Hydrogen isotopic compositions can be expressed in terms of deuterium/hydrogen (D/H) ratio. For example, D/H in the bulk Earth is 149 x 10^{-6} (Lécuyer et al., 1998), whereas the solar wind has a D/H $\leq$ 2 x 10^{-7} (Huss et al., 2012). It is convenient to express D/H as δD (‰) = $([D/H]_{sample}/[D/H]_{standard} - 1) \times 1000$, using Vienna Standard Mean Ocean Water (V-SMOW) for the standard. V-SMOW has a D/H ratio[87] of 155.8 x 10^{-6} (Hagemann et al., 1970). Use of the δD notation is a convenient way to compare lunar hydrogen isotopic values to those of Earth.

Extraterrestrial samples have a complication that terrestrial samples do not have: production of D and H by cosmic radiation. Both isotopes are produced by spallation reactions from high energy cosmic rays in the lunar regolith. If we know the production rate (atoms produced per million years) and the exposure time, we can correct for this effect. Unfortunately, we do not know the production rates well. Estimated production rates[88] from studies of lunar sample 70215 (an 8-kg sample of mare basalt) are 0.46 x 10^{-10} mol/100 Ma for D and 2 x 10^{-8} mol/100Ma for H (Merlivat et al., 1976). These values are consistent with experimentally-determined production rates (Reedy, 1981). The 2-sigma uncertainty in D production in 70215 is 24%, derived almost entirely from the uncertainty in the cosmic ray exposure age for the rock (100 $\pm$ 24 My, 2-sigma

uncertainty, Kirsten and Horn, 1974). Others estimate the uncertainty in the production rates of about 50% (Saal et al., 2013), far greater than the uncertainty in the measurements of δD in lunar samples. Cosmic ray exposure ages of lunar samples have been measured, but not for all. Where no cosmic ray exposure data are available, the corrections can be made by assuming an average age for nearby rocks, but this adds considerable uncertainty that is difficult to quantify. The uncertainty problem is particularly significant for samples with low total H contents (Fig. A2).

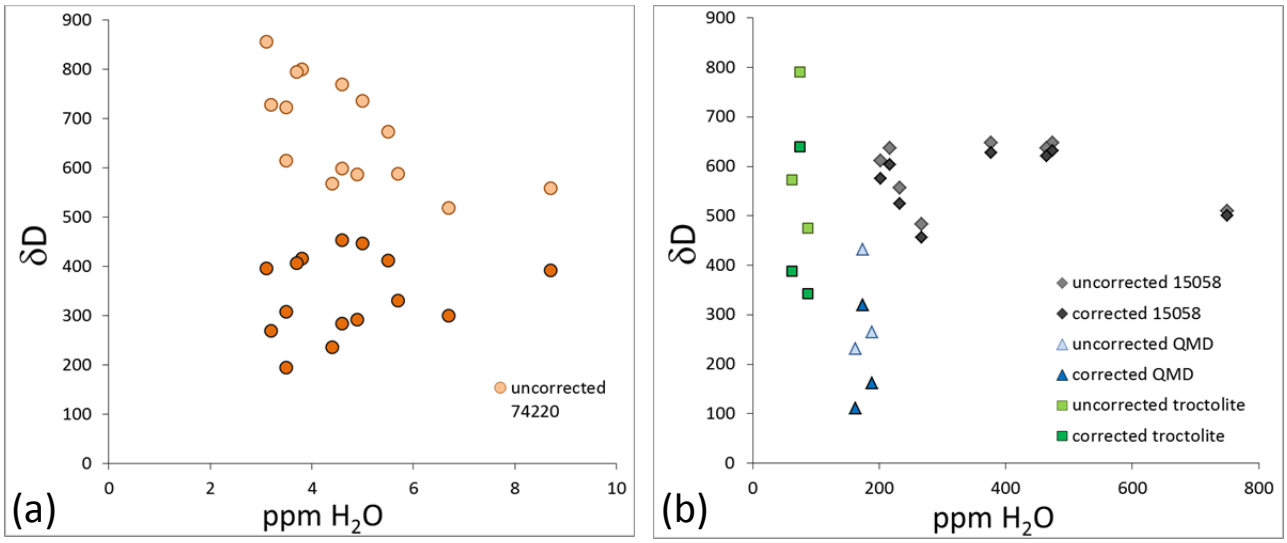

Figure A2. Spallation corrections. δD vs H_2O concentration in (a) low-H samples (Saal et al., 2013), and (b) higher-H samples (Tartèse et al., 2013; Robinson et al., 2013). Error bars are not shown to prevent clutter. Although the correction has large uncertainties, it becomes progressively less significant as total H content increases.

APPENDIX 3: EXTRAPOLATING FROM SAMPLES TO SOURCE

The fundamental goal in measuring water in lunar samples is to determine the water content and its variation in the lunar interior, leading to an accurate assessment of the bulk lunar water content. Melt inclusions are the best source of information about pre-eruptive water contents for magmas because they are essentially capsules of bulk melt sealed inside their host crystals. However, melt inclusions are rare and have only been observed in some lunar samples. The mineral apatite is relatively ubiquitous and found in several rock types.

Approaching the problem of source region water using apatite involves four steps in addition to measuring the OH concentration in apatite: (1) Placing limits on how much crystallization took place before apatite crystallized. (2) Knowing quantitatively how OH partitions between magma and apatite. (3) Constraining how much water was lost as pressure decreased in the magma, especially upon eruption. (4) Estimating the amount of partial melting that was involved in producing the magma that eventually crystallized on the lunar surface.

The OH content of apatite records the OH concentration in the magma (or lava) when the apatite crystallized. In principle, the concentration in the magma can be estimated from the OH in apatite, using crystal-melt distribution coefficients measured experimentally, which range from 0.1 to 0.25 (McCubbin et al., 2010a; Mathez and Webster, 2005). Assuming equilibrium between apatite and magma, this means that the magma contained between 10 and 4 times the OH as measured in the apatite. However, apatite is a very late-forming mineral in basaltic magmas. Because water behaves like an incompatible element at low abundances (Koga et al., 2003; Aubaud et al., 2004; Grant et al., 2007), its concentration increases in the melt as the magma crystallizes, ignoring loss of water. Estimates from published studies of lunar mare basalts that apatite crystallizes after ~95-98% of the magma has solidified (McCubbin et al., 2010a). Estimates from experimental data on silicate liquid immiscibility and observations of KREEP basalts indicates that apatite forms in highly fractionated KREEP basalt magmas after 80–90% crystallization (Tartèse et al., 2014). Thus, for 90% crystallization (10% melt remaining), the inferred initial water content of a magma would be only 10% of the amount recorded by the apatite.

This approach has been used in multiple papers to estimate water abundances in various lunar mantle source regions (McCubbin et al., 2010a; Boyce et al, 2010; Tartèse et al., 2013; Barnes et al., 2014; Tartèse et al., 2014); . However, recent work has shown that the partitioning of H into apatite is not well-represented by simple crystal-melt distribution coefficients (Boyce et al., 2014). During apatite crystallization, OH only becomes compatible after F and Cl are depleted from the melt by their incorporation into apatite (Boyce et al., 2014). Most importantly, OH is not incorporated into apatite independent of the halogens, violating the simple idea of using a composition-independent partition coefficient as done previously (McCubbin et al., 2010a). Nonetheless, if F and Cl concentrations in two magmas are similar, it is reasonable that higher or lower water concentrations in apatite indicates proportionally higher or lower water in the magmas, even if we cannot quantify the absolute concentrations.

The calculations of water loss during eruption of volcanic glass beads indicate 98% loss (Saal et al., 2008). Based on H_2O concentrations in melt inclusions in olivine in submarine Hawaiian basalts (~7000 ppm) compared to degassed melt inclusions in basalts erupted on land (~500-1000 ppm, Hauri, 2002), one can realistically estimate that lavas lose ~90% of their pre-eruptive water. This is highly uncertain, since the low oxygen fugacity of lunar magmas would have led to appreciable H_2 being present in lavas, which could be lost more readily (Hirschmann et al., 2012). On the other hand, water loss from magmas that produced intrusive rocks may have been minimal, but this is yet another uncertain factor, again because of the presence of H_2.

Estimated water content in a magma can be used to estimate the water concentration in the mantle source rock that partially melted to produce the magma. This is not well constrained because of uncertainty in the percentage of partial melting. Petrologic modeling suggests that partial melting of the mantle to produce mare basalt magmas was on the order of a few to 10% and was likely polybaric (Longhi, 2006).

WORK REFERENCED

Ahrens, T.J. Water storage in the upper mantle. *Nature* **342**, 122-123 (1989).

Alexander, C. M. O'D. *et al*. The provenances of asteroids, and their contributions to the volatile inventories of the terrestrial planets, *Science,* **337**, 721-723, doi: 10.1126/science.1223474 (2012).

Aubaud, C., Hauri, E. H., and Hirschmann, M. M. Water partitioning coefficients between nominally anhydrous minerals and basaltic melts. *Geophys. Res. Lett.* **31**, L20611, doi 10.1029/2004GRL021341 (2004).

Baedeker, P.A., Chou, C.L., Sundberg, L.L., Wasson, J.T. (1974) Volatile and siderophilic trace elements in the soils and rocks of Taurus-Littrow. Proc Lunar Sci Conf 5:1625-1643.

Barnes, J.J., Franchi, I.A., Anand, M., Tartèse, R., Starkey, N.A., Koike, M., Sano, Y., and Russell, S.S. Accurate and precise measurements of the D/H ratio and hydroxyl content in lunar apatites using NanoSIMS. *Chem. Geo.* **337-338,** 48-55 (2013).

Barnes, J.J., Tartèse, R.**,** Anand, M., McCubbin, F.M., Franchi, I.A., Starkey, N.A., Russell, S.S. The origin of water in the primitive Moon as revealed by the lunar highlands samples. *Earth Planet. Sci. Lett.* **390**, 244-252 (2014).

Barnes, J.J., Tartèse, R.**,** Anand, M., McCubbin, F.M., Franchi, I.A., Starkey, N.A. , Russell, S.S. The hydrogen isotopic composition of apatites in lunar impact-melt breccias., *45th Lunar Planet. Sci. Conf.,* abstr. 1978 (2014).

Basaltic Volcanism Study Project. *Basaltic Volcanism on the Terrestrial Planets.* Pergamon Press, Inc., New York. 1286 pp (1981).

Bell, D.R. and Rossman, G.R. Water in Earth's mantle: The role of nominally anhydrous minerals. *Science* **255**, 1391-1396 (1992).

Bernatowicz, T.J., Hohenberg, C.M., Hudson B., Kennedy B.M. and Podosek F. Argon ages for lunar breccias 14064 and 15405. *Proc. 9th Lunar Planet. Sci. Conf.*, 905-919 (1978).

Bhattacharya, S. *et al*. Endogenic water on the Moon associated with non-mare silicic volcanism: implications for hydrated lunar interior. *Curr. Sci.* **105**, 685-691 (2013).

Bockelee-Morvan, D. *et al.* Deuterated water in comet C/1996 B2 (Hyakutake) and its implications for the origin of comets. *Icarus* **133**, 147–162 (1998).

Boctor, N.Z., Alexander, C.M. O'D., Wang, J. and Hauri, E. The sources of water in martian meteorites: clues from hydrogen isotopes. *Geochim. Cosmochim. Acta* **67**, 3971–3989 (2003).

Boettcher, A.L. and O'Neil, J.R. Stable isotope, chemical and petrographic studies of high pressure amphiboles and micas: Evidence for metasomatism in the mantle source regions of alkali basalts sand kimberlites. *Am. J. Sci.* **280A**, 594-621 (1980).

Bogard, D.D., Nyquist, L.E., Bansal, B.M., Wiesmann, H. and Shih, C.-Y. 76535: An old lunar rock. *Earth Planet.Sci. Lett.* **26**, 69-80 (1975).

Bottke, W. F., Walker, R. J., Day, J. M. D., Nesvorny, D. and Elkins-Tanton, L. Stochastic late addition to Earth, the Moon, and Mars. *Science* **330**, 1527-1530 (2010).

Bouchet, M., Kaplan, G., Voudon, A., and Bertoletti, M.-J. Spark source spectrometric analysis of major and minor elements in six lunar samples. *Proc. 2nd Lunar Sci. Conf.*, 1247-1252 (1971).

Boyce, J.W., Liu, Y., Rossman, G.R., Guan, Y., Eiler, J.M., Stolper, E.M., and Taylor, L.A. Lunar apatite with terrestrial volatile abundances. *Nature*, **466**, 466-469 (2010).

Boyce, J. W., Tomlinson, S. M., McCubbin F. M., Greenwood, J. P., and Treiman, A. H. The lunar apatite paradox. *Science Express* 20 March 2014 *10.1126/science.1250398* (2014).

Bruno, B.C., Lucey, P.G., and Hawke, B.R. High-resolution UV-visible spectroscopy of lunar red spots. *Proc. 21st Lunar Planet. Sci. Conf.*, 405-415 (1991).

Burnett, D.S., Huneke, J.C., Podosek, F.A., Russ, G.P., Turner, G. and Wasserburg, G.J. The irradiation history of lunar samples. abstr., *Lunar Sci.III.*, 105-107 (1972).

Cameron, A. G. W. and Ward, W. The origin of the Moon (abstract) *Lunar Sci. VII*, 120-122 (1976).

Canup, R. M. Simulations of a late lunar-forming impact. *Icarus* **168**, 433-456 (2004).

Cherniak, D.J., Watson, E.B., and Wark, D.A Ti diffusion in quartz. *Chem. Geo*. **236**, 65-74 (2007).

Cherniak, D.J. Diffusion in accessory minerals: zircon, titanite, apatite, monazite and xenotime. *Rev*. *Mineral*. *Geochem*., **72,** *827-869* (2010).

Compston, W., Berry, H., Vernon, M.J., Chappell, B.W., and Kaye, M.J. Rubidium-strontium chronology and chemistry of lunar material from the Ocean of Storms. *Proc. 2nd Lunar Sci. Conf.*, 1471-1485 (1971).

Crozaz, G., Drozd, R., Hohenberg, C., Morgan, C., Ralston, C. Walker, R. and Yuhas, D. Lunar surface dynamics: Some general conclusions and new results from Apollo 16 and 17. *Proc. 5th Lunar Sci. Conf.,* 2475-2499 (1974).

Delano, J. Pristine lunar glasses: Criteria, data, and implications. *Proc. Lunar Planet. Sci. Conf. 16th,* in *J. Geophys. Res., 91,* D201–D213 (1986).

Deloule, E., Albarède, F., and Sheppard, S.M.F. Hydrogen isotope heterogeneities in the mantle from ion probe analysis of amphiboles from ultramafic rocks. *Earth. Planet. Sci. Lett*. **105**, 543-553 (1991).

Desch, S. J. and Taylor, G. J. A model of the Moon's volatile depletion. *42nd Lunar Planet. Sci. Conf.*, abstr. 1608 (2011).

Desch S.J. and Taylor G. J. Volatile depletion from the protolunar disk. *Euro. Planet. Sci. Cong. 7*, abstr.272 (2012)

Desch, S. J. and Taylor, G. J. Isotopic mixing due to interaction between the protolunar disk and the Earth's atmosphere. *44th Lunar Planet. Sci. Conf.*, abstr.1719 (2013).

Dixon J.E., Stolper E.M., and Holloway J.R.,. An experimental study of water and carbon dioxide solubilities in mid-ocean ridge basaltic liquids: I. Calibration and Solubility Models. *J. Petrol.* **36**, 1607-1631 (1995).

Dodson, M.H. Closure temperature in cooling geochronological and petrological systems. *Contrib.Mineral. Petro*, **40**, 259-274 (1973).

Drake, M.J. Origin of water in the terrestrial planets. *Meteor. Planet. Sci.* **40**, 519-527 (2005).

Drozd, R.J., Kennedy, B.M., Morgan, C.J., Podosek, F.A. and Taylor, G.J. The excess fission Xenon problem in lunar samples. *Proc. 7th Lunar Sci. Conf.,* 599-623 (1976).

Dymek, R. F., Albee, A. L. and Chodos, A. A. Comparative petrology of lunar cumulate rocks of possible primary origin: Dunite 72415, troctolite 76535, norite 78235,and anorthosite 62237. *Proc. 6th Lunar Sci. Conf*. 301-341 (1975).

Eberhardt, P., Reber, M., Krankowsky, D. and Hodges, R.R. The D/H and $^{18}O/^{16}O$ ratios in water from comet P/Halley. Astron. Astrophys. 302, 301–316 (1995).

Elardo, S. M., Draper, D. S., and Shearer, C. K. Jr. Lunar Magma Ocean crystallization revisited: Bulk composition, early cumulate mineralogy, and the source regions of the highlands Mg-suite. *Geochim. Cosmochim. Acta* **75**, 3024-3045 (2011).

Elardo, S. M., McCubbin, F. M., and Shearer, C. K. Jr. Chromite symplectites in Mg-suite troctolite 76535 as evidence for infiltration metasomatism of a lunar layered intrusion. *Geochim. Cosmochim. Acta* **87,** 154-17 (2012).

Elkins-Tanton, L. T. and Grove, T.L. Water (hydrogen) in the lunar mantle: Results from petrology and magma ocean modelling. *Earth Planet. Sci. Lett.* **307,** 173-179 (2011).

Epstein, S. and Taylor, H. P. D/H and $^{18}O/^{16}O$ ratios of H_2O in the "rusty" breccia 66095 and the origin of "lunar water." *Proc. Fifth Lunar Sci. Conf.*, 1839–1854 (1974).

Eugster, O. *et al*. The cosmic-ray exposure history of Shorty Crater samples: the age of Shorty Crater. *Proc. Lunar Planet. Sci. Conf. 8th*, 3059-3082 (1977).

Füri E., Deloule E., Gurenko A., and Marty B. New evidence for chondritic lunar water from combined D/H and noble gas analyses of single Apollo 17 volcanic glasses. *Icarus* **229**, 109-120 (2014).

Gaetani, G.A., O'Leary, J.A., Shimizu, N., Bucholz, C. and Newville, M. Rapid equilibration of H_2O and oxygen fugacity in olivine-hosted melt inclusions. *Geology* **40**, 915-918 (2012).

Geiss, J. and Gloecker, G. Abundances of Deuterium and Helium-3 in the protosolar cloud. *Space Sci. Rev.* **84**, 239-250 (1998).

Gibson, E. K. and Johnson, S. M. Thermal analysis-inorganic gas release studies of lunar samples. *Proc. Second Lunar Sci. Conf.*, 1351–1366 (1971).

Glotch, T.D., *et al.* Highly silicic compositions on the Moon. *Science* **329**, 1510-1513 (2010).

Gooley, R.C., Brett, R., Warner, J.L. and Smyth, J.R. A lunar rock of deep crustal origin: Sample 76535. *Geochim.Cosmochim. Acta* **38**, 1329-1339 (1974).

Graham, C., Kinny, P., Harte, B. and Valley, J. The Nature and Scale of Stable Isotope Disequilibrium in the Mantle: Ion and Laser Microprobe Evidence. *Mineral. Mag.* **58A**, 345-346 (1994).

Grant, K. J., Kohn, S. C., and Brooker, R. A. The partitioning of water between olivine, orthopyroxene and melt synthesized in the system albite-forsterite-H_2O. *Earth Planet. Sci. Lett.* **3260**, 227-241 (2007).

Greenwood, J.P., Itoh, S., Sakamoto, N., Vicenzi, E.P. and Yurimoto, H. Hydrogen isotope evidence for loss of water from Mars through time. *Geophys. Res. Lett*. **35**, L05203 (2008).

Greenwood, J. P. *et al*. Apollo rock samples and the D/H of lunar apatite. 41st *Lunar Planet. Sci. Conf.*, abstr. 2439 (2010).

Greenwood, J. P., Itoh, S., Sakamoto, N., Warren, P., Taylor, L., and Yurimoto, H. Hydrogen isotope ratios in lunar rocks indicate delivery of cometary water to the Moon. *Nature Geosci.* **4,** 79-82 (2011).

Grove, T. L., Till, C. B., and Krawczynski, M. J. The role of H_2O in subduction zone magmatism. *Annu. Rev. Earth Planet. Sci*., **40**, 413-439 (2012).

Hagemann, R., Nief, G., and Roth, E. Absolute Isotopic Scale for Deuterium Analysis of Natural Waters. Absolute D/H ratio for SMOW. *Tellus* **22**, 712−715 (1970).

Hagerty, J.J., Lawrence, D.J., Hawke, B.R., Vaniman, D.T., Elphic, R.C., and Feldman, W.C. Refined thorium abundances for lunar red spots: Implications for evolved, nonmare volcanism on the Moon. *J. Geophys. Res.* **111,** E06002, doi:10.1029/2005JE002592 (2006).

Hallis L. J., Taylor G. J., Nagashima K., Huss G. R. Magmatic water in the martian meteorite Nakhla. *Earth Planet. Sci. Lett*. **359-360**, 84-92 (2012).

Hallis L. J., Huss G.R., Nagashima K., Taylor G.J., Halldórsson S.A., and Hilton D.R. Is Earth's original D/H ratio preserved in the deep mantle? *45th Lunar Planet Sci.Conf.*, abstr.1283 (2014)

Hartmann, W. K. and Davis, D. R. Satellite-sized planetesimals and lunar origin. *Icarus* **24**, 504-515 (1975).

Hartogh, P. *et al.* Ocean-like water in the Jupiter-family comet 103P/ Hartley 2. *Nature* **478**, 218–220 (2011).

Hauri, E., Wang J., Dixon, J.E., King, P.L., Mandeville, C., and Newman, S. SIMS analysis of volatiles in silicate glasses 1. Calibration, matrix effects and comparisons with FTIR. *Chem. Geol*. **183**, 99-114 (2002).

Hauri, E. SIMS analysis of volatiles in silicate glasses, 2: Isotopes and abundances in Hawaiian melt inclusions. *Chem. Geol*. **183**, 115-141 (2002).

Hauri, E. H., Gaetani, G. A., and Green, T. H. Partitioning of water during melting of the Earth's upper mantle at H2O-undersaturated conditions. *Earth Planet. Sci. Lett*. **248**, 715-734 (2006).

Hauri, E. H., Weinreich, T., Saal, A. E., Rutherford, M. C. and Van Orman, J. A. High pre-eruptive water contents preserved in lunar melt inclusions. *Science* **333,** 213-215 (2011).

Hawke, B.R., Lawrence, D.J., Blewett, D.T., Lucey, P.G., Smith, G.A., Spudis, P.D., and Taylor, G.J. Hansteen Alpha: A volcanic construct in the lunar highlands. *J. Geophys. Res.* **E7**, 5069, doi:10.1029/2002JE002013 (2003).

Head, J.W. and McCord T.B. Imbrian-age highland volcanism on the Moon: The Gruithuisen and Mairan domes. *Science* **199**, 1433-1436 (1978).

Hess, P. C., Rutherford, M. J., Guillemette, R. N., Ryerson, F. J., and Tuchfeld, H. A. Residual products of fractional crystallization of lunar magmas: An experimental study. *Proc. 6th Lunar Sci. Conf.*, 895-909 (1975).

Hess, P.C., Rutherford, M.J., Campbell, H.W. Ilmenite crystallization in nonmare basalt: Genesis of KREEP and high-Ti mare basalt. *Proc.9th Lunar Sci. Conf. 705-724* (1978).

Hess, P.C., Horezmpa, P., and Rutherford, M.J. Fractionation of Apollo 15 KREEP basalts. *20th Lunar Planet. Sci. Conf.*, abstr. 1209, 408-409 (1989).

Hildreth, W. Gradients in silicic magma chambers: Implications for lithospheric magmatism. *J. Geophys. Res.* **86** (B11), 10, 153-10,192 (1981).

Hilton, D.R., Gronvold, K., MacPherson, C.G., Castillo, P.T. Extreme $^{3}He/^{4}He$ ratios in northwest Iceland: Constraining the common component in mantle plumes. *Earth Planet. Sci. Lett.* **173**, 53–60 (1999).

Hirschmann, M. M., Wirthers, A. C., Ardia, P., and Foley, N. T. Solubility of molecular hydrogen in silicate melts and consequences for volatile evolution of terrestrial planets. *Earth Planet. Sci. Lett.* **345-348**, 38-48 (2012).

Hui, H., Peslier, A., Zhang, Y., and Neal, C. R. Water in lunar anorthosites and evidence for a wet early Moon. *Nature Geosci.* doi:10.1038/NGEO1735 (2013).

Huss, G. R., Nagashima, K., Burnett, D. S., Jurewicz, A. J. G., and Olinger, C. T. A new upper limit on the D/H ratio in the solar wind. *43th Lunar Planet. Sci. Conf.*, abstr.1709 (2012).

Irving, A.J. Chemical variation and fractionation of KREEP basalt magmas. *Proc.8th Lunar Sci. Conf.*, 2433-2448 (1977).

Jackson, M. G., *et al.* Evidence for the survival of the oldest terrestrial mantle reservoir. *Nature* **466**, 853-856 (2010).

Jambon, A. Earth degassing and large-scale geochemical cycling of volatile elements. In: Carroll, M.R., Holloway, J.R. (Eds.), Volatiles in Magmas. *Min. Soc. Am., Rev. Min.* **30**, 479-517 (1994).

James, O.B. and Hammarstrom, J.G. Petrology of four clasts from consortium breccia 73215. *Proc.8th Lunar Sci. Conf.*,,2459-2494 (1977).

Jolliff, B.L. Fragments of quartz monzodiorite and felsite in Apollo 14 soil particles. *Proc. 21st Lunar Planet. Sci. Conf.*, 101-118 (1991).

Jolliff, B.L., Korotev, R.L., and Haskin, L.A. Geochemistry of 2-4mm particles from Apollo 14 soil (14161) and implications regarding igneous components and soil-forming processes. *Proc. 21st Lunar Planet. Sci. Conf.*, 193-219 (1991).

Jolliff, B. L., Floss, C., McCallum, I. S., Schwartz, J. M. Geochemistry, petrology, and cooling history of 14161,7373: A plutonic lunar sample with textural evidence of granitic-fraction separation by silicate-liquid immiscibility. *Am. Mineral.* **84**, 821-837 (1999).

Jolliff, B.L., Gillis, J.J., Haskin, L.A., Korotev, R.L., and Wieczorek, M.A. Major lunar crustal terrains: Surface expressions and crust-mantle origins. *J.Geophys. Res.* **105** (E2), 4197-4216 (2000).

Jolliff, B. L. *et al.* Non-mare silicic volcanism on the lunar farside at Compton-Belkovich. *Nature Geosci.* **4**, 566-571 (2011).

Jovanovic, S. and Reed, G.W., jr. Cl and P_2O_5 systematics: Clues to early lunar magmas. *Proc. 6th Lunar Sci. Conf.,* 1731-1751 (1975).

Kirsten, T., Deubner, J., Horn, P., Kaneoka, I., Kiko, J., Schaeffer, O.A. and Thio, S.K. The rare gas record of Apollo 14 and 15 samples. *Proc. 3rd Lunar Sci. Conf.* 1865-1889 (1972).

Kirsten, T. and Horn, P. Chronology of the Taurus-Littrow region III: ages of mare basalts and highland breccias and some remarks about the interpretation of lunar highland rock ages. Proc. 5 th Lunar Sci. Conf. 1451-1475 (1974).

Klima, R., Cahill, J., Hagerty, J., and Lawrence, D. Remote detection of magmatic water in Bullialdus Crater on the Moon. *Nature Geosci.* doi:10.1038/NGEO1909 (2013).

Koga, K., Hauri, E., Hirshmann, M., and Bell, D. Hydrogen concentration analyses using SIMS and FTIR: comparison and calibration for nominally anhydrous minerals. *Geochem. Geophys. Geosys.* **4**, 1019, doi: 10.1029/2002GC000378 (2003).

Latham, G. V. *et al*. Apollo 11 passive seismic experiment. *Proc. Apollo 11 Lunar Science Conf.*, 2309-2320 (1970).

Lécuyer, C., Gillet, P., and Robert, F. The hydrogen isotope composition of seawater and the global water cycle. *Chem. Geo.* **145**, 249-261 (1998).

Liu, Y., Guan, Y., Zhang, Y., Rossman, G.R., Eiler, J.M., and Taylor, L.A. Direct measurement of hydroxyl in the lunar regolith and the origin of lunar surface water. *Nature Geosci.* **5**: 779-782 (2012).

Longhi, J. Experimental petrology and petrogenesis of mare volcanics. *Geochim. Cosmochim. Acta* **56**, 2235-2251 (1992).

Longhi, J. Petrogenesis of picritic mare magmas: Constraints on the extent of early lunar differentiation. *Geochim. Cosmochim.Acta* **70**, 5919-5934. (2006).

Lucey, P.G., Blewett, D.T., and Jolliff, B.F. Lunar iron and titanium abundance algorithims based on final processing of Clementine ultraviolet-visible images. *J. Geophys. Res.* **105** (E5): 20297-20305 (2000).

Lugmair, G.W. and Marti, K. Exposure ages and neutron capture record in lunar samples from Fra Mauro. *Proc. 3rd Lunar Sci. Conf.*, 1891-1897 (1972).

Lugmair, G.W., Marti, K., Kurtz, J.P. and Scheinin, N.B. History and genesis of lunar troctolite 76535 or: How old is old? *Proc. 7th Lunar Sci. Conf.,* 2009-2033 (1976).

Malin, M.C. Lunar red spots: Possible pre-mare materials. *Earth Planet. Sci. Lett.* **21**, 331-341 (1974).

Mathez, E. A., and Webster, J. D. Partitioning behavior of chlorine and fluorine in the system apatite-silicate melt-fluid. *Geochim. Cosmochim. Acta*, **69**, 1275-1286 (2005).

Maxwell, J. A., Peck, L. C., and Wiik, H. B. Chemical composition of Apollo 11 lunar samples 10017, 10020, 10072, and 10084. 1369-1374 (1970).

McCubbin, F. M., Nekvasil, H. and Lindsley, D. H. Evidence for water in lunar magmatic minerals? A crystal chemical investigation. *38th Lunar Planet. Sci. Conf.*, abstr. 1354 (2007).

McCubbin, F. M., Steele, A., Hauri, E.H., Nekvasil, H., Yamashita, S., and Hemley, R.J. Nominally hydrous magmatism on the Moon. *Proc. Natl. Acad. Sci. USA* **107,** 11223-11228 (2010a).

McCubbin, FM. *et al*. Detection of structurally bound hydroxyl in apatite from Apollo mare basalt 15058,128 using TOF-SIMS. *Am Mineral* **9,** 1141-1150, doi: 10.2138/ am.2010.3448 (2010b).

McCubbin, F.M. *et al*, Fluorine and chlorine abundances in lunar apatite: Implications for heterogeneous distributions of magmatic volatiles in the lunar interior. *Geochim. Cosmochim. Acta* **75**, 5073–5093 (2011).

McCubbin, F.M.**,** Hauri, E.H., Elardo, S.M., Vander Kaaden, K.E., Wang, J., and Shearer, C.K.,. Hydrous melting of the martian mantle produced both depleted and enriched shergottites. *Geology* **40**, 683-686 (2012).

Meier, R. *et al*. A determination of the HDO/H_2O ratio in comet C/1995 01 (Hale-Bopp). *Science* **279**, 842–844 (1998).

Merlivat, L., Leiu, M., Neif, G., and Roth, E. Spallation deuterium in rock 70215. *Proc. Lunar Sci. Conf. 7th*, 649-658 (1976).

Michael, P.J. The concentration, behavior and strorage of H_2O in the suboceanic upper mantle: implications for mantle metasomatism. *Geochim. Cosmochim. Acta* **52**, 555–566 (1988).

Minitti, M. E., Leshin, L. A., Darby Dyar, M., Ahrens, T. J., Guan, Y. and Luo, S. N. Assessment of shock effects on amphibole water contents and hydrogen isotope compositions: 2. Kaersutitic amphibole experiments. *Earth Planet. Sci. Lett*. **266**, 288–302 (2008).

Morgan, J.W., Ganapathy, R., Higuchi, H., Krahenbuhl, U. and Anders, E. Lunar basins: Tentative characterization of projectiles from meteoritic elements in Apollo 17 boulders. *Proc. 5th Lunar Sci. Conf.*, 1703-1736 (1974).

Morris, R.V., Taylor, G.J., Newsom, H.E., Keil, K., and Garcia, S.R.. Highly evolved and ultramafic lithologies from Apollo 14 soils. *Proc. 20th Lunar Planet. Sci. Conf.*, 61-75 (1990).

Morris, R.V. The surface exposure (maturity) of lunar soils; some concepts and I_s/FeO compilation. *Proc. 9th Lunar Planet. Sci.* 2287-2297 (1978).

Morrisson, G.H., Gerard, J.T., Potter, N.M., Gangadharam, E.V., Rothenberg, A.M., and Burdo R.A. Elemental abundances of lunar soil and rocks from Apollo 12. *Proc. 2nd Lunar Sci. Conf.*, 1169-1185 (1971).

Mottl, M. J., Glazer, B. T., Kaiser, R. I. and Meech, K. J. Water and astrobiology. *Chemie der Erde* **67,** 253-282 (2007).

Nash, W.P. and Crecraft, H.R. Partition coefficients for trace elements in silicic magmas. *Geochim. Cosmochim. Acta* **49**, 2309-2322 (1985).

Newman, S. and Lowenstern, J.B. VolatileCalc: a silicate melt-H_2O-CO_2 solution model written in Visual Basic for Excel. *Comp. and Geosci.* **28**, 597-604 (2002).

Paniello, R.C., Day, J. M. D., and Moynier, F. Zinc isotopic evidence for the origin of the Moon. *Nature* **490,** 376-379 (2012).

Pernet-Fisher, J.F., Howarth, G.H., Liu, Y., Chen, Y., and Taylor, L.A. Estimating the lunar mantle water budget from phosphates: Complications associated with silicate-liquid-immiscibility. *Geochim. Cosmochim. Acta* **144**, 326-341 (2014).

Quick, J.E., Albee, A.L., Ma, M.-S, Murali, A.V., and Schmitt, R.A. Chemical compositions and possible immiscibility of two silicate melts in 12013. *Proc. 8th Lunar Sci. Conf.* **8**, 2153-2189 (1977).

Reedy, R.C. Cosmic-ray-produced stable nuclides: Various production rates and their implications. *Proc. Lunar Sci. Conf.* **12B**, 1809-1823 (1981).

Robinson, K.L. and Taylor, G.J. Intrusive and extrusive lunar felsites. *42nd Lunar Planet Sci. Conf.,* abstr. 1257 (2011).

Robinson, K.L., Taylor, G.J., Hellebrand, E., and Nagashima, K. KREEP, KREEP derivatives, and the Lunar D Enrichment? *Euro. Planet. Sci. Cong. 2012*, abstr. 283 (2012).

Robinson, K.L., Taylor, G.J., and Nagashima, K. D/H of intrusive Moon rocks: Implications for lunar origin. *44th Lunar Planet Sci. Conf.*, abstr.1327 (2013).

Robinson, K.L. and Taylor, G.J. Heterogeneous distribution of water in the Moon. *Nature Geosci.* **7**, 401-408 (2014).

Roedder, E. and Weiblen, P.W. Lunar petrology of silicate melt inclusions, Apollo 11 rocks. *Proc. Apollo 11 Lunar Sci.Conf.,, Geochim. Cosmochim.Acta* **34**, suppl. 1, 801-837 (1970).

Roedder, E. and Weiblen, P.W. Petrology of silicate melt inclusions, Apollo 11 and Apollo 12 and terrestrial equivalents. *Proc. 2nd Lunar Sci. Conf.,* 507-528 (1971).

Rutherford, M. J., Dixon, S., and Hess, P. Ilmenite saturation at high pressure in KREEP basalts: Origin of KREEP and Hi-TiO_2 mare basalts (abstract). *9th Lunar Planet. Sci.*, 966–967 (1980).

Rutherford, M. J., Hess, P.C., and Daniel, G.H. Experimental liquid line of descent and liquid immiscibility for basalt 70017. *Proc. 5th Lunar Sci. Conf.*, 569-583 (1974).

Rutherford, M.J., Hess, P.C., Ryerson, F.J., Campbell, H.W., and Dick, P.A. The chemistry, origin and petrogenetic implications of lunar granite and mozonite. *Proc. 7th Lunar Sci. Conf.,* 1723-1740 (1976).

Ryder, G. and Martinez, R. R. Evolved hypabyssal rocks from station 7, Apennine Front, Apollo 15. *Proc. 21st Lunar Planet. Sci. Conf.*, 127-50 (1991).

Ryder, G. Lunar sample 15405: Remnant of a KREEP basalt-granite differentiated pluton. *Earth Planet. Sci. Lett.* **29**, 255–268 (1976).

Ryder G., Quenching and disruption of lunar KREEP lava flows by impacts. Nature **336**, 751–754 (1988).

Ryder, G., Bogard, D., and Garrison, D. Probable age of Autolycus and calibration of lunar stratigraphy. *Geology* **19**, 143–146 (1991).

Ryder, G., Stoeser, D. B., Marvin, U. B., and Bower, J. F. Lunar granites with unique ternary feldspars. *Proc.6th Lunar Planet. Sci. Conf.,* 435-449 (1975).

Saal, A.E., Hauri, E.H., Langmuir, C.H. and Perfit, M.R. Vapor undersaturation in primitive mid-ocean ridge basalt and the volatile content of the Earth's Upper Mantle. *Nature* **419**, 451-455 (2002).

Saal, A.E., Hauri, E. H., Rutherford, M. J., and Cooper, R. F. The volatile contents (CO_2, H_2O, F, S, Cl) of the lunar picritic glasses. 38th *Lunar Planet. Sci. Conf.*, abstr. 2148 (2007).

Saal, A.E., Hauri, E.H., Lo Cascio, M., Van Orman, J.A., Rutherford, M.C., and Cooper, R.F. Volatile content of lunar volcanic glasses and the presence of water in the Moon's interior. *Nature* **454,** 192-195 (2008).

Saal, A.E., Hauri, E.H., Van Orman, J.A., and Rutherford, M.J. Hydrogen isotopes in lunar volcanic glasses and melt inclusions reveal a carbonaceous chondrite heritage. *Science* **340**, 1317-1320 (2013).

Sarafian, A. R., Nielsen, S.G., Marschall, H.R., McCubbin, F.M., Monteleone, B.D. Early accretion of water in the inner solar system from a carbonaceous chondrite-like source. *Science* **346**, 623-626 (2014).

Schwartz J.M. and McCallum I.S. Inferred depths of formation of spinel cataclasites and troctolitic granulite,76535 using new thermodynamic data for Cr-spinel. *30th Lunar Planet. Sci. Conf.,* abstr. 1308 (1999).

Seddio, S.M., Jolliff, B.L., Korotev, R.L., and Zeigler, R.A. Petrology and geochemistry of lunar granite 12032,366-19 and implications for lunar granite petrogenesis. *Am. Mineral.,* **98**, 1697-1713 (2013).

Sharp, Z.D., Shearer, C.K., McKeegan, K.D., Barnes, J.D., and Wang, Y.Q. The chlorine isotope composition of the Moon and implications for an anhydrous mantle. *Science* **329**, 1050-1053 (2010).

Sharp, Z. D., McCubbin, F. M., and Shearer, C. K. A hydrogen-based oxidation mechanism relevant to planetary formation. *Earth Planet. Sci. Lett.* **380**, 88-97 (2013).

Shaw, A. M., *et al.* Long-term preservation of slab signatures in the mantle inferred from hydrogen isotopes. *Nature Geosci*. **5**, 224-228 (2012).

Shearer, C.K. and Floss, C. Evolution of the Moon's mantle and crust as reflected in trace-element microbeam studies of lunar magmatism. In Origin of the Earth and Moon (R. Canup and K. Righter, eds.), Univ. of Arizona Press, Tucson, pp. 339-359 (1999).

Shearer, C.K., and Papike, J.J. Early crustal building processes on the Moon: Models for the petrogenesis of the magnesian suite. *Geochim. Cosmochim. Acta* **69**, 3445-3461 (2005).

Shearer, C. K., *et al*. Thermal and Magmatic Evolution of the Moon. *New Views of the Moon: Reviews in Mineralogy and Geochemistry* **60**, 365-518 (2006).

Shervais, J.W., and Taylor, L.A. Micrographic granite: More from Apollo 14. 13th Lunar Planet. Sci. Conf., abstr., 696-697 (1983).

Shervais, J.W. and McGee, J.J. KREEP cumulates in the western lunar highlands: Ion and electron microprobe study of alkali-suite anorthosites and norites from Apollo 12 and 14. *Amer. Mineral.* **84**, 806-820 (1999).

Snyder, G. A., Taylor, L. A., and Halliday, A. N.. Chronology and petrogenesis of the lunar highlands alkali suite: Cumulates from KREEP basalt crystallization. *Geochim. Cosmochim. Acta* **59**, 1185–1203 (1995).

Starkey, N. A. *et al.* Helium isotopes in early Iceland plume picrites: Constraints on the composition of high 3He/4He mantle. *Earth Planet. Sci. Lett.* **277**, 91–100 (2009).

Stuart, F. M., Lass-Evans, S., Fitton, J. G., and Ellam, R. M. High $^{3}He/^{4}He$ ratios in picritic basalts from Baffin Island and the role of a mixed reservoir in mantle plumes. *Nature* **424**, 57-59 (2003).

Tartèse, R. and Anand, M. Late delivery of chondritic hydrogen into the lunar mantle: Insights from mare basalts. *Earth Planet. Sci. Lett.* **361**, 480-486 (2013).

Tartèse, R., Anand, M., Barnes, J. J., Starkey, N. A., Franchi, I. A., and Sano, Y. The abundance, distribution, and isotopic composition of Hydrogen in the Moon as revealed by basaltic lunar samples: Implications for the volatile inventory of the Moon. *Geochim. Cosmochim. Acta* **122**, 58-74 (2013).

Tartèse, R., Anand, M., McCubbin, F.M., Elardo, S.M., Shearer, C.K., and Franchi, I.A. Apatites in lunar KREEP basalts: The missing link to understanding the H isotope systematics of the Moon. *Geology* **42**, 363-366 (2014).

Taylor, G.J., Warner, R.D., Keil, K., Ma, M-.S., and Schmitt, R.A. Silicate liquid immiscibility, evolved lunar rocks, and the formation of KREEP. *Proc. Conf. Lunar Highlands Crust,* 339-352 (1980).

Taylor G. J., Martel L. M. V, and Spudis P. D. The Hadley-Apennine KREEP Basalt Igneous Province. *Meteor. Planet. Sci.* **47,** 861-879 (2012).

Taylor, G.J. and Robinson, K.L. (2015) Radically heterogeneous distribution of volatiles in the Moon. *46th LPSC*, Abst. # 2815.

Taylor, L.A., Mao, H.K. and Bell P.M. Identification of the hydrated iron oxide mineral akaganeite in Apollo 16 lunar rocks. *Geology* **2**, 429-432 (1974).

Taylor, L.A., Mao, H.K. and Bell, P.M. "Rust" in the Apollo 16 rocks. *Proc. 4th Lunar Sci. Conf.* 829-839 (1973).

Thompson, A.B. Water in the Earth's upper mantle. *Nature* **358**, 295-302 (1992).

Tittmann, B. R. *et al*. Internal friction quality-factor Q under confining pressure. *Proc. Lunar Sci. Conf. 8th*, 1209-1224 (1977).

Tittmann, B. R, Clark, V. A, and Spencer, T. Compressive strength, seismic Q, and elastic modulus. *Proc. Lunar Planet. Sci. Conf. 11th*, 1815-1823 (1980).

Toksoz, M.N., Dainty, A.M., Solomon, S.C. and Anderson, K.R. Structure of the Moon. *Rev. Geophys. Space Phys*. **12**, 539–567 (1974).

Turcotte, D.L. and Schubert, G. Geodynamics: Applications of Continuum Physics to Geological Problems., Wiley, 450pp. (1982)

Tuttle, O.F. and Bowen, N.L. Origin of granite in the light of experimental studies in the system $NaAlSi_3O_8$-$KAlSi_3O_8$-SiO_2-H_2O, *Geol. Soc. Am. Mem*. **74**, 151 pp. (1958).

Wadhwa, M. Redox conditions on small bodies, the Moon, and Mars. *Rev. Mineral. Geochem.* **68**, 493-510 (2008).

Wagner, C., Deloule, E., Mokhtari and A. Richterite-bearing peridotites and MARID-type inclusions in lavas from North Eastern Morocco: Mineralogy and D/H isotopic studies. *Cont. Min. Petrol*. **124**, 406–421 (1996).

Wanke H., *et al.* Apollo 12 samples: Chemical composition and its relation to sample locations and exposure ages, the two component origin of the various soil samples and studies on lunar metallic particles. *Proc. 2nd Lunar Sci. Conf.,* 1187-1208 (1971).

Wanke, H., *et al*. New data on the chemistry of lunar samples: Primary matter in the lunar highlands and the bulk composition of the Moon. *Proc. 6th Lunar Sci. Conf.*, 1313-1340 (1975).

Wanke H., *et al*. Chemistry of lunar highland rocks: A refined evaluation of the composition of the primary matter. *Proc. 7th Lunar Sci. Conf.*, 3479-3499 (1976).

Wark, D.A. and Watson, E.B. TitaniQ: a titanium-in-quartz geothermometer. *Contrib. Mineral. Petro.* 152: 743-754. doi: 10.1007/s00410-006-0132-1 (2006).

Warner, R.D., Taylor, G.J., Mansker, W.L., and Keil, K. Clast assemblages of possible deep-seated (77517) and immiscible-melt (77538) origins in Apollo 17 breccias. *Proc. 9th Lunar Planet. Sci. Conf.,* 941-958 (1978).

Warren, P.H., and Wasson, J.T. The origin of KREEP. *Rev. Geophys.* **17**, 73-88 (1979).

Warren, P.H., Taylor, G.J, Keil, K., Shirley, D.N., and Wasson, J.T. Petrology and chemistry of two “large” granite clasts from the Moon. *Earth Planet. Sci. Lett.* **64**, 175-185 (1983).

Warren, P.H., Jerde, E.A., and Kallemeyn, G.W. Pristine Moon rocks: a “large” felsite and a metal-rich ferroan anorthosite. *Proc. 18th Lunar Planet. Sci. Conf., J. Geophys. Res.* **92**, B4, E303-E313 (1987).

Warren, P. H. and Taylor, G. J. The Moon. In *Treatise on Geochemistry*, vol. 1 (A. Davis, ed.), 213-242, Elsevier (2014).

Wasson, J.T., Boynton, W.V., Kallemeyn, G.W., Sundberg, L.L., and Wai, C.M. Volatile compounds -released during lunar lava fountaining. *Proc. 7th Lunar Sci. Conf.*, 1583-1595 (1976).

Watson, L.L., Hutcheon, I.D., Epstein, S. and Stolper, E.M. Water on Mars: clues from D/H and water contents of hydrous phases in SNC meteorites. *Science* **265**, 85–90 (1994).

Whitaker, E.A. Lunar color boundaries and their relationship to topographic features. *Moon* **4**, 348-355 (1972).

Wieczorek, M.A., *et al.* The crust of the Moon as seen by GRAIL. *Science* **339**, 671-675 (2013).

Wilson, L. and Head, J.W. Lunar Gruithuisen and Mairan domes: Rheology and mode of emplacement. *J. of Geophys. Res.* **108**, E5, 5012, doi:10.1029/2002JE001909 (2003) .

Wolf, R and Anders, E. Moon and Earth: Compositional differences inferred from siderophiles, volatiles and alkalis in basalts. *Geochim. Cosmochim. Acta* **44**, 2111-2124 (1980).

Wood, C.A. and Head, J.W. Geologic setting and provenance of spectrally distinct premare material of possible volcanic origin (abst.). *Conf. Origin Mare Basalts* (1975)

Xia, Q-K., Deloule, E., Wu, Y-B., Chen, D-G. and Cheng, H. Anomalously high δD values in the mantle. *Geophys. Res. Lett*. **29**, 4-1–4-4. doi:10.1029/2001GL013887 (2002).

Yurimoto, H., Kurosawa, M., and Sueno, S. A. Hydrogen analysis in quartz crystals and quartz glasses by secondary ion mass spectrometry. *Geochim. Cosmochim. Acta* **53**, 751-755 (1989).

Zhang, Y. Geochemical Kinetics. Princeton University Press, 631pp. (2008).

Zhang, Y. "Water" in lunar basalts: The role of molecular hydrogen (H_2), especially in the diffusion of the H component. *42nd Lunar Planet. Sci.Conf.*, abstr. 1957 (2011).